REAL-TIME HARDWARE-IN-THE-LOOP MODELLING AND SIMULATION OF A GRID CONNECTED SOLAR ENERGY SYSTEM

By

KALUNGA DESIRE MULEMBO

Thesis Submitted in partial fulfilment of the requirements for the degree

Master of Engineering in Energy

Faculty of Engineering and Built Environment

Cape Peninsula University of Technology

Supervisor: Dr. Ali Almaktoof

Co-Supervisor: AProf. K. Aboalez
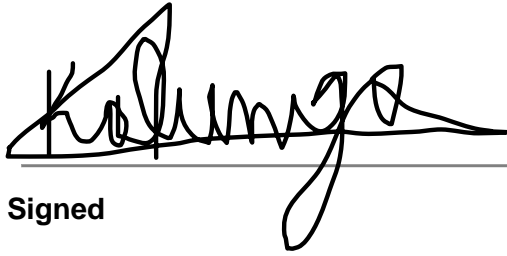
Bellville Campus

December 2023

DECLARATION

I, Desire Kalunga Mulembo, declare that the contents of this dissertation/thesis represent my own unaided work, and that the dissertation/thesis has not previously been submitted for academic examination towards any qualification. Furthermore, it represents my own opinions and not necessarily those of the Cape Peninsula University of Technology.

December 2023

Signed

Date

ABSTRACT

The growing concern for environmental conservation and the ever-increasing global energy demand have thrust renewable energy systems (RESs) into the spotlight. RESs offer a compelling solution by simultaneously reducing harmful emissions and harnessing an essentially boundless source of primary energy. Among RESs, photovoltaic (PV) systems have emerged as a popular choice for both residential and grid-connected renewable energy applications. This study is dedicated to achieving seamless power synchronization between two distinct energy sources such as Photovoltaics (PV) systems and the utility grid. To accomplish this objective, a novel maximum power point tracking (MPPT) algorithm is introduced. This algorithm is meticulously designed to efficiently regulate the switching element of a DC-DC boost converter.

It excels at swiftly tracking the maximum power point while ensuring voltage stability, irrespective of fluctuations in solar radiation. The incorporation of precise speed control is pivotal in extracting maximum power from PV systems. Consequently, the proposed system offers an effective mechanism for achieving harmonious power synchronization. The central focus of this research revolves around the evaluation of system performance and control techniques for the seamless integration of PV systems into the utility grid. Successful integration hinges on the ability to align the frequencies and voltages of PV systems with those of the grid. To achieve this synchronization and enable the injection of alternating current into the grid, the study employs the phase-locked loop synchronization technique (PLL).

This method is thoroughly elucidated, simulated using MATLAB/Simulink, and validated in Typhoon HIL 402 real-time simulator. Furthermore, the study addresses the performance evaluation and control engineering aspects of PV systems integrated into utility grids. This encompasses the synchronization of alternating current outputs of grid-powered systems through proportional-integral (PI) control methods. The research employs simulations and testing using software like MATLAB/Simulink and Typhoon HIL 402 real-time simulator to scrutinize and optimize synchronization control and the performance of PV systems in grid-connected applications. The findings of this research hold promise for countries with similar grid structures, such as South Africa, which can benefit from advancements in PV technology and grid-connected renewable energy systems.

ACKNOWLEDGEMENTS

DEDICATION

I dedicate this dissertation to the remarkable individuals who have been a constant source of inspiration and support throughout my academic journey:

Late Father: Desire Kalunga Mulembo

Mother: Marie Kitenge

Brothers: Philippe Mulembo, Emma Mulembo, Moise Mulembo,and David Mulembo

Sisters: Mulembo Carine, Mulembo Gisele, Mulembo Sarah and Mulembo Rose

Lastly, I dedicate this thesis to all those who have contributed to my growth and development as a researcher and an individual. Your advice, feedback, and contributions have been instrumental in shaping this work, and I am thankful for your valuable insights.

`

Table of Contents

Table of Figures

Table of Tables

GLOSSARY

AC:	Alternative current
ANF:	Adaptive Notch Filter
CDPES:	Center for Distributed Power Electronics Systems
DP:	Phase detector
DC:	Direct current
E:	Energy
EGI:	Electric generation injecting
FF:	Fill factor
FOCV:	Fractional Open Circuit Voltage
FSCC:	Fractional Short Circuit Current
FSCC:	Fractional Short Circuit Current
G GPV:	Generator Photovoltaic
GHG:	Greenhouse Gas
GCES:	Grid-connected energy system
GPS	Grid connecting photovoltaic system
H	Planck's constant
HIL	Hardware-in-the-Loop
IEA	International Energy Agency
IGBT	Insulated-gate bipolar transistor
IC:	Incremental Conductance
INC	Incremental Conductance
I_{opt}:	Optimum Current

(I_{sc}):	Short-Circuit Current
IPT:	Instantaneous Power Theory
LED:	Light Emitting Diodes
LG:	line to ground
LN:	Line to Neutral
MPC:	Model Predictive Control
MPC:	Model Predictive Control
MPP:	Maximum Power Point
MPPT:	Maximum power point tracking
MPC:	Model Predictive Control
MtCO2e:	Metric tons of carbon dioxide equivalent
N:	Negative
N_P:	Number of photovoltaic arrays connected in parallel
N_s:	Number of solar cells connected in series
P:	Positive
PI:	Proportional Integral
PV:	Photovoltaic
PLL:	Phase lock loop
PID:	Proportional Integral derivative
PWM:	Pulse Width Modulated
$\mathbf{P_{MA}}$:	Total power output of the photovoltaic system or array
$\mathbf{P_M}$:	Power output of a single photovoltaic module or array
PN:	Positive-Negative
P&O:	Perturb and Observe

R_s :	Series resistance
R_{sh}:	Parallel shunt resistor
RESs:	energy demand has thrust renewable energy systems
SEA:	Sustainable Energy Africa
SIO2:	Silicon Dioxide
SRF:	Synchronize rotating reference frame
TF:	Transfer function
TO:	Gate turn-off Thyristor
USAID	United States Agency for International Development
V_{oc}:	Open-Circuit Voltage
VCO:	Voltage-controlled oscillator
WRI CAIT:	World Resources Institute Climate Analysis Indicator Tool.
VBS:	Vector-Based Synchronization

CHAPTER ONE: INTRODUCTION

1.1. Introduction

In recent years, the global transition towards sustainable and clean energy sources has gained significant momentum, with solar energy emerging as a leading contender in the race to replace fossil fuels (Bank, 2023). Consequently, the integration of solar energy systems into power grids has become a pressing concern for researchers, policymakers, and engineers alike (Pal & Sahay, 2018). This research delved into the intricacies of designing, modelling, and simulating such systems in a real-time environment.

By employing hardware-in-the-loop (HIL) techniques, this study aims to provide valuable insights into the dynamic behaviour of grid-connected solar energy systems and pave the way for their efficient and reliable integration into existing power networks. Through a systematic exploration of the challenges and opportunities inherent in HIL implementations, this dissertation seeks to contribute to the ongoing efforts to optimise the performance and stability of solar energy systems, thereby accelerating the global shift towards a more sustainable and greener future.

A country's economy and development depend on the availability and stability of reliable, affordable, and clean energy (Kabeyi & Olanrewaju, 2020). As industry and population increase, so does the demand for energy, which affects the scarcity of energy resources and increases the demand for fossil fuels, which in turn affects the environment through increased pollution. In industrial and public sectors such as hospitals, schools, and commercial sectors, electrical equipment accounts for the majority of energy consumption; this sector consumes about 80% of energy in most developed countries (Consumption & Resources, 2016).

Efforts to transition to more reliable, affordable, and clean energy sources, such as renewable energy (e.g., solar, wind, hydropower), and energy efficiency measures can help address the challenges associated with increasing energy demand, resource scarcity, and environmental pollution (Garcia & Hawes, 2021). Investing in the research and development of new technologies, promoting energy conservation and efficiency measures, and adopting policies and regulations to incentivize the use of clean energy can all contribute to sustainable energy practices and support economic and social development while minimising environmental impacts.

Uses of renewable energy, such as solar energy from Photovoltaic (PV) cells, have become increasingly important in addressing the challenges of limited supply and environmental damage associated with non-renewable energy sources like fossil fuels.

PV cells, which convert sunlight directly into electricity, have become a popular choice for home applications and grid-connected renewable energy systems (Fofang & Tanyi, 2020).

PV systems can be connected in parallel to increase current or in series to increase voltage, and they can also be combined in parallel and series to monitor output current and voltage. With advancements in technology, newer PV cells can be integrated into the grid without the need for isolation using generation injection techniques. This allows renewable energy to be fed back into the main grid through grid-connected energy systems (GCES), which utilize natural processes like solar energy, wind, and hydrolysis to generate power (Yasmeena & Das, 2015). The excess energy produced by GCES can be put back into the grid, reducing the need for expensive energy storage equipment like generators.

Research has focused on the performance evaluation and control engineering of PV systems integrated into utility grids, including the synchronization of alternating current outputs of grid-powered systems using proportional-integral (PI) control methods. Simulations and testing using software like MATLAB/Simulink and HIL simulators have been used to analyze and optimize the synchronization control and performance of PV systems in grid-connected applications.

Countries with similar grid structures, such as South Africa, can benefit from the advancements in PV technology and grid-connected renewable energy systems. By incorporating more renewable energy into the grid, countries can reduce their reliance on fossil fuels, decrease environmental pollution, and improve energy security and sustainability in the long term (Kojima, 2016). However, it is important to continue research and development efforts in renewable energy technologies to further improve their efficiency, reliability, and affordability for widespread adoption and maximum impact on economic and environmental sustainability.

1.2. Research problem statement

In South Africa, the increasing demand for energy coupled with the reliance on non-renewable energy sources has resulted in a severe shortage of energy. The country is grappling with frequent power outages and an unsustainable energy supply system. This situation not only impedes industrial growth and economic development but also has negative consequences for the daily lives of citizens and the environment.

To address this energy shortage issue, there is an urgent need to transition to renewable energy sources such as grid-tied systems. Grid-tied systems are connected to the local utility grid, allowing for the use of both solar energy and grid electricity. By implementing grid-tied systems, South Africa

can harness its abundant sunshine to meet the growing energy demand while reducing its reliance on non-renewable sources and mitigating environmental impact.

1.3. Background of the research problem

According to data from WRI CAIT, South Africa's greenhouse gas emissions have increased by 142 MtCO2e from 1990 to 2012, with an average annual growth rate of 1.7% (USAID, 2014). This increase in emissions is a cause for concern, as it contributes to global climate change and has negative environmental and socio-economic impacts.

The dominant sources of South Africa's greenhouse gas emissions are coal-fired power plants, which account for 83% of the country's energy production, and natural gas, which accounts for 6% (Ibrahim et al., 2021). The country's heavy reliance on fossil fuels for energy generation has resulted in significant carbon emissions, contributing to the overall increase in greenhouse gas emissions.

The background of the research problem is further compounded by the country's growing energy demand due to population and industrial growth, resulting in energy shortages. This has led to increased concessions for energy growth in the country to meet the rising energy demand. However, the reliance on fossil fuels for energy production has adverse environmental and social consequences, including climate change impacts, air pollution, and health issues (Ibn-Mohammed et al., 2017).

Renewable energy sources, such as wind and solar, offer potential solutions to reduce greenhouse gas emissions and increase energy supply in South Africa (Garcia & Hawes, 2021). The integration of renewables into the grid system, such as through feed-in tariffs and grid chain expansion, can facilitate the adoption of renewable energy and diversify the energy mix (IEA, 2022). This background sets the stage for the research problem, which aims to investigate strategies for mitigating greenhouse gas emissions and increasing energy supply in South Africa through the integration of renewable energy sources into the energy system.

1.4. The Objectives of the research

The aims of this project is to design and implement a MATLAB and HIL model and simulation of a grid-connected solar energy system. The Objective of this projects is following by:

1. Developing a HIL model of a grid-connected solar energy system using MATLAB/Simulink software and Validate in Typhoon-HiL400.

2. Implementing the HIL system with hardware components that emulate the behavior of the solar panel, inverter, battery storage, and grid connection.
3. Designing and implementing control algorithms to optimize the operation of the solar energy system.
4. Testing the HIL system in real-time using various scenarios and conditions, such as changes in solar irradiance and load demand.

1.5. Project limitation

Limitations: The project had the following limitations:

1. The project not involve the physical construction or installation of solar panels.
2. The project focused on a grid-connected solar energy system and may not be applicable to off-grid systems.
3. The project assumed ideal conditions for the solar energy system components and may not account for real-world factors such as degradation and aging of components.
4. The project required a significant amount of hardware and software resources, which may limit the scale of the simulation.
5. The project was limited by the availability and accuracy of data on solar irradiance and load demand.

1.6. Organization of the Thesis

To validate a smart configuration grid in the context of strong integration of renewable energy resources, the proposed thesis currently focuses on the design part of the control system, based on the Phase-Locked Loop (PLL) method and approaches to real-time simulation. Grid-connecting photovoltaic systems (GPS) require significant attention to the design method. This ensures that the integration of the two different energy supplies is synchronized to ensure efficient and reliable functionality. The following outlines how this project is set up:

Chapter 2 Literature Review:

This chapter covers an in-depth literature review on various topics related to grid-connected PV systems, as mentioned in the project description. It reviewed the current state of research on solar energy, PV cells and modules, temperature and irradiation effects on PV performance, different types of PV systems, grid-connected PV system characteristics, DC-DC converter control system,

and maximum MPPT techniques. The chapter provided a comprehensive understanding of the existing knowledge in the field and serve as a foundation for the design part of the thesis.

Chapter 3 Modeling of Grid-Connected PV Systems:

Focused on the modeling and control aspects of grid-connected PV systems. It began with the modeling of photovoltaic generators, particularly using the single-diode model, considering temperature and irradiance effects. The chapter then explored the mathematical modeling of DC-DC Boost converters and methods for controlling them to optimize power output. It delved into the modeling of DC-AC converters and the role of grid-tied inverters in converting DC to AC for grid connection. Additionally, it discussed the control system for grid-connected PV systems, emphasizing the use of PLL and Proportional-Integral controllers for effective synchronization and power management.

Chapter 4 Modeling using MATALAB Simulink and Typhoon HIL:

This chapter discussed on the modeling and designing, of grid-tied photovoltaic systems in MATLAB and Typhoon HIL-402. Additionally, there was an exploration of the design and calculation aspects of the Boost converter and the LCL filter.

Chapter 5: Simulation Results and Discussions

This chapter presented, simulations were conducted to acquire results for grid-connected system. These simulations were executed using SIMULINK software, with the primary aim of evaluating the performance of the PV system in a grid-connected configuration. To ensure the accuracy and alignment of our findings with real-world scenarios, we employed the Typhoon hardware-in-the-loop system for thorough validation of our simulations.

Chapter 6: Summary of findings, Conclusions, and Recommendations

This chapter provided the summarized for the main findings of the thesis and draw conclusions based on the research conducted. It highlighted the contributions of the thesis to the field of grid-connected PV systems and the validation of a smart configuration grid.

References: This chapter provided a comprehensive list of all the references cited in the thesis, following the appropriate citation style.

Appendices: This section included any additional information that is relevant to the thesis but not included in the main text, such as simulation settings, data, and additional analyses.

1.7. Summary

Chapter 1 introduces the thesis "Real-Time Hardware-in-the-Loop Modelling and Simulation of a Grid-connected Solar Energy System." It outlines the increasing significance of renewable energy, particularly solar power, in meeting energy demands and addresses the challenges of grid synchronisation. The chapter defines the research problem as the need for effective synchronisation techniques and control strategies in grid-connected solar power systems.

Key objectives include designing and implementing a real-time hardware-in-the-loop simulation to enhance system performance. The scope is clearly defined, focusing on specific aspects of the solar power system, while acknowledging hardware and software limitations. The chapter concludes with an overview of the thesis structure, including subsequent chapters on literature review, methodology, results, conclusion, and future work. This initial chapter sets the groundwork for the detailed research that follows.

CHAPTER TWO: LITERATURE REVIEW

2.1 Introduction

The sun is a nearly limitless source of energy. All other energies on Earth, including so-called renewable energies like wind, biomass, thermal, chemical, kinetic, and even electrical energy, are thought to have originated from this source, which also produces radiation and heat (J. Sreedevi, N. Ashwin, 2016). The latter is created by turning solar energy from photon energy into electricity. When a material is exposed to the sun, this process determines how much electricity it can produce. The photovoltaic effect is as shown; he had been found by French physicist Antoine Becquerel in 1839 (Approach, 2019). This finding has undergone evolution and advancement over time. Bell Telephone Laboratories produced the first solar cell made of crystalline silicon in the United States in 1954.

This PV cell had a conversion efficiency of 4%. Eventually, the efficiency was increased to 11% in Bell Labs (Approach, 2019). At this time, a new era of solar energy production was ushered in by the PV effect. The American spacecraft Vanguard I, which had six panels coated in silicon cells with an average efficiency of 6%, was launched in 1958. (Berrada & El Mrabet, 2020). Since all of the satellites are equipped, PV modules that were chosen to reduce the weight/electrical power ratio supplied. Before the relaunch seen in the 1990s, the PV and other renewable energy experienced their first "terrestrial" boom in the early 1980s (Fofang & Tanyi, 2020).

Initially, the use of silicon PV cells in space applications allowed for relatively quick but incremental learning and competence (Ibn-Mohammed et al., 2017). Since then, its use has grown significantly and spread around the globe. Today, remote sites are powered by photovoltaic energy (Yasmeena & Das, 2015). In order to lessen the emissions of gases into the atmosphere caused by fossil fuels, complete farms of the magnitude of Megawatts are erected all over the world (Munguia et al., 2020). They are either independent or linked to the main electrical network. The description of the photovoltaic system and its workings will be the main topics of this chapter.

Chapter 2 serves as a comprehensive exploration of the existing body of knowledge related to solar energy, photovoltaic cells, and grid-connected solar energy systems. This chapter aims to provide the necessary context for understanding the current state of the art and identifying gaps in the literature, thereby justifying the need for this research. The literature review begins with an introduction, followed by an examination of the global status of photovoltaic energy and an in-depth analysis of solar energy and its conversion through photovoltaic cells. Further, this chapter investigates the electrical properties of photovoltaic cells, the influence of temperature and

irradiation, the various types of PV systems, and their components. Subsequently, it delves into the design aspects of grid-connected photovoltaic systems and discusses the advantages and disadvantages of photovoltaic energy. Lastly, the chapter explores the role of simulation tools and real-time simulators in the context of solar energy systems.

2.2. The world situation of photovoltaic energy

Photovoltaic energy, which harnesses solar radiation to generate electricity, has emerged as a promising technology to address the pressing global challenges of increasing energy demand, mitigating climate change, and promoting sustainable development (Ibn-Mohammed et al., 2017). The capacity of installed PV has been rapidly expanding in recent years, driven by sustainable energy legislation, strong commitments from nations, advancements in technology, and cost reduction efforts.

According to estimates, the global installed PV capacity reached around 400 GW by the end of 2017, and it is projected to increase to 4500 GW by 2050 (Chowdhury et al., 2020). This exponential growth in PV capacity reflects the increasing adoption of solar energy as a viable and sustainable source of electricity worldwide (IEA, 2022).

Figure 2.1 presents a visual representation of the global capacity and annual additions of PV energy around the world. The graph highlights the significant growth in PV capacity over the years, with a steep increase in annual additions in recent times, indicating the accelerated deployment of PV systems globally.
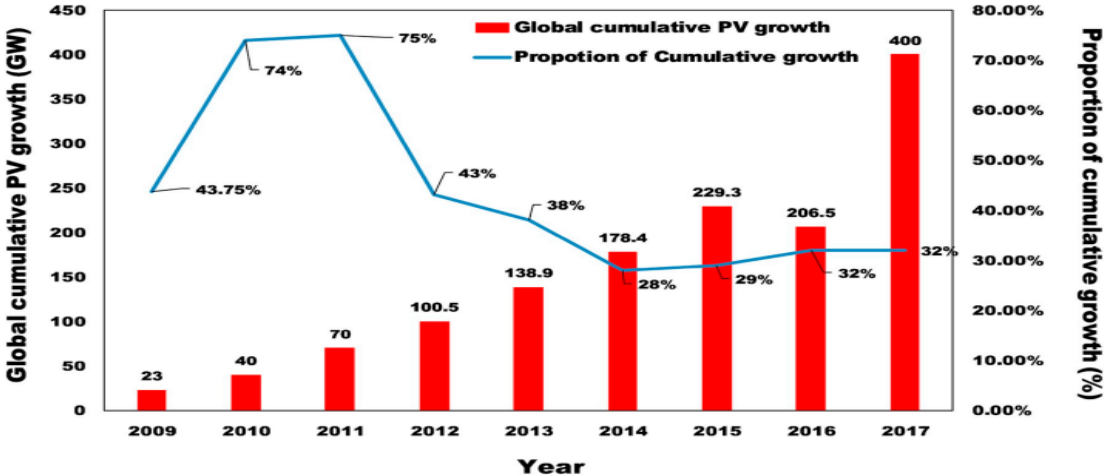
Figure 2.1: Global growth of solar PV capacity

This rapid expansion of PV energy can be attributed to various factors, including favorable government policies and incentives, increasing awareness about the need for renewable energy, advancements in PV technology, and declining costs of PV modules and systems (Brunarie et al., 2009). Governments and international organizations have implemented sustainable energy legislation, such as feed-in tariffs, net metering, and renewable portfolio standards, to promote the adoption of PV energy and reduce greenhouse gas emissions (SEA, 2017).

Furthermore, the commitment of nations towards reducing their dependence on fossil fuels and transitioning to clean energy sources has been a driving force behind the growth of PV energy. Many countries have set ambitious targets for renewable energy deployment, including PV, as part of their efforts to mitigate climate change and achieve sustainable development goals (Kojima, 2016).

Advancements in PV technology, such as improvements in PV module efficiency, durability, and reliability, have also contributed to the growth of PV capacity. Moreover, the decreasing costs of PV modules and systems, due to economies of scale, technological innovation, and increased competition, have made PV energy more affordable and accessible to a wider range of users (Sultana & U, 2016).

The global situation of PV energy is characterized by rapid expansion in installed capacity, driven by sustainable energy policies, national commitments, technological advancements, and cost reductions. PV energy has emerged as a promising solution to address the challenges of increasing energy demand, climate change, and sustainable development, and its growth trajectory is expected to continue in the coming years.

2.3. Solar energy

Solar energy is derived from the Sun, which took approximately 100 million years to form. The Sun's nuclear fusion reactions involving hydrogen atoms create helium (He) and release energy in the form of heat and radiation, including thermal energy(Szabo, 2018). Solar energy can be converted into different types of energy, such as chemical, kinetic, thermal, biomass, and electric energy (Fraas, 2015).

Electric energy, specifically, is generated when solar radiation is converted into electricity through a process known as the photoelectric effect. This phenomenon was discovered by Antoine Becquerel, a French physicist, in 1839 (Hempstead, 1977). The photoelectric effect involves the

ability of certain substances, known as photoelectric materials, to generate electricity when exposed to sunlight.

Solar energy can be harnessed using various technologies, such as photovoltaic (PV) cells or solar panels, which directly convert sunlight into electricity through the photoelectric effect (Szabo, 2018). PV cells are typically made of semiconductor materials, such as silicon, which absorb sunlight and generate an electric current. This electricity can be used to power electrical devices, homes, businesses, and even be fed back into the grid (Chowdhury et al., 2020).

Solar energy is a clean, renewable, and abundant source of energy that has numerous benefits, including reducing greenhouse gas emissions, mitigating climate change, and promoting sustainable development (Approach, 2019). It is a promising alternative to fossil fuels, and advancements in solar technology continue to improve the efficiency and affordability of solar energy systems, making it an increasingly viable solution for meeting our energy needs in a sustainable manner.

2.4. Photovoltaic cell

The PV cell converts sunlight directly into electricity through the photovoltaic effect, and multiple PV cells are typically interconnected in a solar panel to generate higher voltage and power levels for practical applications (Salah, 2019).

2.4.1. Principle of operation of a PV cell

A PV cell typically consists of two layers of silicon, with one layer being positively doped with a material such as boron (P zone) and the other layer being negatively doped with a material such as phosphorus (N area) (Ibn-Mohammed et al., 2017). These two layers are brought together to form a PN junction, where the excess electrons from the N layer diffuse to the P layer, and the excess holes from the P layer diffuse to the N layer, this creates an internal electric field at the junction.

The PV cell is usually protected by a plate that serves as an anode on the P side and a plate that serves as a cathode on the N side (Salah, 2019). When sunlight strikes the surface of the PV cell, photons are absorbed, generating electron-hole pairs in the semiconductor material(Salah, 2019). The electric field at the PN junction then causes the free electrons and holes to be separated, with electrons being pushed towards the N side and holes being pushed towards the P side (Salah, 2019). Figure 2.2 below shows Solar cell construction.

When an external circuit is connected to the PV cell, the accumulated electrons flow through the circuit towards the P side, and the accumulated holes flow towards the N side, generating an electric current that can be collected by very fine metal wires on the surface of the cell (Ibn-Mohammed et al., 2017). This generated electric current can be used to power various electrical devices or stored in batteries for later use, providing a source of clean and renewable electricity.
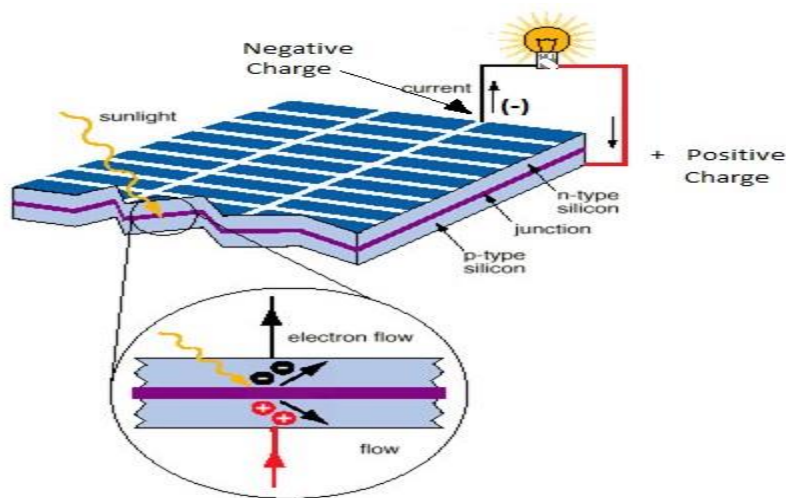
Figure 2.2: Solar cell construction

Photons are elementary particles of light that exhibit properties of both particles and waves (Ibrahim et al., 2019). They are quanta of electromagnetic radiation, which means they can behave both as particles and waves depending on how they are observed or measured (Mohammad Bagher, 2015). The energy (E) of a photon is directly proportional to its frequency (f), and the constant of proportionality is Planck's constant (h) (Tunahan Işık Isik, 2015). This relationship is described by the equation:

$$E = f * h$$
<div align="right">Equation 2.1</div>

Where E represents the energy of the photon, f represents the frequency of the electromagnetic wave, and h represents Planck's constant. Planck's constant (h) is a fundamental constant of nature and has a value of approximately $6.62607015 * 10^{-34}$ joule-seconds (J·s) (Yi, 2012). It was introduced by the German physicist Max Planck in his groundbreaking work on the theory of quantum mechanics, and it plays a crucial role in describing the behavior of photons and other particles at the atomic and subatomic scale (Ngoc et al., 2019).

When a photon is absorbed by a semiconductor in a photovoltaic cell, it produces an electron and a "hole." This photon will, in fact, transmit its energy to an electron (negative particle), which will then free itself from the attraction of its nucleus, leaving a "hole" (positively charged) behind him. To generate an electric current, the positive ("holes") and negative (electrons) charges must be separated and then drawn apart (Aleem et al., 2020).

This is when the PN junction's internal electric field comes into play, pushing the electrons back into the N zone and thus separating the charges. The charge carriers are then collected via a grid at the front that serves as an anode and a contact at the back that serves as the cathode (Aleem et al., 2020). Then, between these electrodes, a DC voltage of about 0.5 V is obtained (Aleem et al., 2020).

2.4.2. Types of PV Cells

Many semiconductor materials are used in the fabrication of a PV cell. Indeed, three major technologies are available on the market: crystalline silicon, thin films, and organic cells. However, crystalline silicon commands a market share of more than 80% (Mohammad Bagher, 2015). This is because silica, also known as silicon dioxide ($SiO2$), is a mineral that is abundant on our planet and thus less expensive. It's also non-toxic (Zina et al., 2017). and accounts for 25% of the mass of our planet's crust, making it the second most common element after oxygen (Zina et al., 2017). Each cell type has its own performance and cost. Currently, there are three main types of cells (Mohammad Bagher, 2015).

Monocrystalline silicon cells are typically a consistent blue color (Mohammad Bagher, 2015). It has the best yield among all (between 12 to 18% or even up to 24% in the laboratory) (Mohammad Bagher, 2015). It has the highest yield (between 12 and 18%, or up to 24% in the laboratory) (Mohammad Bagher, 2015). It has a tendency to lose ground due to its high manufacturing cost, as shown in Figure 2.3a, the polycrystalline silicon cell is the most present technology on the photovoltaic power generation market, and their manufacturing cost is much lower (Fofang & Tanyi, 2020).

However, their yield is average, ranging from 11% to 15% or even up to 19.8% in the laboratory Figure 2.3b, which shows a typical example of a polycrystalline silicon cell; and the performance of amorphous silicon cells is poor. In the laboratory, it ranges from 5% to 8% and can reach 13% (Mohammad Bagher, 2015). They are gray or brown in color, as shown in Figure 2.3c, with an example of an amorphous silicon cell below (Shariar & Control, 2016).
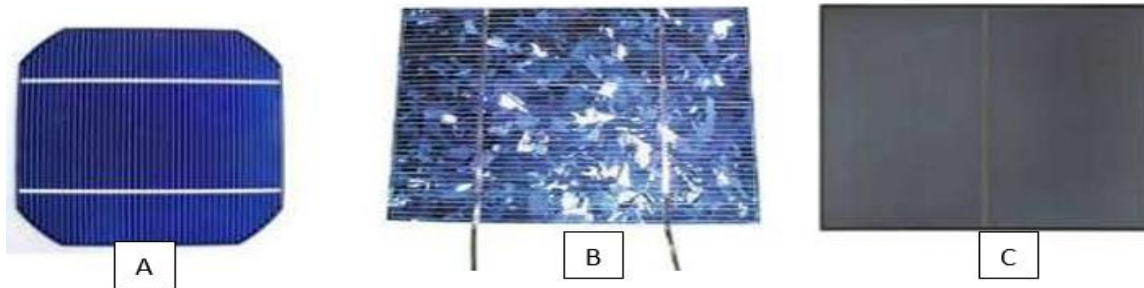
Figure 2.3: a) Monocrystalline silicon, b) Polycrystalline silicon and c) Amorphous silicon

Solar cell technologies are crucial for harnessing solar energy and converting it into electricity. They are classified into three main types based on the materials used: silicon-based solar cells, semiconductor compound solar cells, and emerging or novel materials solar cells. These types have evolved over time, each offering unique advantages and potential advancements Figure 2.4 shown the classification of cell technologies used.
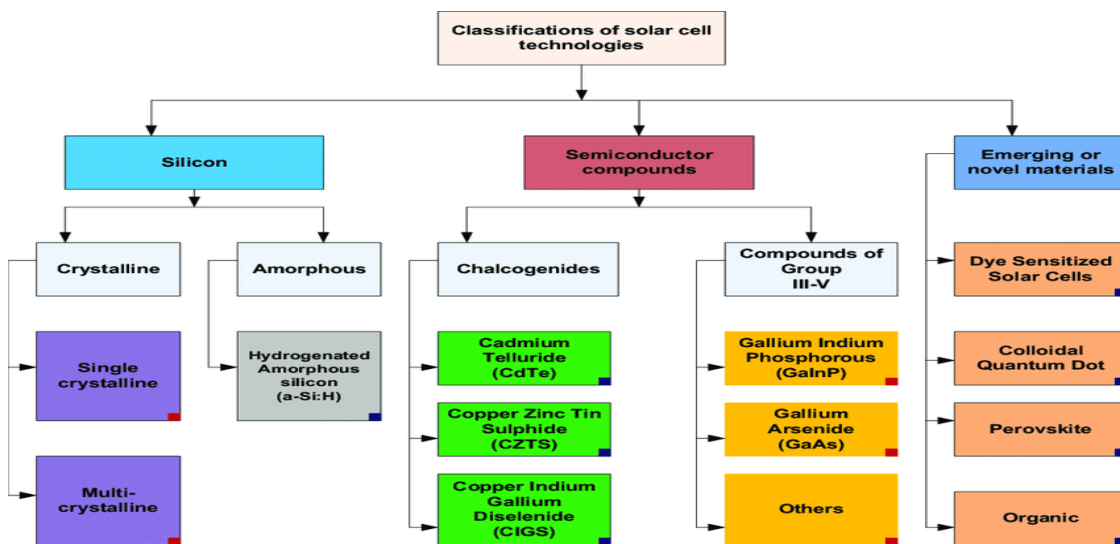
Figure 2.4: Solar cell technology types.

2.4.3. Cell equivalent circuit

A photovoltaic (PV) cell can be represented by an electrical equivalent circuit shown in Figure 2.5 bellow, which consists of various components that model its behavior (Yasmeena & Das, 2015). The figure shows five parameters of a PV cell's electrical equivalent circuit, which includes a current

generator connected in parallel with a diode. Additionally, there are two resistors that are included in the cell's electrical composition and affect its operation:

Series resistance (R_s) or internal resistance): This resistor models the resistance of the semiconductor material used in the PV cell, as well as losses in contact with the collector grids and their resistivity, It represents the overall resistance to current flow within the PV cell (Zina et al., 2017; El-basit & Soliman, 2016).

Parallel shunt resistor (R_{sh}): This resistor simulates the leakage currents caused by the edge effects of the PN junction in the PV cell. It represents the parallel path for current flow, which can be due to the imperfections in the cell's construction or materials (Zina et al., 2017; El-basit & Soliman, 2016).
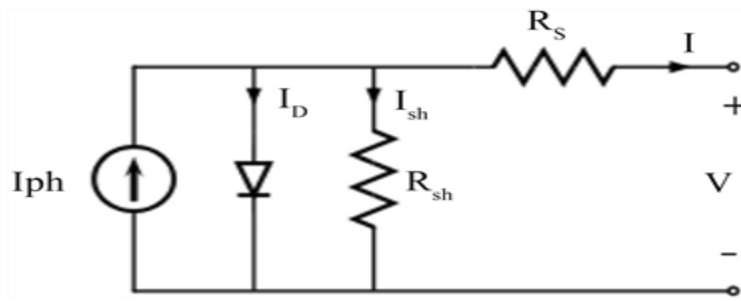
Figure 2.5: PV cell equivalent circuit.

To determine the current generated by the PV cell's mathematical model, Kirchhoff's law, which is a fundamental law of circuit analysis, can be applied. Kirchhoff's law states that the sum of currents entering a junction in a circuit must be equal to the sum of currents leaving the junction, and the sum of voltages around any closed loop in a circuit must be zero (El-basit & Soliman, 2016). By considering the electrical equivalent circuit and applying Kirchhoff's law, the behavior of a PV cell can be modeled and analyzed for various operating conditions (Zina et al., 2017).

The operation of the PV cell as a generator can be mathematically formalized using system equations derived from Kirchhoff's laws (Zina et al., 2017).

The equation (2.2) represents the current (I) generated by the PV cell, and it includes several parameters:

$$I = I_{ph} - I_o \cdot \left[exp \left(\frac{q.(v+IR_s)}{V_r} \right) - 1 \right] - \frac{(V+IR_s)}{R_{sh}} \qquad \text{Equation 2.2}$$

Where:

$V_r = \dfrac{K.T.m}{q}$ Equation 2.3

I_{ph}: Represents the photocurrent, which is the current generated by the cell due to the absorption of photons from sunlight.

I_o: Represents the reverse saturation current of the diode, which is a characteristic parameter of the PV cell and depends on the temperature, material properties, and other factors.

q: Represents the charge of an electron.

v: Represents the voltage across the PV cell.

R_s: Represents the series resistance, which models the resistance of the semiconductor material used in the PV cell, as well as losses in contact with the collector grids and their resistivity.

V_r: Represents the thermal voltage of the cell, which is calculated using Equation 2.3 where K is the Boltzmann constant, T is the temperature in Kelvin, and m is the ideality factor of the diode.

R_{sh}: Represents the parallel shunt resistance, which models the leakage currents caused by the edge effects of the PN junction in the PV cell.

Equation 2.4 is obtained by substituting the expression for V_r from Equation 2.3 into equation (2.2). These equations are commonly used in PV cell modelling and analysis to study the performance of PV cells under different operating conditions and design parameters (El-basit & Soliman, 2016).

$$I = I_{ph} - I_o.\left[exp(\frac{q.(v+IR_s)}{K.T.m}) - 1\right] - \frac{(V+IR_s)}{R_{sh}}$$ Equation 2.4

Where:

I: Represents currant source

K: Represents Boltzmann's constant

T: Represents Absolut temperature in kelvin

m: Represents Diode ideality factor it depends on the technology of the PV module.

The amount of energy produced by a photovoltaic (PV) cell is directly proportional to the amount of light it receives, as the PV cell generates electricity through the absorption of photons from sunlight (Li et al., 2021b). When more light is incident on the PV cell, it will generate a higher photocurrent,

resulting in a higher output power (Li et al., 2021a). Temperature also plays a significant role in the performance of a PV cell. The temperature affects the I-V (current-voltage) characteristics of the PV cell, which describes the relationship between the current and voltage output of the cell (Chhetri et al., 2014).

Typically, an increase in temperature leads to a decrease in the performance of a PV cell. The reverse saturation current (I_o) of the diode in the PV cell, as mentioned in the previous equations, is affected by temperature (Li et al., 2021b). As the temperature increases, the I_o of the diode generally increases, resulting in an increase in the losses and a decrease in the overall efficiency of the PV cell, Additionally, the thermal voltage (V_r) of the cell, which is calculated based on the temperature, also affects the I-V characteristics of the PV cell (Li et al., 2021a).

Therefore, both light intensity and temperature are important factors that influence the performance of a PV cell, and they need to be considered in the design, operation, and analysis of PV systems.

2.4.4. Characteristic of PV cells.

The I-V (current-voltage) and P-V (power-voltage) characteristics of a photovoltaic (PV) cell are important parameters that describe the behavior of a PV cell and provide valuable information for its performance analysis (Padmanaban et al., 2022). Figure 2.6 typically shows the I-V and P-V curves of a PV cell.
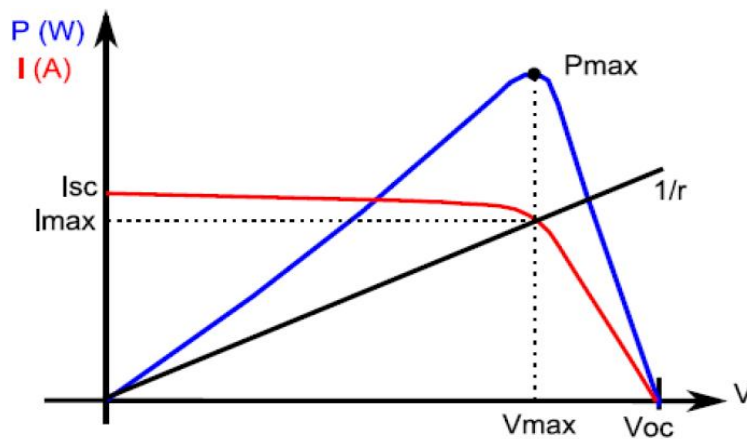
Figure 2.6: Characteristic of cells

Based on the I-V characteristic, the following four main quantities can be studied:
Short-Circuit Current (I_{sc}): This is the current that flows through the PV cell when the voltage across the terminals of the cell is zero (i.e., short-circuited) (Santhoshi et al., 2019). It represents the

maximum current that the PV cell can produce under ideal conditions (maximum sunlight intensity, optimal temperature, etc.). Open-Circuit Voltage (V_{oc}): This is the voltage across the terminals of the PV cell when the current through the cell is zero (i.e., open-circuited) (Santhoshi et al., 2019). It represents the maximum voltage that the PV cell can generate under ideal conditions.

Optimum Current (I_{opt} or I_{max}): This is the current at which the PV cell generates its maximum output power. It is usually slightly lower than the short-circuit current (I_{sc}) due to the effect of series resistance (R_s) in the cell (Ibn-Mohammed et al., 2017).

Optimum Voltage (V_{opt} or V_{max}): This is the voltage at which the PV cell generates its maximum output power. It is usually slightly lower than the open-circuit voltage (V_{oc}) due to the effect of parallel shunt resistance (R_{sh}) in the cell (Zina et al., 2017).

These quantities are important for analyzing the performance of a PV cell and optimizing the design and operation of PV systems for maximum power output (Zina et al., 2017). They can be determined experimentally or calculated from the I-V and P-V characteristics of the PV cell.

$$V_{oc} = V_T * ln(\frac{I_{ph}}{I_o} + 1)$$ Equation 2.5

Where:

$$V_T = \frac{\alpha KT}{e}$$ Equation 2.6

2.4.5. Fill factor

The fill factor (FF) of a solar cell is a measure of its efficiency in converting sunlight into electricity. It is defined as the ratio of the cell's maximum power (P_{max}) to the product of the short-circuit current (I_{sc}) and the open-circuit voltage (V_{co}) of the cell. Mathematically, it is expressed as (Sharma & Purohit, 2014):

Fill Factor (FF) = $\frac{P_{max}}{I_{sc}*V_{co}}$ Equation 2.7

The fill factor is always less than or equal to one, and the closer it is to one, the more effective the solar cell is at converting sunlight into electricity. A fill factor of 1 would mean that the solar cell is operating at its maximum possible efficiency. Efficient solar cells typically have a fill factor around 0.7, although this value may vary depending on various factors such as temperature, irradiance, and the type of solar cell technology used (Shariar & Control, 2016)(Shariar & Control, 2016).

The fill factor decreases with increasing temperature due to the impact of parasitic resistances, which cause losses in the solar cell's performance(Sharma & Purohit, 2014). The formula for fill factor allows researchers and engineers to quantify the efficiency of a solar cell and analyze the impact of parasitic resistances on its performance. By optimizing the fill factor, solar cell manufacturers can improve the overall efficiency and performance of solar panels for various applications. The energy conversion efficiency (η) of a solar cell is a measure of how effectively it converts incident solar radiation into electrical power(Sharma & Purohit, 2014). It is defined as the ratio of the maximum power output (P_{max}) of the solar cell to the power of incident solar radiation (P_i) received at the surface of the cell. Mathematically, it is expressed as:

Energy Conversion Efficiency (η) = $\frac{P_{max}}{P_i}$ Equation 2.8

The energy conversion efficiency is a key parameter for evaluating the performance of a solar cell, as it represents the percentage of incident solar energy that is converted into usable electrical power. A higher efficiency indicates a more effective solar cell that can generate more electricity from the same amount of sunlight (Ngoc et al., 2019).

Solar cell efficiency can vary depending on various factors such as the type of solar cell technology, temperature, irradiance, and spectral distribution of the incident solar radiation. State-of-the-art solar cells can achieve energy conversion efficiencies of over 40% in laboratory settings, while commercial solar panels typically have efficiencies ranging from 15% to 25% (Amelia et al., 2016).

Improving the energy conversion efficiency of solar cells is an ongoing area of research and development in the field of photovoltaics, with the aim of making solar energy more economically viable and environmentally sustainable as a renewable energy source.

2.4.6. Operation at maximum power point

The maximum power point (MPP) refers to the optimal operating point of a photovoltaic (PV) system where it generates the maximum possible power output (De Brito et al., 2013). This point is typically achieved by adjusting the voltage and current of the PV system to their optimal values, denoted as V_{opt} and I_{opt} respectively, or sometimes referred to as V_{mpp} and I_{mpp}. At the MPP, the PV system operates at the most efficient point on its current-voltage (I-V) characteristic curve (De Brito et al., 2013).

The maximum power (P_{max}) that can be obtained from a PV system at the MPP is given by the equation:

$P_{max} = V_{max} * I_{max}$ Equation 2.9

where V_{max} represents the optimal voltage and I_{max} represents the optimal current at the MPP. This point is located at the "elbow" of the I-V curve, where the PV system operates at the highest possible power output (De Brito et al., 2013).

Achieving and maintaining operation at the MPP is essential for maximizing the power output and efficiency of a PV system. This is typically done through a technique called MPPT, which involves continuously adjusting the voltage and/or current of the PV system to keep it operating at or near the MPP, even under changing environmental conditions such as varying solar irradiance and temperature. MPPT techniques are commonly used in PV systems to ensure that they operate at their optimal performance and generate the highest possible power output (Kotak & Tyagi, 2013).

2.5. Photovoltaic module

A photovoltaic module, also known as a solar panel, is a device that consists of multiple interconnected solar cells (Zina et al., 2017). Solar cells are typically made from semiconducting materials, such as silicon, which can convert sunlight directly into electricity through the photovoltaic effect (Zabihian, 2021). Other materials, such as thin-film materials like cadmium telluride or copper indium gallium selenide, can also be used in solar cells (Mohammad Bagher, 2015). The cells in a photovoltaic module are usually connected in series, parallel, or a combination of both to achieve the desired electrical characteristics (Zina et al., 2017).

2.5.1. Series Connection

Figure 2.7 shown series connection, the cells are connected one after the other, forming a chain. The positive terminal of one cell is connected to the negative terminal of the next cell, and so on. This increases the total voltage of the module while keeping the current constant. Series connection is used to increase the voltage output of the module, which is important in applications where higher voltage is required, such as grid-connected systems or systems with long cable runs (Zina et al., 2017; El-basit & Soliman, 2016).

The equation (2.10) represents the open-circuit voltage of a photovoltaic array that is formed by connecting Ns solar cells in series.

$V_{oc-Array} = V_{oc} * N_s$ Equation 2.10

Where:

$V_{oc-Array}$: represents the open-circuit voltage of the photovoltaic array, which is the voltage across the array when no current is flowing through it. It is typically measured with the array disconnected from any load.

V_{oc}: represents the open-circuit voltage of a single solar cell, which is the voltage across a single cell when no current is flowing through it. It is a characteristic parameter of the solar cell and depends on its material, design, and operating conditions.

N_s: represents the number of solar cells connected in series to form the photovoltaic array.
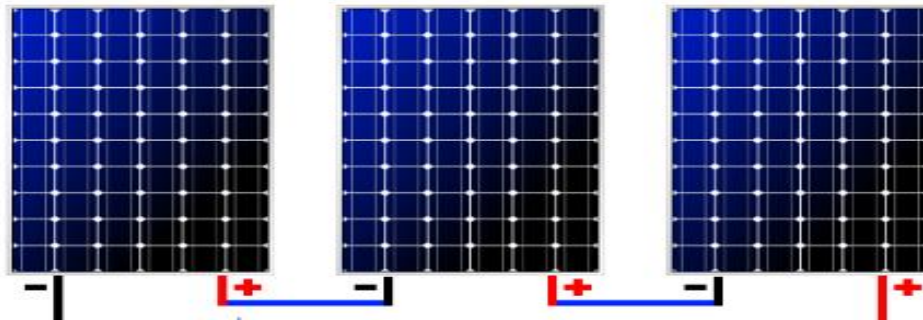
Figure 2.7: Series of module

2.5.2. Parallel Connection

Figure: 2.8 shown a parallel connection, the cells are connected side by side, with all the positive terminals connected together and all the negative terminals connected together. This keeps the voltage constant while increasing the total current output of the module (Zina et al., 2017). Parallel connection is used to increase the current output of the module, which is important in applications where higher current is required, such as off-grid systems or systems with shading issues (Zina et al., 2017; El-basit & Soliman, 2016).

The equation (2.11) represents the short-circuit current of a photovoltaic array that is formed by connecting Np solar cells in parallel.

$$I_{sc-Array} = I_{sc} * N_p$$ Equation 2.11

Where:

$I_{sc-Array}$: Represents the short-circuit current of the photovoltaic array, which is the current flowing through the array when the voltage across it is shorted to zero. It is typically measured with the array connected to a short circuit.

I_{sc}: represents the short-circuit current of a single solar cell, which is the current generated by a single cell when it is shorted to zero voltage. It is a characteristic parameter of the solar cell and depends on its material, design, and operating conditions.

N_p: Represents the number of solar cells connected in parallel to form the photovoltaic array.
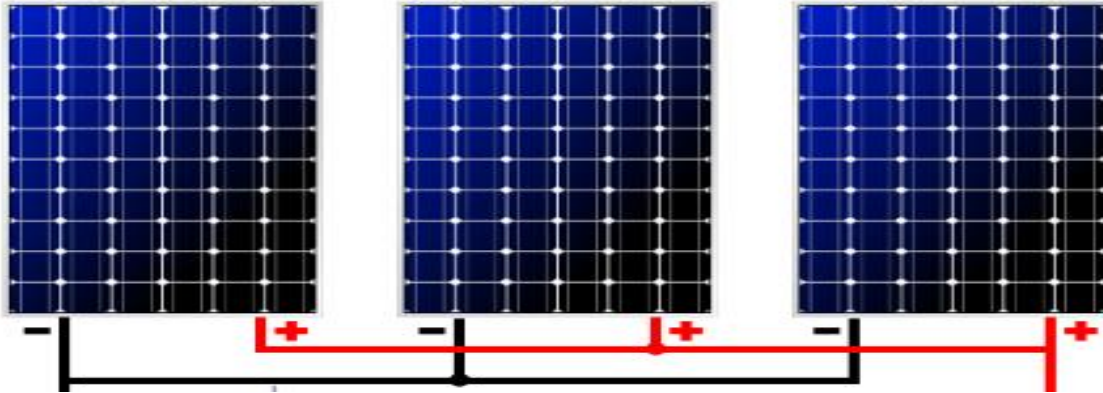
Figure 2.8: Series-parallel of module

2.5.3. Series-Parallel Connection

Some cases, a combination of series and parallel connections may be used to achieve the desired electrical characteristics. For example, multiple cells can be connected in series to form strings, and then these strings can be connected in parallel to increase both voltage and current output (Zina et al., 2017). Series-parallel connection allows for customization of the module's electrical characteristics to meet specific system requirements Figure 2.9 shown the combination Series-Parallel Connection.

The Equation 2.12 represents the total power output of a photovoltaic system or array.

$$P_{MA} = N_P * N_s * P_M$$
Equation 2.12

P_{MA}: represents the total power output of the photovoltaic system or array, which is the total amount of electrical power that can be generated by the system or array.

N_P: represents the number of photovoltaic arrays connected in parallel, which is the number of arrays that are connected side by side with their positive and negative terminals connected together to form a parallel connection. This configuration increases the current output of the system or array.

N_s: represents the number of solar cells connected in series in each photovoltaic array, which is the number of cells that are connected end to end with their positive and negative terminals connected

together to form a series connection. This configuration increases the voltage output of the system or array.

P_M: represents the power output of a single photovoltaic module or array, which is the amount of electrical power that can be generated by a single module or array under given operating conditions.

According to the equation, the total power output of the photovoltaic system or array (PMA) is equal to the product of the number of photovoltaic arrays connected in parallel (NP), the number of solar cells connected in series in each array (NS), and the power output of a single module or array (PM) (Zina et al., 2017). This equation reflects how the power output of a photovoltaic system or array can be increased by connecting multiple arrays in parallel and/or multiple cells in series, depending on the desired system configuration and performance requirements.
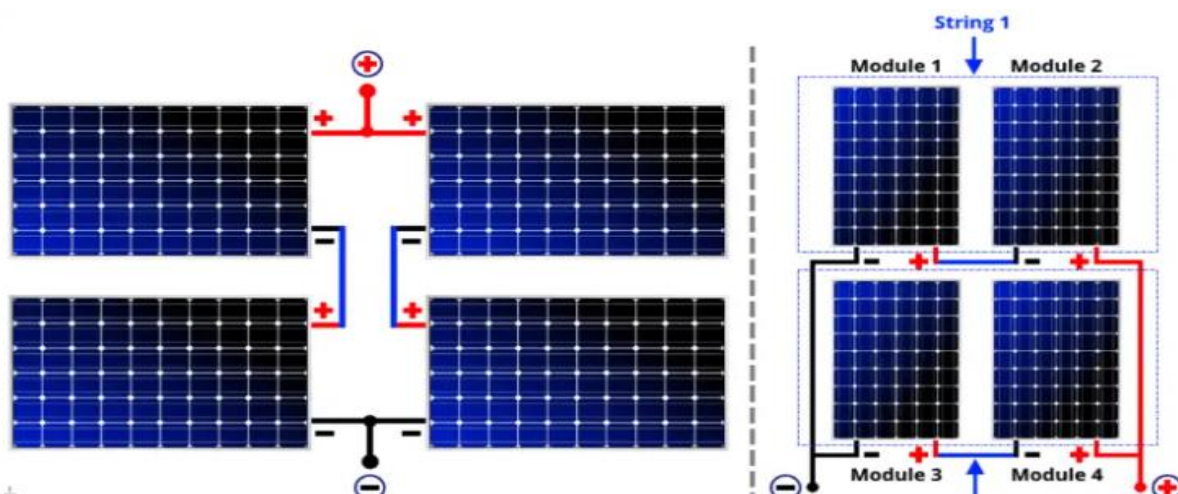
Figure 2.9: Series-parallel of module

2.6. The influence of temperature on PV modules

Temperature has a significant influence on the performance of photovoltaic (PV) modules, as the electrical properties of the semiconductor material used in PV cells are temperature sensitive. As the temperature of a PV module increases, it can cause a decrease in the overall power output of the module. This is due to several factors, including the reduction in open-circuit voltage and the change in short-circuit current (Li et al., 2021b; Li et al., 2021a).

V and P-V characteristics are graphical representations of the electrical performance of a PV module, showing the relationship between current, voltage, and power output under varying conditions. The variations in temperature can impact these characteristics, as explained in the previous response (Motahhir et al., 2018).

At higher temperatures, the open-circuit voltage tends to decrease, while the short-circuit current remains relatively unchanged (Kotak & Tyagi, 2013). This can result in a decrease in the power output of the PV module, as shown in Figure 2.10.

This reduction in power output can have a direct impact on the overall performance and efficiency of a PV system, especially in hot environments or during peak temperature periods (Dubey et al., 2013).
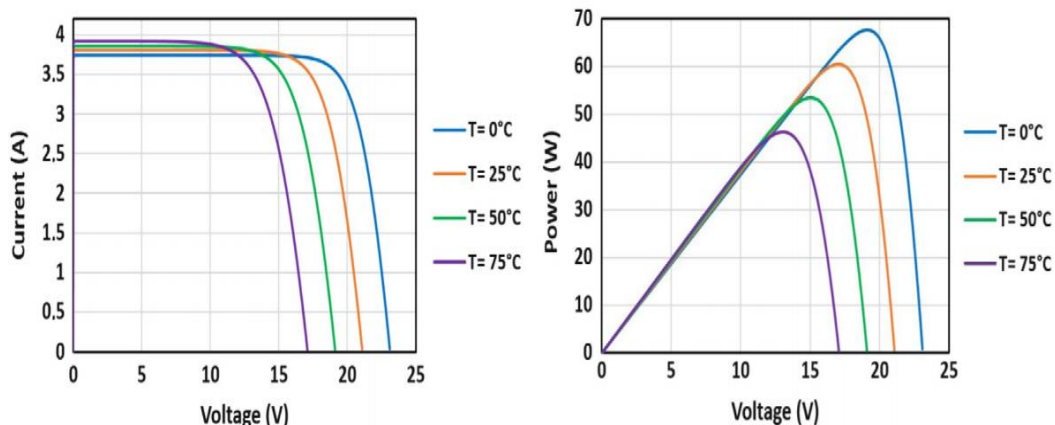
Figure 2.10: I-V and P-V characteristics of a PV module at various temperatures under constant sunlight.

Open-circuit voltage (V_{oc}) is the maximum voltage that a PV module can produce when no load is connected to it. As the temperature increases, the open-circuit voltage of a PV module tends to decrease. The rate of decrease is typically around -0.4% per degree Celsius (°C) or Kelvin (K) according to research studies (Dubey et al., 2013).

This decrease in open-circuit voltage can result in a reduction in the power output of the PV module, as the module may not be able to generate the same voltage levels needed for efficient power production.

On the other hand, short-circuit current (I_{sc}) is the maximum current that a PV module can produce when the output is shorted. The short-circuit current of a PV module is relatively less affected by temperature compared to the open-circuit voltage. It tends to vary little with temperature, according to research studies (Amelia et al., 2016).

The combined effect of the decrease in open-circuit voltage and the relatively unchanged short-circuit current with increasing temperature can result in a significant reduction in the power output of a PV module

It is important to consider the temperature effect on PV modules during system design and operation, and take appropriate measures to mitigate the impact of temperature on system performance. This may include using proper ventilation and cooling techniques, optimizing module placement and orientation, and selecting PV modules with better temperature coefficient characteristics to minimize the loss of power due to temperature.

2.7. Influence of Irradiation on PV modules

Irradiation, or the amount of light intensity incident on a PV module, has a significant influence on its performance characteristics, as described in the statement (Ibrahim et al., 2019). The short-circuit current, which is the current output of the PV module when the voltage is zero, is particularly sensitive to changes in irradiation (Ibrahim et al., 2019). It is directly proportional to the irradiation, meaning that as the irradiation increases, the short-circuit current also increases see Figure 2.11.
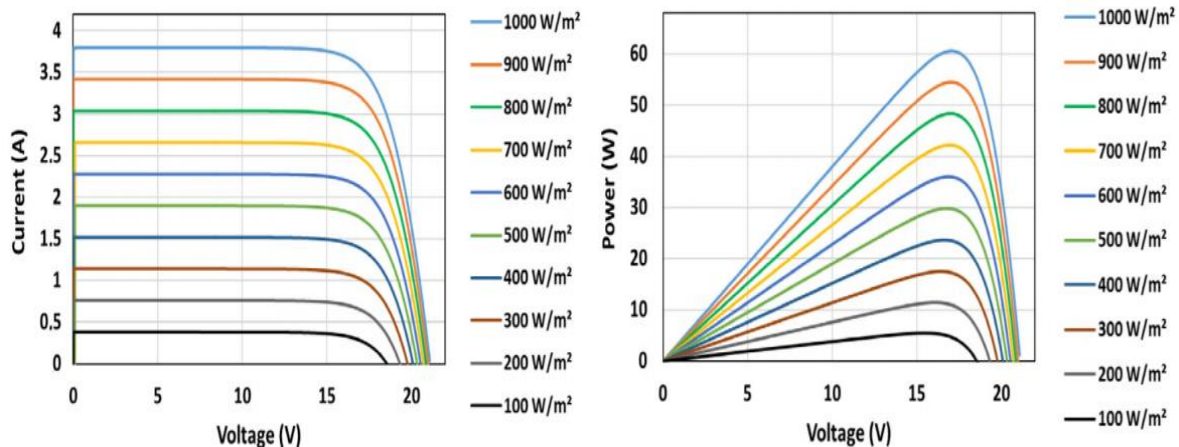
Figure 2.11: PV module I-V and P-V characteristics for various types of irradiation at a constant temperature.

The current-voltage (I-V) characteristic of a PV module is directly proportional to the incident radiation, meaning that as the irradiation increases, the current output of the module also increases, resulting in a displacement of the I-V curve along the current axis (EL Tayyan, 2013; Padmanaban et al., 2022)

This is because a higher amount of light energy leads to more electron-hole pairs being generated in the PV module, resulting in a higher current output (Ibrahim et al., 2019).

On the other hand, the open circuit voltage, which is the voltage output of the PV module when the current is zero, is only slightly affected by changes in irradiation. The open circuit voltage is

determined by the characteristics of the PV materials and the temperature, and it tends to remain relatively constant with changes in irradiation (Ibrahim et al., 2019).

However, despite the open circuit voltage being minimally affected, the power output of the PV module, which is the product of current and voltage, increases dramatically with increasing irradiation (Amelia et al., 2016). This is because although the increase in open circuit voltage is small, the increase in short-circuit current due to higher irradiation results in a much greater increase in power output. This is reflected in the P-V (power-voltage) characteristic of the PV module, where the maximum power point, or the point of highest power output, shifts towards higher voltages with increasing irradiation (EL Tayyan, 2013).

2.8. Types of PV systems and their main components.

There are several types of photovoltaic (PV) systems, each with its own unique characteristics and main components.

2.8.1. Off-grid PV system

Also known as standalone or isolated PV system, this type of PV system is not connected to the utility grid and is designed to provide electricity in remote or isolated areas where grid electricity is not available (Fofang & Tanyi, 2020). It typically consists of PV modules, charge controllers, batteries for energy storage, an inverter, and sometimes, a backup generator, Figure 2.12 represent off grid systems.
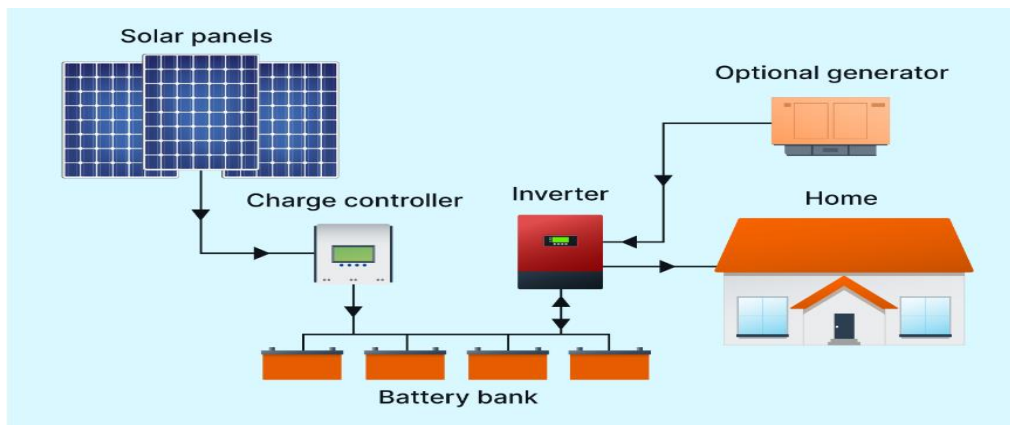
Figure 2.12: Off grid PV systems.

The PV modules generate electricity from sunlight, which is stored in batteries for later use. The charge controller regulates the charging and discharging of the batteries, and the inverter converts

the DC electricity from the batteries into AC electricity for powering electrical loads (Brunarie et al., 2009).

2.8.2. Hybrid PV system

Also known as a hybrid renewable energy system, this type of PV system combines PV technology with other renewable energy sources such as wind or hydropower, along with energy storage (Berrada & El Mrabet, 2020)e. It can be grid-connected or off-grid, depending on the application and requirements. Hybrid PV systems typically consist of PV modules, other renewable energy sources, energy storage (such as batteries), charge controllers, inverters, and sometimes, a backup generator. These systems provide flexibility in utilizing multiple renewable energy sources and energy storage to optimize power generation and consumption, Figure 2.13 represent hybrid renewable energy system.
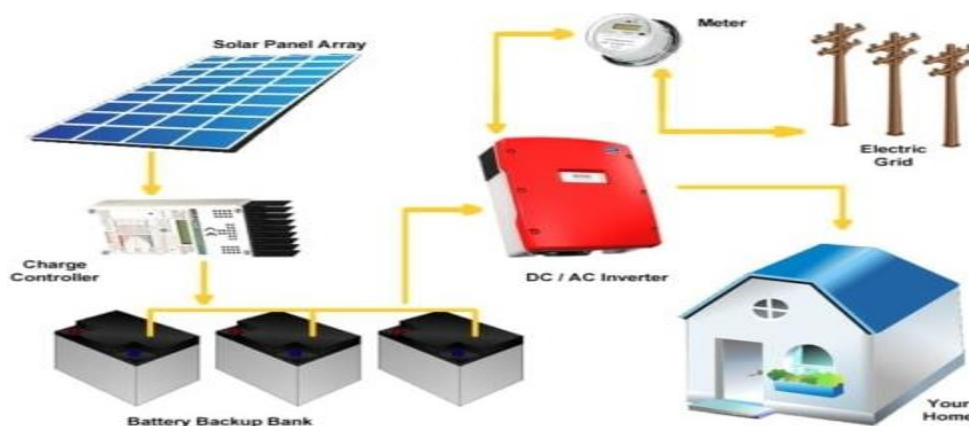
Figure 2.13: hybrid renewable energy system

2.8.3. Grid-connected PV system

Also known as grid-tied or grid-connected solar system, this type of PV system is connected to the utility grid (Argyrou et al., 2017). It typically consists of PV modules, an inverter, and sometimes, a monitoring system. The PV modules generate electricity from sunlight, and the inverter converts the DC (direct current) electricity produced by the PV modules into AC (alternating current) electricity that can be fed into the utility grid. Grid-connected PV systems are the most common type of PV system and do not require energy storage as excess electricity can be fed back into the grid and used later when needed Figure 2.14 represent grid-tied or grid-connected solar system (Singh et al., 2019).
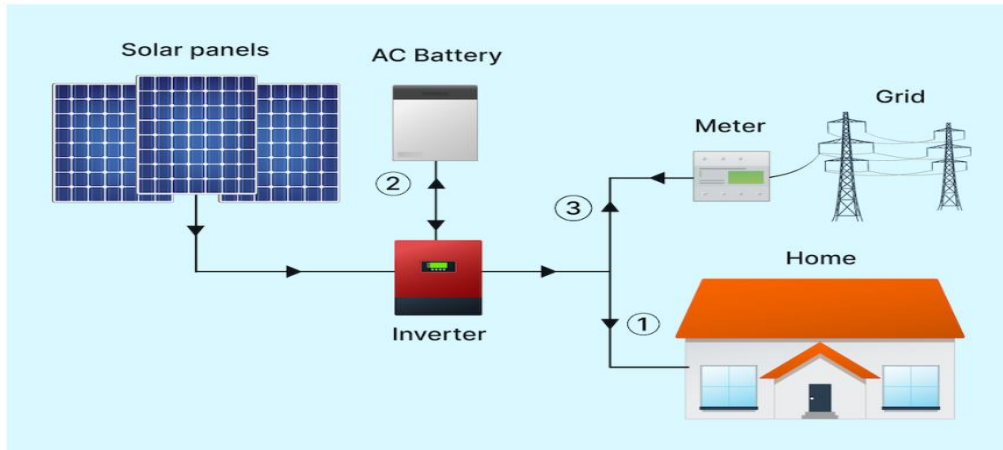
Figure 2.14: Grid connected Solar Energy System

2.9. The main components of PV systems

Photovoltaic systems are renewable energy installations that convert sunlight into electricity. They consist of several main components:

a) PV modules: These are the panels that contain PV cells, which generate electricity from sunlight.

b) Inverters: These convert the DC electricity produced by the PV modules into AC electricity that can be used to power electrical loads or fed into the grid.

c) Batteries: These are used in off-grid or hybrid PV systems for energy storage, allowing for electricity to be stored for use during periods of low sunlight or high demand.

d) Charge controllers: These regulate the charging and discharging of batteries in PV systems, preventing overcharging or over discharging and ensuring efficient battery performance.

e) Backup generators (in some cases): These are used in off-grid or hybrid PV systems as a backup power source during extended periods of low sunlight or high energy demand.

f) Monitoring systems: These provide real-time monitoring and control of the PV system, allowing for performance tracking, fault detection, and system optimization.

It's important to note that the specific components and configurations of a PV system may vary depending on the type of system, location, size, and intended application

2.10. Characteristic of a grid-connected photovoltaic system

Overall, a grid-connected PV system is a complex and sophisticated system that requires careful design and implementation to ensure optimal performance and reliability (Romero-cadaval et al.,

2013). The Figure 2.15 shown the basic grid-connected PV system's block diagram the following are some of the characteristics of a grid-connected photovoltaic (PV) system:

a) Inverter: An inverter is a crucial component of a grid-connected PV system. It converts the DC electricity generated by the PV panels into AC electricity, which is compatible with the electricity grid.

b) Power converters: The adaptation stage of a grid-connected PV system can consist of one or more power converters based on electronics. These converters are responsible for regulating the voltage and current of the PV system to match the requirements of the inverter and the electricity grid.

c) High efficiency: Due to advancements in power electronics, grid-connected PV systems can now achieve high efficiency in converting solar energy into usable electricity. This efficiency is critical for maximizing the energy output of the PV system and reducing its operating costs.

d) DC-DC converter: In some grid-connected PV systems, a DC-DC converter is used to connect the PV generator to the inverter via an intermediate DC bus system. This configuration allows for greater flexibility in controlling the voltage and current of the PV system.

e) Integration with the electricity grid: A grid-connected PV system is designed to seamlessly integrate with the electricity grid. This integration requires compliance with certain technical standards and regulations to ensure the safety and reliability of the electricity supply.
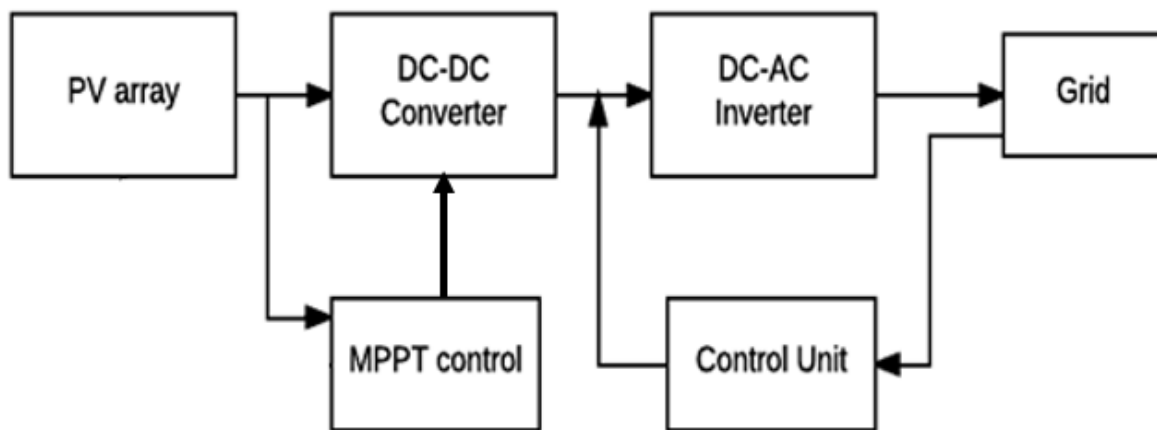
Figure 2.15: Grid-connected PV system's block diagram

2.11. DC-DC Converter characteristic

As mentioned in the description, a DC-DC converter is a power electronic device that can vary the output voltage from a DC input voltage. The converter consists of several components, including two capacitors (C1 and C2), an inductor, and a switch (controlled by GTO thyristors, bipolar transistors, or insulated gate field-effect transistors)(Kotak & Tyagi, 2013).

The DC-DC converter operates in a switching mode, where the switch is rapidly turned on and off to transfer energy from the input to the output (W. Hart Danial, 2011). During the on-time of the switch, energy is stored in the inductor, and during the off-time, the energy is released into the output (RASHID, 2001; W. Hart Danial, 2011). The two capacitors (C1 and C2) help to smooth out the output voltage, while the inductor helps to reduce the ripple current (Hart Danial, 2011).

The performance of the DC-DC converter depends on the efficiency of the components used, as well as the control strategy used to operate the switch (Fathah, 2013). In the ideal case, all components have zero resistance and zero losses, resulting in a high-efficiency converter. However, in practice, there are losses due to the resistance of the components, switching losses, and other parasitic effects (De Brito et al., 2013).

The DC-DC converter offers great flexibility in terms of output voltage regulation, and can be used in a wide range of applications such as power supplies for electronics, electric vehicles, and renewable energy systems, the schematic-diagram of DC to DC converter. The converter can also be used in combination with other power electronic devices to form complex power conversion systems (Hart Danial, 2011).

2.11.1. Types of DC-DC converters

There are several types of DC-DC converters, each with its unique characteristics and applications. Some of the commonly used types of DC-DC converters include:

a) Buck converter: A buck converter steps down the input voltage to a lower output voltage and is widely used in applications where high efficiency and low output voltage are required, such as in laptops, mobile phones, and Light Emitting diode (LED) lighting.

b) Boost converter: A boost converter steps up the input voltage to a higher output voltage and is commonly used in applications such as battery charging, electric vehicles, and solar energy systems.

c) Buck-boost converter: A buck-boost converter can either step up or step down the input voltage to match the desired output voltage and is commonly used in applications such as LED lighting, battery charging, and motor control.

d) Flyback converter: A flyback converter is a type of isolated converter that can step up or step down the input voltage and is commonly used in applications such as telecommunication, medical equipment, and industrial control.

e) Forward converter: A forward converter is a type of isolated converter that steps down the input voltage and is commonly used in high power applications such as industrial control and power supplies for servers.

2.12. Control System of Grid connected PV Systems

The control system of a grid-connected PV system is essential to ensure the safe and efficient integration of solar power into the grid. The main purpose of the control system is to maintain synchronization between the PV system and the grid by regulating the voltage, current, frequency, and phase of both sources (Tripathi & Singh, 2020).

The control structure of a PV system can be divided into two major elements: the input controller and the output controller. The input controller, also known as the maximum MPPT controller, is responsible for maximizing the power output from the PV array by controlling the boost converter (Argyrou et al., 2017). The MPPT controller continuously tracks the maximum power point of the PV array and adjusts the duty cycle of the boost converter to maintain it (Manna et al., 2023).

The output controller, on the other hand, is responsible for regulating the power output of the PV system to match the grid requirements. The output controller consists of a DC-AC inverter and an LCL filter, which convert the DC power from the PV array to AC power and filter out the harmonics (Jiang et al., 2018). The output controller performs two main functions:

a) Active and reactive power control: The output controller regulates the active and reactive power output of the PV system to match the grid requirements. The DC-link controller is used to maintain the DC voltage of the inverter, which affects the active power output, while the output voltage and frequency are regulated to control the reactive power output (Merai et al., 2019).

b) Synchronization with the grid: The output controller synchronizes the PV system with the grid by regulating the voltage, current, frequency, and phase of both sources. The synchronization

is crucial to prevent damage to the PV system and the grid and to ensure a stable power supply to the load (Yasmeena & Das, 2015).

2.13. Maximum Power Point Tracker System

The choice of control method depends on various factors such as the type of energy source, the capacity of the system, and the grid requirements. A well-designed control system is essential to ensure the safe and efficient operation of grid-connected PV systems. The output power of a PV module is affected by various factors, including solar irradiation, temperature, and shading. The MPPT is an electronic device used in PV systems to track and adjust the operating point of the PV array to ensure that it operates at its MPP under varying conditions (Manna et al., 2023).

The MPP is the point at which the PV module output power is at its maximum for a given set of conditions, such as solar irradiation and temperature. The MPPT controller continuously monitors the voltage and current of the PV array and adjusts the load impedance to ensure that the array is always operating at its MPP (Sharma & Purohit, 2014).

As mentioned, temperature has a significant impact on the output power of a PV module. Generally, the output power of a PV module decreases as its temperature increases, and vice versa (Pal & Sahay, 2018). This is due to the negative temperature coefficient of the PV module's voltage and the positive temperature coefficient of its current.

Therefore, the MPPT controller must be able to adjust the load impedance to compensate for changes in temperature and other factors to ensure that the PV array always operates at its MPP and produces the maximum possible power output (Sharma & Purohit, 2014).

2.13.1. MPPT Methods

MPPT methods have been extensively studied in the literature, and there are several approaches that differ in terms of their reliance on PV array, implementation complexity, accuracy, and cost-effectiveness. Esram and Chapman (2007) conducted a comprehensive review and analysis of 19 MPPT methods and presented a comparison of their performance characteristics in Table 2.1, (Esram & Chapman, 2007).

Similarly (De Brito et al., 2013) experimentally evaluated the performance of various MPPT methods and reported their findings in Table 2.2. These tables can be used to identify the most suitable MPPT method for a specific PV application based on the system's requirements and constraints (De Brito et al., 2013). Some of the commonly used MPPT methods include Perturb and Observe (P&O), Incremental Conductance (INC), Fractional Open Circuit Voltage (FOCV), and Fractional

Short Circuit Current (FSCC). P&O and INC are among the most widely used MPPT methods due to their simplicity, ease of implementation, and relatively low cost (Argyrou et al., 2017).

FOCV and FSCC are more accurate but require more complex hardware and may be more expensive to implement (De Brito et al., 2013).Overall, the selection of an appropriate MPPT method depends on the specific requirements and constraints of the PV system, such as the type and size of the PV array, the operating conditions, and the cost-effectiveness of the implementation.

Table 2.1: Comparison of MPPT Technique's Major Characteristics

PV Array Dependent?	True MPPT?	Analog or Digital?	Periodic Tuning	Convergence Speed	Implementation Complexity	Sensed Parameters
No	Yes	Both	No	Varies	Low	Voltage-Current
No	Yes	Digital	No	Varies	Medium	Voltage-Current
Yes	No	Both	Yes	Medium	Low	Voltage
Yes	No	Both	Yes	Medium	Medium	Current
Yes	Yes	Digital	Yes	Fast	High	Varies
Yes	Yes	Digital	Yes	Fast	High	Varies
No	Yes	Analog	No	Fast	Low	Voltage-Current
Yes	Yes	Digital	Yes	Slow	High	Voltage-Current
No	No	Both	No	Medium	Low	Voltage
No	No	Analog	No	Fast	Low	Voltage-Current
No	Yes	Digital	No	Fast	Medium	Voltage-Current
Yes	No	Digital	Yes	Slow	High	Voltage-Current
Yes	No	Digital	Yes	Fast	Medium	Irradiance
Yes	Yes	Digital	Yes	N/A	Medium	Irradiance
Yes	Yes	Both	Yes	Fast	High	Temperature
Yes	No	Both	Yes	Fast	Medium	Voltage-Current
Yes	No	Both	Yes	N/A	Low	Current
Yes	No	Digital	No	N/A	High	None
No	Yes	Digital	No	Fast	Medium	Voltage-Current

Table 2.2: Comparison of Major MPPT Technique Characteristics.

Technique	Dependency of PV Array	Tracking tractor (TF)	Implementation	Accurate?	Sensors
Dete	No	Poor	Very Simple	No	N/A
Vete	Yes	Reasonable	Simple	No	V
P&O	No	Good	Simple	Yes	V,I
IC	No	Good	Medium	Yes	V,I
Modified P&O	No	Very-Good	Complex	Yes	V,I
P&O Based On PI	No	Excellent	Medium	Yes	V,I
Modified IC	No	Very-Good	Complex	Yes	V,I
IC Based on PI	No	Excellent	Medium	Yes	V,I
Beta	Yes	Excellent	Medium	Yes	V,I
System Oscillation	Yes	Reasonable	Simple	No	V
Ripple Correlation	No	Good	Complex	Yes	V
Temperature	Yes	Very-Good	Simple	Yes	V Temperature

The Incremental Conductance (IC) and Perturb and Observe (P&O), also known as Hill Climbing method, are widely used MPPT approaches due to their simplicity, effectiveness, and independence from the PV array characteristics (Manna et al., 2023).

The IC method continuously compares the incremental conductance of the PV array with a reference conductance and adjusts the operating point to maintain maximum power output (De Brito et al., 2013). The P&O method perturbs the PV array voltage or current and measures the corresponding change in power output to determine the MPP (Ibrahim et al., 2019).

Both methods have been extensively studied in the literature and have been shown to perform well under various operating conditions. They are relatively simple to implement and do not require detailed knowledge of the PV array characteristics, making them popular choices for small-scale PV systems.

However, it's worth noting that IC and P&O methods may not always provide the optimal MPP in certain operating conditions, such as partial shading or rapidly changing irradiance levels. In such cases, more advanced MPPT algorithms, such as the Fractional Short Circuit Current (FSCC) or Model Predictive Control (MPC), may be required to achieve higher accuracy and efficiency.

Therefore, the selection of an appropriate MPPT method should be based on the specific requirements and operating conditions of the PV system to ensure optimal performance and maximum power output.

2.14. DC-link Controller and Active & Reactive Powers

According to (Jaalam et al., 2016), the DC-link controller in a grid-connected PV system typically consists of two cascaded loops: an internal current loop and an external voltage loop. The DC-link controller's primary function is to manage the DC-link voltage and control the flow of active and reactive power between the PV array and the grid, as noted by (Merai et al., 2019). The internal current loop is responsible for controlling grid current and eliminating harmonic distortion, which are crucial for ensuring high-quality power production. A proportional-integral (PI) controller is commonly used to construct the current loop, adjusting the PWM switching signals to maintain the required current waveform, as reported by (Gao & Barnes, 2016).

In contrast, the external voltage loop regulates the power flow between the PV array and the grid by regulating the DC-link voltage. A PI controller is also used to construct the voltage loop, modulating the duty cycle of the PWM signals to modify the DC-link voltage (Jaalam et al., 2016). The controller can be implemented in a variety of reference frames, including stationary, synchronous, and rotational reference frames, depending on the system's operating conditions and control objectives.

The DC-link controller is a critical component of a grid-connected PV system, as it ensures the regulation of the DC-link voltage, manages power flow, and guarantees high-quality power output with low harmonic distortion (Merai et al., 2019). To achieve optimal performance under various operating conditions, the controller can be constructed using different reference frames and PI control algorithms.

2.14.1. Natural Reference Frame (abc frame)

Figure 2.16 depicts the control structure in the abc frame. This controller's DC-link voltage (U_{dc}) controller adjusts the active current reference (I_d^*) to match the required active power. In addition, the reactive power controller establishes the reactive current reference (I_q^*). Making use of the dq to abc transformation (Krause et al., 2010), the grid voltages' phase angle (θ) is utilized to construct the three current controller references ($i_a^*,\ i_b^*\ i_d^*$). The measured currents ($i_a,\ \ i_b, i_c$) are then compared to the current references, and the error signals are supplied into three current controllers.

The current controller outputs (U_a^*, $U_b^* U_d^*$)are utilized as a reference to regulate the three-phase inverter switches(Inverters & Techniques, 2020; Yasmeena & Das, 2015; Blaabjerg et al., 2006). A Proportional Integral (PI) controller or a Proportional Resonant (PR) controller can be used to implement the current controllers. Nonlinear controllers (hysteresis or dead beta), on the other hand, are commonly utilized because of their high dynamics (Blaabjerg et al., 2006).
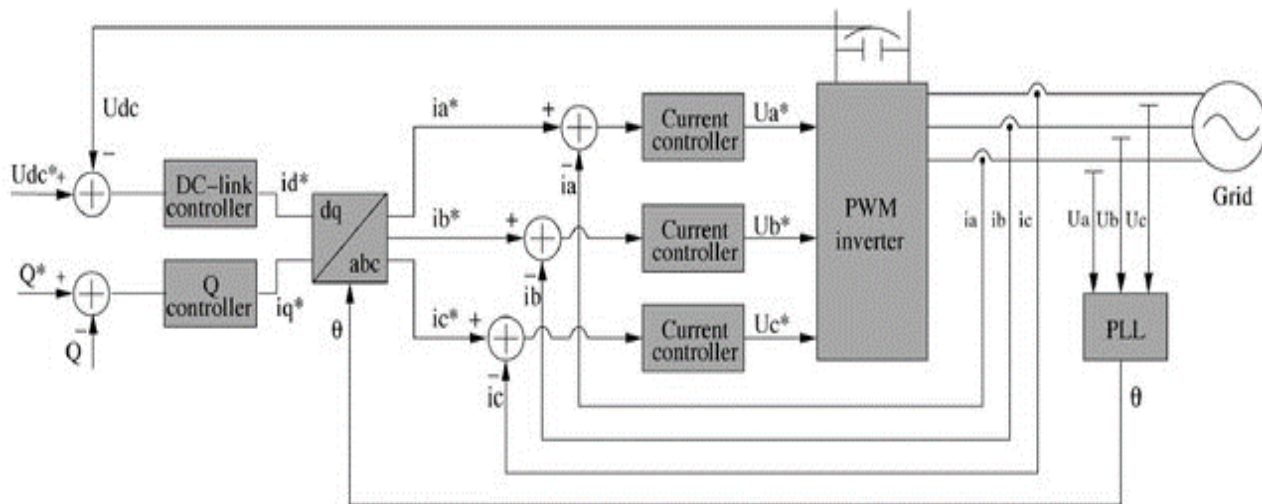
Figure 2.16: Control Structure in Natural Reference frame

2.14.2. Synchronous Reference Frame (dq frame)

Figure 2.17 depicts the control structure in the dq frame. The dc-link voltage controller generates the active current reference (I_d^*) , much like in natural reference frame control. The reactive power controller establishes the reactive current reference (I_q^*). The phase angle of the grid voltage (θ) is used to change the voltages on the grid (U_a , U_b, U_c) and grid currents (i_a, i_b, i_c) into a d_q frame that spins in synchrony with the grid voltage.

As a result, the controller variables become dc values, simplifying the design of the controller and filter. Because PI controllers work well while regulating DC variables, they are commonly used to create current controllers in the synchronous reference frame. (Inverters & Techniques, 2020; Yang et al., 2015; Jiang et al., 2018).
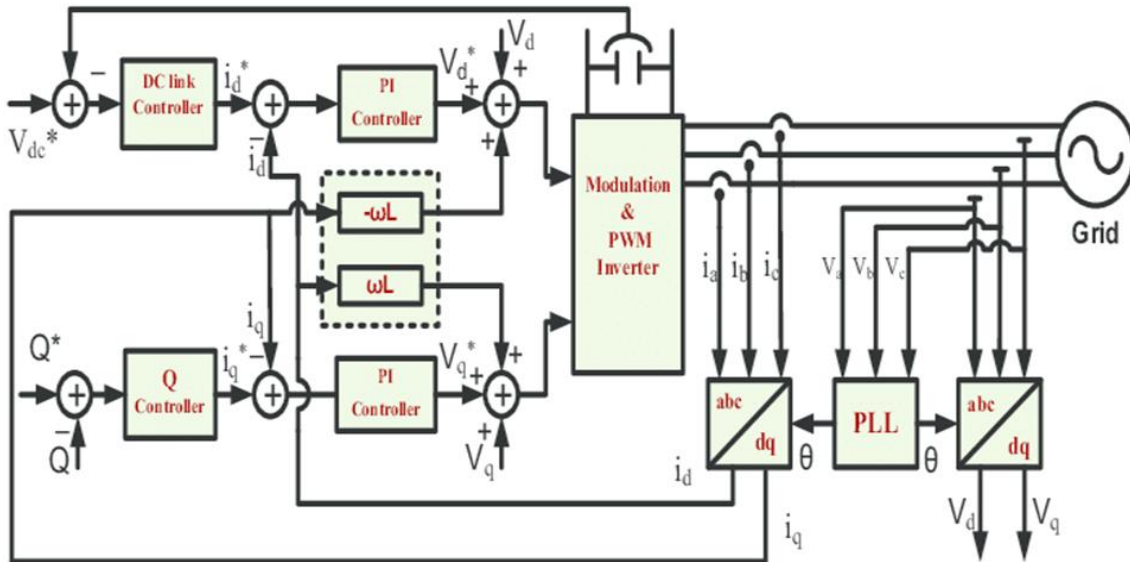
Figure 2.17: Synchronous Reference Frame Control Structure

2.14.3. Stationary Reference Frame (αβ frame)

Figure 2.18 depicts the control organization in a frame. Grid currents (i_a, i_b, i_c) are changed into $\alpha\beta$ frame (i_α, i_β) in this construction. After that, the measured values are compared to active and reactive current references. (i_α^*, i_β^*) in order to create inverter control signals. In this scenario, the current controllers are implemented utilizing PR controllers (Inverters & Techniques, 2020; Blaabjerg et al., 2006).
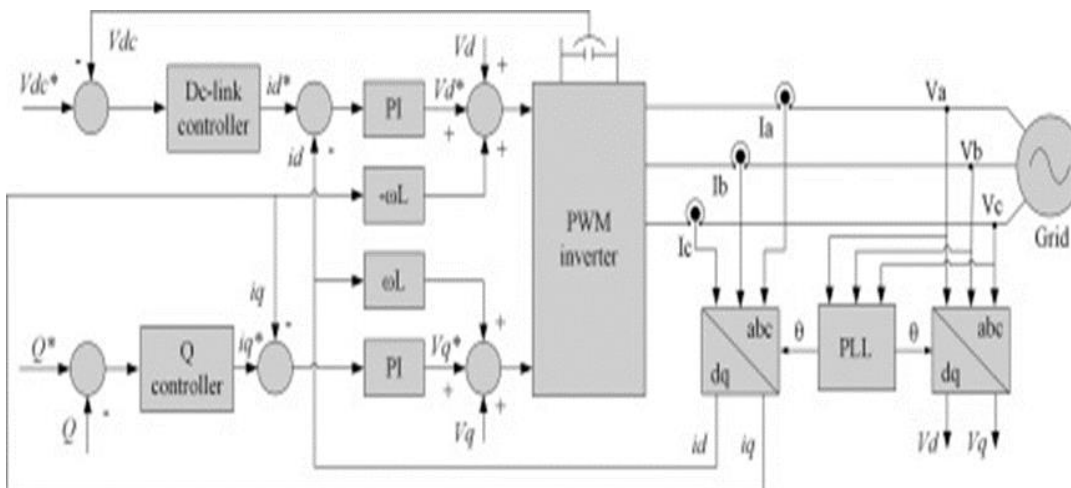
Figure 2.18: Structure of Control in a Stationary Reference Frame

2.15. Types of control algorithms

PD, PID, and PI are types of control algorithms commonly used in engineering and control systems. They are used to regulate and stabilize a system's behavior by adjusting the system's input or output. In contrast, integrating multiple energy sources involves combining different forms of renewable energy, such as solar, wind, and hydro power, to create a more reliable and efficient energy system. This integration is achieved through various methods such as hybrid systems, energy storage, and smart grids.

Hybrid systems combine different energy sources to provide a more consistent and reliable source of energy, while energy storage systems help to store excess energy generated during peak production periods for later use. Smart grids, on the other hand, use advanced technologies to manage the flow of energy between different sources and optimize energy usage (Basilio & Matos, 2002; Surya & Singh, 2019) .

So, to summarize, PD, PID, and PI are types of control algorithms used in engineering and control systems, while integrating multiple energy sources involves combining different forms of renewable energy through methods such as hybrid systems, energy storage, and smart grids.

2.15.1. The PID Controller

A PID controller is a type of feedback controller that is commonly used in industrial control systems. It combines three control modes: proportional (P), integral (I), and derivative (D) control to improve the control performance of a system (Iqbal, n.d.). The proportional control mode is responsible for generating an output signal that is proportional to the error between the desired set point and the current process variable (Basilio & Matos, 2002; Surya & Singh, 2019).

The integral control mode integrates the error over time, which helps to eliminate steady-state errors. The derivative control mode calculates the rate of change of the error, which can help to anticipate future changes in the process variable and adjust the control output accordingly. (Iqbal, n.d.). The relationship between the P, I, and D control modes is described by the time-domain PID controller equation:

$$u(t) = k_p + k_d \frac{d}{dt}e(t) + k_i \int e(t)dt \hspace{4cm} \text{Equation 2.13}$$

where u(t) is the control output at time t, e(t) is the error between the desired set point and the current process variable at time t, K_p, K_i, and Kd are the proportional, integral, and derivative gain coefficients, respectively.

By adjusting the values of these gain coefficients, the PID controller can be optimized to provide the desired control performance for a given system

The PID controller has the following transfer function:

$$K(s) = k_p + k_d s + \frac{k_i}{s}$$
Equation 2.14

The following are the controller gains for the three basic forms of control:: $(k_p, \quad k_d, k_i)$ The proportional component acts as a static controller, the derivative term accelerates system responsiveness, and the integral term reduces steady-state error (Basilio & Matos, 2002; Surya & Singh, 2019). Figure 2.19 shown the PID controller three fundamental control modes.
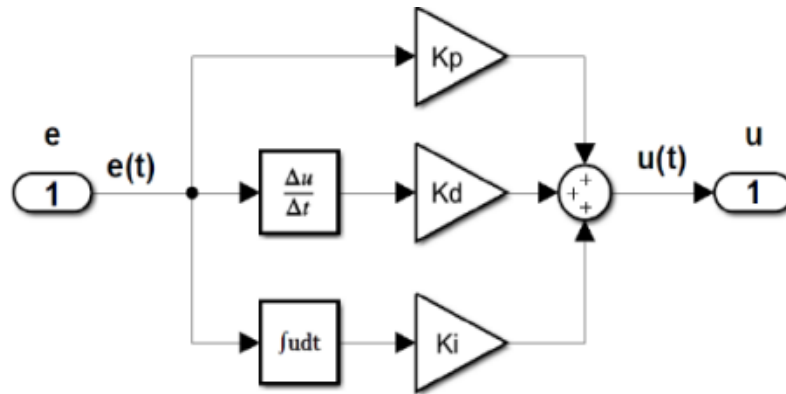
Figure 2.19: The PID controller represents three fundamental control modes

Polynomial with Closed Loop Characteristics:

Assume G(s) $=\frac{n(s)}{d(s)}$, is a closed-loop characteristic polynomial with a PID controller to minimize noise, a first-order filter may be added to the PID controller; the modified controller transfer function is as follows.

$$K(s) = k_p + \frac{k_i}{s} + \frac{k_d s}{T_f s + 1}$$
Equation 2.15

Furthermore, by combining low-pass and high-pass filters, the filter makes the controller transfer function acceptable and hence realizable. The control system design objectives may mandate the

usage of only a subset of the three main controller modes. Two prominent solutions are the proportional-derivative controller and the proportional-integral controller (Wang, 2020).

2.15.2. PD Controller
The transfer function describes a PD controller:

$$K(s) = k_p + k_d s = k_d (s + \frac{k_p}{k_d})$$ Equation 2.16

As a result, a PD controller modifies the loop transfer function with a single zero. The following is the closed-loop characteristic polynomial: The phase contribution of the PD controller rises from 0° at low frequencies to 90° at high frequencies (Basilio & Matos, 2002; Surya & Singh, 2019).

For practical purposes, a pole with a tiny time constant may be added to the PD controller. The pole helps to reduce the loop gain at high frequencies, which is good for disturbance rejection. The enhanced PD controller is described by the transfer function (Wang, 2020).

$$K(s) = k_p + \frac{k_d s}{T_{fs} + 1}$$ Equation 2.17

The modified PD controller is very similar to a first-order phase-lead controller and is used to improve the transient responsiveness of the system (Wang, 2020).

2.15.3. PI Controller
The transfer function describes a PI controller:

$$K(s) = k_p + \frac{k_i}{s} + \frac{k_p (s + \frac{k_i}{k_p})}{s}$$ Equation 2.18

As a result, the PI controller adds a pole at the origin (an integrator) and a finite zero to the feedback loop. PI controllers are frequently used in the design of servomechanisms because the presence of an integrator in the loop causes the error to a constant input to be zero in steady-state. Controller zero is frequently situated near the origin in the difficult s-plane.

A closed-loop system pole with a substantial time constant is introduced by the AA pole-zero pair. (Wang, 2020). The location of the zero point can be altered. Such that the slow mode's contribution to total system responsiveness remains negligible. The PI controller's block diagram is seen in the Figure 2.20:
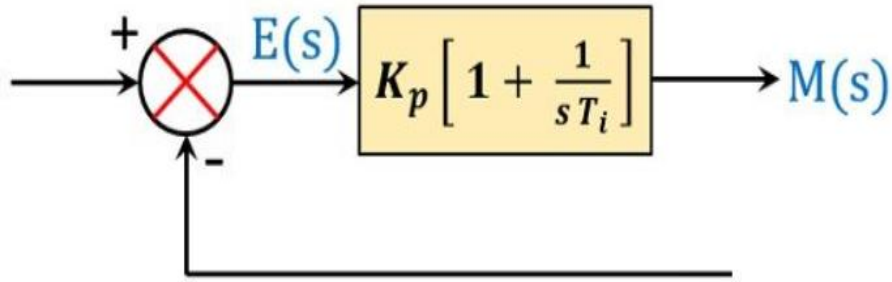
Figure 2.20: PI controller's block diagram

2.15.4. The PI-PD Controller

The PD and PI components of a PI-PD controller can be combined as follows:

K(s) = $(k_p + \frac{k_i}{s})(1 + k_d s)$ or $K(s) = (k_p + k_d s)(1 + \frac{k_i}{s})$ Equation 2.19

By adding two zeros and an integrator pole, the PI-PD controller alters the loop transfer function. The PI portion's zero may be close to the origin, whereas the PD portion's zero is placed at an optimum spot to enhance transient responsiveness. The PI-PD controller, which is similar to a regular PID controller, is described by the transfer function (Wang, 2020; Gao & Barnes, 2016):

K(s) = $k_p + k_d s + \frac{k_i}{s} = \frac{k_d s^2 + k_p s + k_i}{s}$ Equation 2.20

The PID controller improves the system's transient and steady-state performance. Furthermore, it provides stability and resilience to the closed-loop system.

2.15.5. Grid-tied Inverter

In the current control method, an inverter and a PWM switching mechanism are used to closely follow the sinusoidal reference current command (Pal & Sahay, 2018). The PWM switching mechanism is a crucial component of a grid-tied inverter, responsible for generating the desired sinusoidal current waveform and ensuring stable operation (Haider et al., 2012). The switching frequency is chosen to prevent resonance, and the modulation schemes are selected based on the system requirements and operating conditions (Chapman, 2012).

To ensure stable operation and prevent resonance, the switching frequency is typically chosen to be much higher than the resonant frequency of the system (Merai et al., 2019). The resonant frequency can be calculated using the formula:

$$f_{res} = \frac{f_{sw}}{10} \hspace{6cm} \text{Equation 2.21}$$

Where:

f_{sw}: switching frequency

f_{res}: resonance frequency

The value of f_{res} is usually kept below the fundamental frequency of the output waveform to prevent resonance and ensure stable operation (Chapman, 2012). The three-phase full-bridge inverter is a common topology used in grid-tied inverters, which can generate sinusoidal output waveforms by applying different PWM modulation schemes to the switch commands (Chapman, 2012). The modulation schemes can be selected based on the system requirements and operating conditions, such as the desired switching frequency, output voltage amplitude, and harmonic distortion level.(Haider et al., 2012).

Synchronization approaches for grid-connected series and shunt inverter. Grid-connected inverters require synchronization with the grid to ensure that the inverter output voltage and frequency are in phase and synchronized with the grid voltage and frequency. Some of the synchronization strategies that have been proposed in literature include (Singh et al., 2019):

a) Phase-Locked Loop (PLL) based synchronization
b) Adaptive Notch Filter (ANF) based synchronization
c) Instantaneous Power Theory (IPT) based synchronization
d) Vector-Based Synchronization (VBS)
e) Model Predictive Control (MPC) based synchronization

Each approach has its own advantages and limitations and the choice of synchronization strategy depends on various factors such as the type of inverter, application, and performance requirements. In this study, the PLL will be used to achieve accurate synchronization of PV systems with the grid.

2.15.6. The Phase Locked Loop (PLL)

The PLL is a widely used control system in power electronics and electrical engineering applications(Jiang et al., 2018). Its main purpose is to synchronize the output signal with the input signal, and it is commonly used to track the grid voltage signal.

The PLL uses a Voltage-controlled oscillator (VCO) to generate an output signal that matches the phase and frequency of the input signal (Gao & Barnes, 2016). The input signal is compared with the output signal using a phase detector, and the resulting error signal is filtered and used to adjust the frequency of the VCO (Izah & Prastiyanto, 2018). This process continues until the output signal is phase-locked to the input signal.

In three-phase systems, the PLL uses an inverse Park transformation to convert the three-phase network voltages into a two-dimensional reference frame (Natesan & Venkatesan, 2016). The q-axis component of this reference frame is set to zero to achieve angle synchronization with the grid voltage signal. The PLL algorithm includes three essential components: the phase detector, the loop filter, and the VCO (Izah & Prastiyanto, 2018).

The PLL is a critical component in power electronics and electrical engineering applications, and its use is essential for achieving accurate synchronization between the input and output signals. Figure 2.21 shown the basis block diagram of PLL.
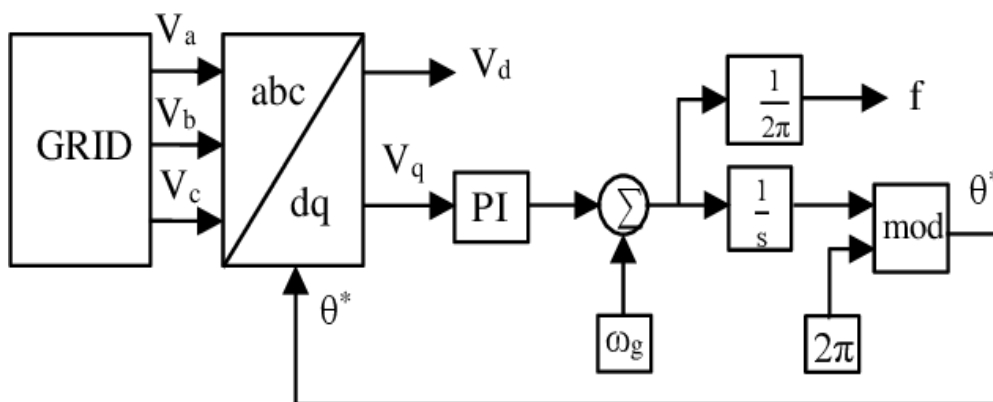
Figure 2.21: PLL basis block diagram

(Jaalam et al., 2016) provided an overview of grid-connected series and shunt inverter synchronization methodologies. These synchronization strategies are summarized in Figure 2.22.
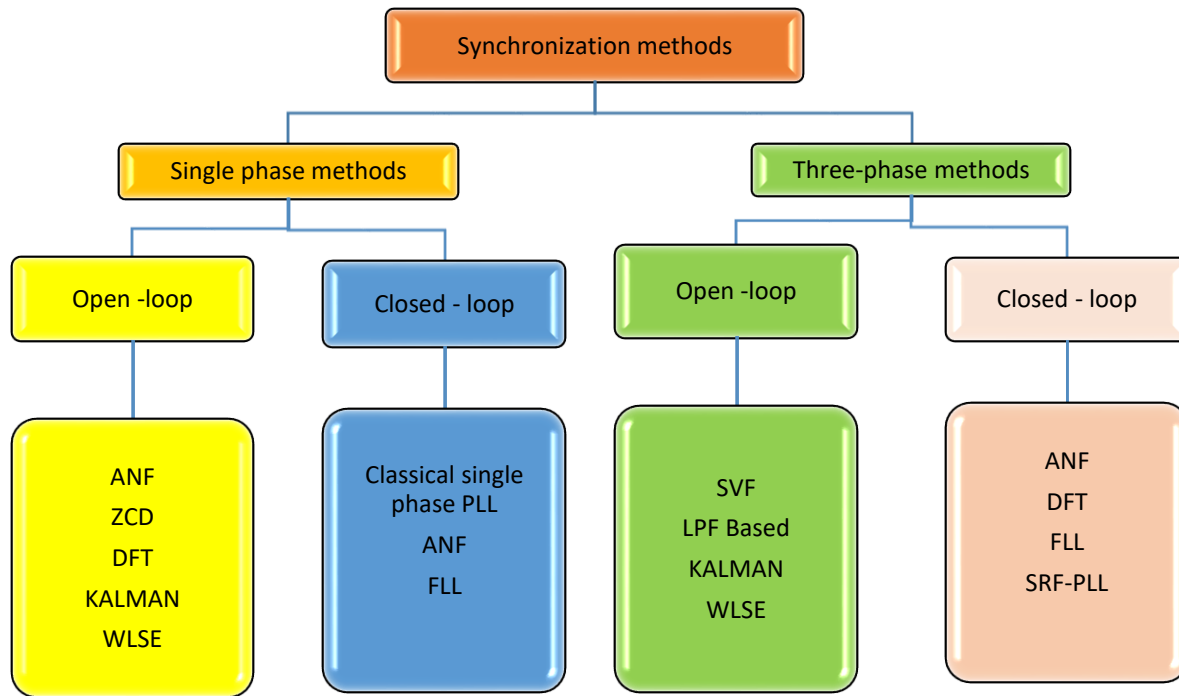
Figure 2.22: Classification of synchronization Methods

Dynamic/convergence time, accuracy, distortion rejection capabilities, noise immunity, phase and frequency adaptively, computational burden, single or three-phase usage, and structural simplicity are all factors to consider when evaluating synchronization strategies. (Jaalam et al., 2016).

2.16. PV System Grid Faults

On photovoltaic (PV) systems connected to the grid, several types of faults can be considered. Here are some examples:

a) **Symmetrical faults**

These faults occur when the fault impedance is the same for all three phases of the PV system. Symmetrical faults can include three-phase short-circuits, where all three phases are shorted to each other, or three-phase open-circuits, where all three phases are disconnected from each other (Sapountzoglou et al., 2019; Mano Raja Paul et al., 2021; Rakesh et al., 2020).

b) **Unsymmetrical faults**

These faults occur when the fault impedance is different for each of the three phases of the PV system. Unsymmetrical faults can include single-phase short-circuits or open-circuits,

where only one phase is affected while the other two phases remain normal (Sapountzoglou et al., 2019; Mano Raja Paul et al., 2021; Rakesh et al., 2020).

c) **LG (L-G) faults**

These faults occur when a line conductor comes into contact with ground, creating a fault path between one phase and ground. LG faults can cause imbalances in the system's voltage and current, and can lead to issues such as unbalanced power flow, increased losses, and potential damage to equipment (Sapountzoglou et al., 2019; Mano Raja Paul et al., 2021; Rakesh et al., 2020).

d) **LN (L-N) faults**

These faults occur when a line conductor comes into contact with another line conductor, creating a fault path between two phases. LN faults can cause imbalances in the system's voltage and current, and can result in issues such as unbalanced power flow, increased losses, and potential damage to equipment (Sapountzoglou et al., 2019; Mano Raja Paul et al., 2021; Rakesh et al., 2020).

It's important to note that fault characteristics and impacts can vary depending on the specific PV system configuration, grid integration method, fault location, and other factors. Conducting a comprehensive literature review on these different types of faults in PV systems connected to the grid can provide valuable insights into fault detection, protection, and mitigation techniques, as well as their effects on system performance and reliability (Sapountzoglou et al., 2019; Mano Raja Paul et al., 2021; Rakesh et al., 2020).

2.17. LCL filter

An LCL filter is a type of filter that is commonly used in grid-connected photovoltaic systems to reduce the amount of harmonic distortion and ripple current in the output waveform of the inverter (Saïd-Romdhane et al., 2016). The LCL filter is typically used in combination with the inverter to convert the DC output of the PV panels into AC power that can be fed into the electrical grid.

The LCL filter consists of three components: an inductor, a capacitor, and another inductor, arranged in an L-C-L configuration. The first inductor is connected in series with the output of the inverter, while the capacitor is connected in parallel with the load (Saïd-Romdhane et al., 2016).

The second inductor is connected in series with the load. The values of the inductors and capacitor are selected to achieve a specific cutoff frequency that will filter out the unwanted harmonics.

The LCL filter is preferred over other types of filters because it provides better attenuation of the harmonic distortion and ripple current while also minimizing the voltage drop across the filter. This is important because voltage drop can reduce the efficiency of the PV system (Saïd-Romdhane et al., 2016).

2.18. Advantages and disadvantages of photovoltaic energy

There are numerous advantages and disadvantages associated with photovoltaic energy. The following outlines both the positive and negative aspects of this form of energy production:

2.18.1. The main advantages of PV

There are several advantages of using PV energy:

1. Renewable and sustainable: Solar energy is a renewable and sustainable source of energy that does not rely on finite resources such as coal, oil, or natural gas. As long as the sun shines, solar panels can generate electricity (James, 2021).

2. Environmentally friendly: Solar energy is a clean and green source of energy that does not produce harmful greenhouse gases or pollutants. It helps to reduce the carbon footprint and mitigate the effects of climate change (James, 2021).

3. Low maintenance: PV systems require very little maintenance, as there are no moving parts that can break down or wear out. The panels only need to be cleaned periodically to ensure optimal performance (James, 2021).

4. Energy independence: PV systems can provide energy independence and security, especially in remote or off-grid locations. They can also reduce reliance on foreign oil and other fossil fuels (James, 2021).

5. Cost-effective: The cost of PV systems has decreased significantly over the years, making it a more cost-effective option for generating electricity, especially in areas with high electricity costs or unreliable grid infrastructure (Villegas Aguilar, 2018).

6. Modular and scalable: PV systems are modular and may be scaled up or down based on energy requirements. As a result, they are appropriate for a wide range of applications, from residential to commercial and industrial (Villegas Aguilar, 2018).

2.18.2. The disadvantages of PV

While photovoltaic (PV) energy is a promising source of renewable energy, it also has a number of disadvantages. Some of the main disadvantages of PV energy include:

1. Intermittency: The amount of energy produced by a solar panel depends on the amount of sunlight it receives. This means that the amount of energy produced by PV systems can vary significantly from day to day and season to season, making it difficult to rely on as a consistent source of power (Villegas Aguilar, 2018).

2. Cost: While the cost of PV panels has come down dramatically in recent years, the initial cost of building a PV system can still be rather expensive. Furthermore, the expense of maintaining and repairing a PV system might be substantial. (Villegas Aguilar, 2018).

3. Land use: Large-scale PV systems require significant amounts of land to install, which can be a challenge in densely populated areas or in areas where land is already in short supply (James, 2021).

4. Environmental impact: The production and disposal of PV panels can have environmental impacts, including greenhouse gas emissions and the release of toxic materials (James, 2021).

5. Performance degradation: PV panels can experience a decrease in performance over time due to a variety of factors, including weathering and physical damage (Villegas Aguilar, 2018).

6. Energy storage: PV systems require energy storage solutions in order to provide power when sunlight is not available. However, energy storage systems can be expensive and may require additional land use (Villegas Aguilar, 2018).

7. Geographic limitations: PV systems may not be suitable for all geographic locations, as they require a certain amount of sunlight to generate power effectively. This means that some areas may not be able to fully rely on PV energy as a primary source of power.

2.19. Simulation tools and real time simulator

Simulation tools like MATLAB/Simulink and real-time simulators like Typhoon HIL play an important role in the design, testing, and validation of complex electrical systems and components. MATLAB/Simulink provides an environment for engineers to simulate and analyze the behavior of electrical systems and components. It offers a range of building blocks for simulating various components and systems, and engineers can design their own custom blocks as needed. With MATLAB/Simulink, engineers can simulate multi-domain systems, incorporate temperature and attitudinal effects, and instantly see the outcomes of their simulations.

On the other hand, real-time simulators like Typhoon HIL offer a hardware-based approach to simulation and testing. These simulators can run complex, real-time simulations of micro grid and power electronics control systems. Typhoon HIL uses patented numerical methods, ultra-low latency processors, and specialized software architecture to achieve high-fidelity simulation results. Engineers in various industries can use HIL solutions to speed up time to market, reduce testing costs, and improve the quality and reliability of their products. Simulation tools and real-time simulators are essential for engineers working on complex electrical systems and components.

These tools help engineers design and test their systems before they are implemented, which can lead to cost savings and improved system performance. We used both MATLAB/Simulink and Typhoon HIL for the project. With these tools, you can design and simulate your electrical systems and components, as well as test and validate their performance in real-time. By using simulation tools and real-time simulators, we can identify potential issues and optimize the design before implementing it, which can save time and money in the long run and the result will be discussing.

2.20. Summary

In this chapter, the fundamentals of grid-connected photovoltaic (PV) systems and the worldwide status of photovoltaic energy were examined. Solar energy and the construction of photovoltaic cells, as well as the properties of photovoltaic modules, were deliberated. The impacts of temperature and irradiance on the performance of PV modules were considered. Furthermore, various types of PV systems and their constituent elements were investigated, leading to an analysis of the attributes of a grid-connected photovoltaic system.

The chapter then delved into the control systems used in grid-connected PV systems, including MPPT, DC-link controller, and active and reactive powers. We also discussed the integration method and synchronization approaches for grid-connected series and shunt inverter applications. Other topics covered include PV system grid faults, the LCL filter, and the advantages and disadvantages of photovoltaic energy.

Finally, we looked at simulation tools and real-time simulators, with the next chapter set to cover mathematics modeling and design methodologies. Overall, this chapter provided a comprehensive introduction to grid-connected PV systems and the factors that affect their performance, laying the foundation for further understanding of the mathematical modeling and design methodologies necessary for their optimal operation.

CHAPTER THREE: MODELING OF GRID-CONNECTED PV SYSTEMS

3.1. Introduction

By directly converting the radiation from solar cells, or cells, an electronic device, photovoltaic energy is produced. It is a power generator consequently; a photovoltaic panel's module is made up of a collection of several cells (Yasmeena & Das, 2015). The amount of sunlight and the surrounding temperature affect the PV panel's power (Motahhir et al., 2018). Depending on the demands of the consumer, the energy produced can go through various transformations (mechanical, luminous, chemical). In fact, in order to supply a load, one must use a device acting as an interface that allows one to modify (transform) the features of the source in order to ensure that it operates properly (and to introduce transfer adjustment means of energy) (Berrada & El Mrabet, 2020). This chapter will look at the solar generator, how physical factors (such temperature and light) and electrical phenomena affect these functions, as well as DC-DC converters.

This Chapter delves into the development and analysis of mathematical models for various components and subsystems within a grid-connected solar energy system. The chapter begins with an exploration of the modelling and simulation of photovoltaic generators and their performance. Additionally, the influence of temperature and irradiance on solar cells is examined through simulations, highlighting the importance of considering these factors in the design and optimization of solar energy systems. Subsequently, the chapter focuses on modelling and simulating DC-DC converters, specifically boost converters, which play a crucial role in the power conditioning stage of the system. Finally, the chapter investigates the association and interaction between photovoltaic panels, boost converters, and interleaved chopper systems, with an emphasis on the impact of temperature and illuminance variations.

3.2. Modelling of a photovoltaic generator

The principal component within a solar energy generation system is the photovoltaic generator. The operation of a photovoltaic generator closely resembles that of a current source modulated by a diode. Its inherent nonlinearity is effectively characterized through several mathematical models. This study, in particular, places its focus on the five-parameter models, illustrated in the electrical circuit depicted in Figure 3.1.

These models function as follows: for an individual PV cell, they portray the conventional single-diode concept of a PV generator; and when applied to a solitary module, they present PV as an aggregation of identical cells interconnected in a series-parallel configuration.
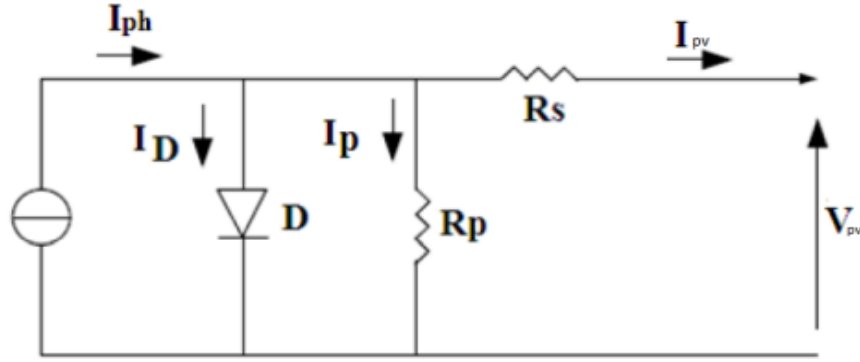
Figure 3.1: PV electrical circuit

Kirchhoff's law is used to derive the following characteristic equation. (Zina et al., 2017; Salah, 2019) (El-basit & Soliman, 2016).

$$I_{pv} = I_{ph} - I_D - I_p \qquad\qquad \text{Equation 3.1}$$

The currents I_{ph}, I_D and I_p are illustrated by the relationships.

$$I_{ph} = I_{Sc} + (K_i(T - T_n)) \cdot \frac{G}{G_o} \qquad\qquad \text{Equation 3.2}$$

The relationships express saturation current:

$$I_o = I_{rs} \cdot \left(\frac{T}{T_n}\right)^3 \cdot \left[exp^{\frac{q.E_{go} \cdot \left(\frac{1}{T_n} - \frac{1}{T_s}\right)}{n.K}}\right] \qquad\qquad \text{Equation 3.3}$$

The following expression can be used to get the reverse saturation current:

$$I_{rs} = \frac{I_{sc.}}{e^{\left(\frac{q.V_{oc}}{n..k.T.N_s}\right)} - 1} \qquad\qquad \text{Equation 3.4}$$

The current through the shunt resistor is calculated using this equation:

$$I_{Sh} = \frac{V + R_{s.}.I}{R_{sh}} \qquad\qquad \text{Equation 3.5}$$

We obtain the output current by changing Equation 3.1 with Equations 3.3, 3.4, and 3.5:

$$I = I_{ph} - \left[exp\left(\frac{q.(V + R_{s.}.I)}{n.K..T.N_s}\right) - 1\right] - I_{Sh} \qquad\qquad \text{Equation 3.6}$$

Where:

I_{pv}: Current generated by the photovoltaic cell.

I: The current circulating in the resistor R_s is also the current I_{pv}.

I_o: Saturation current

I_D: The current flows through the diode.

I_{ph}: Photon current

I_p: The current flowing through the shunt resistance R_P

K_i: Coefficient of cell temperature.

T_{oc}: Cell operating temperature.

I_{Scn}: Nominal short-circuit current of the cubicle.

G_o: Illuminance for STC (the standard test conditions used in this project are 1000).

T_r: Reference temperature [K].

G: Irradiance.

T_n: Nominal operating temperature of the cell which is given by the manufacturer (datasheet).

I_S: Diode saturation current.

I_{Sc}: The short-circuit current of the cells.

E_g: Threshold energy.

q: Elementary electric charge ($1.6x10^{-19}C$).

A: Diode power factor.

K: Boltzmann constant ($1.381x10^{-23}$ J/K).

N_S: Number of cells in series per module.

M_S: Number of modules in series.

R_s: Series resistance of the cell.

R_p: Cell shunt resistance.

3.3. Modelling of DC-DC Boost converter

The boost converter, also referred to as a step-up converter, is illustrated in Figure 3.2. This type of power converter is recognized for its capability to produce an output voltage greater than the input voltage. It comprises four primary components: an inductor, a power electronic switch such as an Insulated-gate bipolar transistor (IGBT), a diode, and a capacitor. The operation of the boost converter is controlled using Pulse Width Modulation (PWM). (Manna et al., 2023).

Give thorough explanations of the Boost converter and PWM. PWM controls the Boost converter by flicking the switch on and off at a high frequency (referred to as the switching frequency) (Fathah, 2013; Pal & Sahay, 2018). For continuous current conduction, the relationship between the input voltage and the output voltage is described as follows.

$$V_{o=} \frac{V_{pv}}{1-D}$$ Equation 3.7
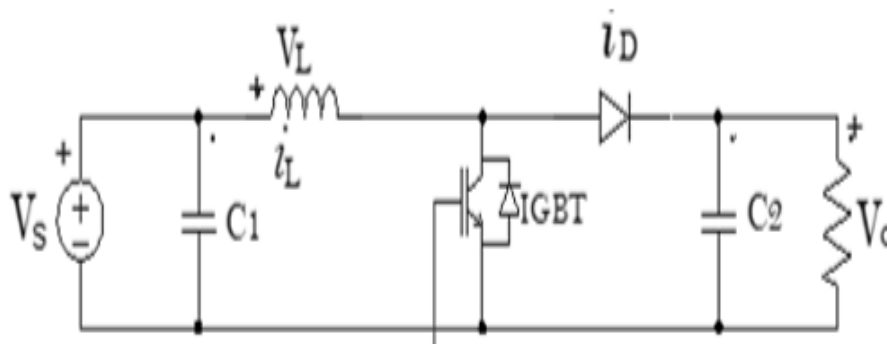
Figure 3.2: Boost convertor control

Where D is the duty cycle, which is equal to the percentage of time the switch is ON and has values ranging from 0 to 1; that is, Vo is the boost output voltage, Vpv is the PV array output voltage, and so on.

$$V_{o=} \frac{T_{ON}}{T_{ON}-T_{OFF}}$$ Equation 3.8

3.4. Function of Boost converter

The boost converter's function is to change the input voltage into a greater output value. A boost chopper's block diagram is shown in Figure 3.3 (W. Hart Danial, 2011).
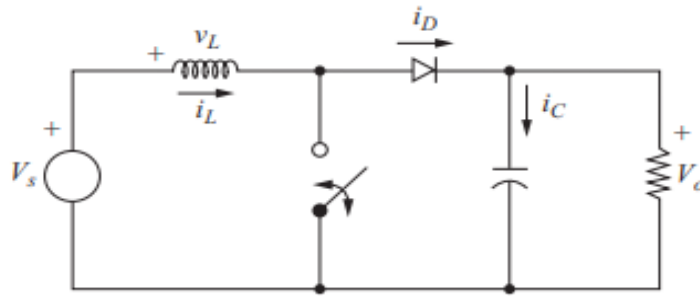
Figure 3.3: Boost Equivalent circuit diagram.

To study this diagram, we must make the representation of the equivalent circuit for the two states of the switch (open and closed) and then draw the mathematical model linking the input/output variables Figure 3.4 shown the one circuit of boost converter when switch is on (W. Hart Danial, 2011). The diode is biased in the opposite way when the switch is closed.
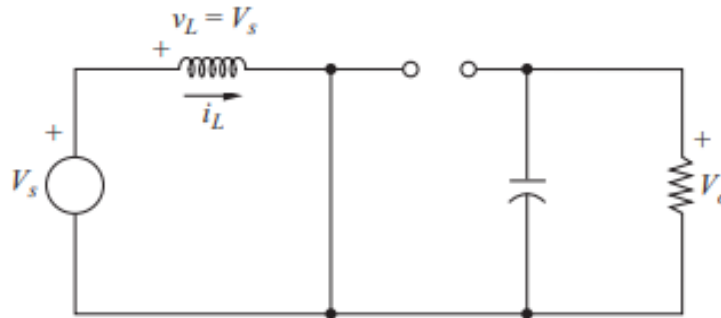
Figure 3.4: Equivalent diagram Boost converter circuit when switch is on.

$$v_L = V_S = L\frac{di_L}{dt} \quad or \quad = \frac{di_L}{dt} = \frac{V_L}{L}$$ Equation 3.9

The corrected inductor current is computed by

$$\frac{\Delta i_L}{\Delta t} = \frac{\Delta i_L}{DT} = \frac{V_S}{L}$$

Solving for Δi_L for the switch closed,

$$(\Delta i_L)_{closed} = \frac{V_S DT}{L}$$ Equation 3.10

For the route created by the source, inductor, and closed switch, Kirchhoff's voltage law is applicable. As seen in Figure 3.5, when the switch is closed, the current increases linearly since its rate of change is constant (W. Hart Danial, 2011).
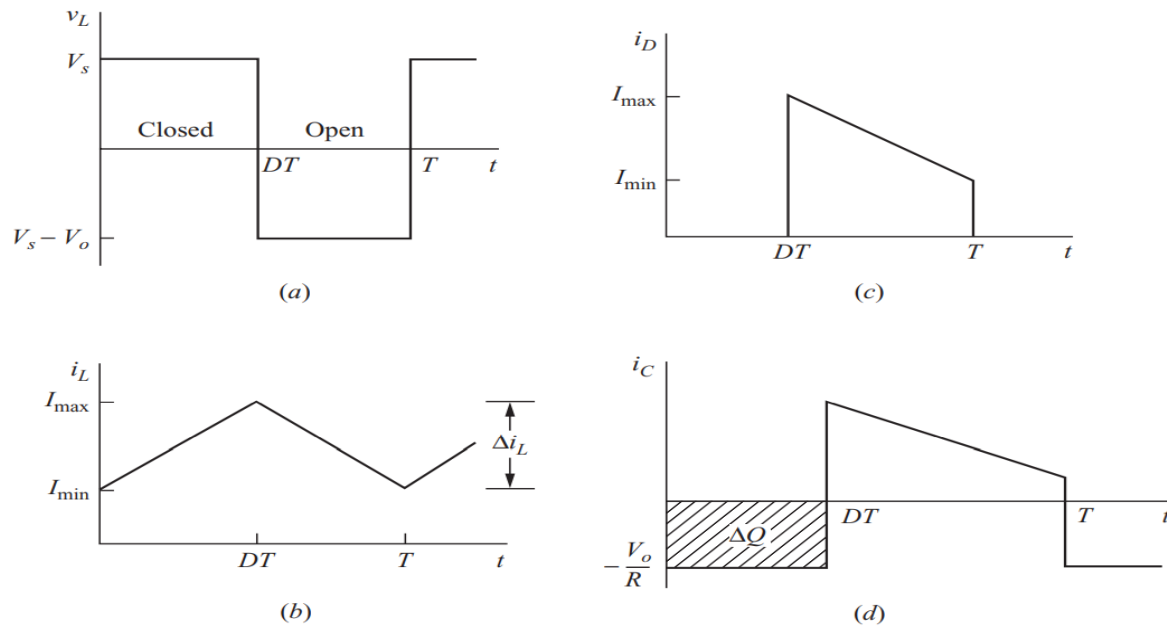
Figure 3.5: Boost converter waveforms. (a) Inductor voltage; (b) Inductor current; (c) Diode current; (d) Capacitor current

Examination of the Off Switch: Yet, when the switch is opened for a period of time, $(1 - \alpha)$. T_S, the stored energy in the coil is dissipated and controls the flow of current in the Wheel diode free D. Figure 3.6 (Hart Danial, 2011), illustrates this operation:
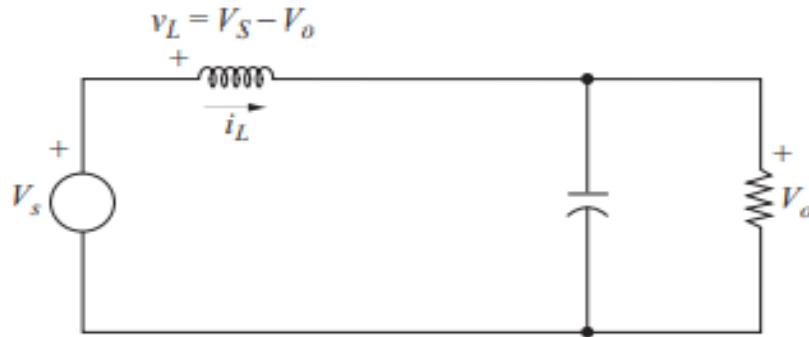
Figure 3.6: Equivalent diagram of a boost convertor when Swish off .

The voltage across the inductor, supposing a constant output voltageV_o, is as follows (W. Hart Danial, 2011):

$$v_L = V_S - V_o = L * \frac{di_L}{dt}$$

$$\frac{di_L}{dt} = \frac{V_S - V_o}{L}$$

54

Since the inductor current's rate of change is constant, the current must vary linearly while the switch is open. When the switch is open, the inductor current fluctuates as follows (W. Hart Danial, 2011):

$$\frac{\Delta i_L}{\Delta t} = \frac{\Delta i_L}{(1-D)T} = \frac{V_S - V_o}{L}$$

Solve Δi_L,

$$(\Delta i_L)_{Open} = \frac{(V_S - V_o)(1-D)T}{L} \qquad \text{Equation 3.11}$$

The net change in inductor current must be zero for steady-state functioning Equation 3.10 and Equation 3.11 *(W. Hart Danial, 2011)*:

$$(\Delta i_L)_{Open} + (\Delta i_L)_{closed} = 0$$

$$\frac{V_S DT}{L} + \frac{(V_S - V_o)(1-D)T}{L} \qquad \text{Equation 3.12}$$

Solve V_o $\qquad V_S * (D + 1 - D) - V_o * (1 - D) = 0$

$$V_o = \frac{V_S DT}{1-D}$$

Additionally, for periodic operation, the average inductor voltage must be zero. Calculating the typical inductor voltage

$$V_L = V_S D + (V_S - V_o)(1 - D) = 0$$

Knowing that the average power given by the source must equal the average power absorbed by the load resistor allows one to determine the average current in the inductor.

The power output is $\quad P_o = \frac{V_o^2}{R} = V_o I_o$

And input power is $V_S I_S = V_S I_L$. Using Equation 3.12, to calculate input and output powers.

$$V_S I_L = \frac{V_o^2}{R} = \frac{[\frac{V_S}{1-D}]^2}{R} = \frac{V_S^2}{(1-D)^2 R}$$

IL can be expressed by solving for the average inductor current and making various substitutes.

$$I_L = \frac{V_S}{(1-D)^2 R} = \frac{V_o^2}{V_S R} = \frac{V_o I_o}{V_S} \qquad \text{Equation 3.13}$$

The average value and current change from Equation (3.10) are used to compute the maximum and minimum inductor currents

$$I_{max} = I_L + \frac{\Delta i_L}{2} = \frac{V_S}{(1-D)^2 R} + \frac{V_S DT}{2L}$$

Equation 3.14

$$I_{min} = I_L - \frac{\Delta i_L}{2} = \frac{V_S}{(1-D)^2 R} - \frac{V_S DT}{2L}$$

Equation 3.15

In the boost converter, the minimal inductance and switching frequency combination for continuous current is as follows:

$$L_{min} = \frac{D(1-D)^2 R}{2f}$$

Equation 3.16

In a boost converter intended for continuous-current operation, an inductor value greater than v_{Lmin} will be employed. It is useful in terms of design to express L in terms of a desired Δi_L.

$$L = \frac{V_S DT}{\Delta i_L} = \frac{V_S D}{\Delta i_L f}$$

Equation 317

The capacitor current waveform, given in Figure 3.5d, may be used to compute the peak-to-peak output voltage ripple *W. Hart Danial, 2011*. The capacitor charge change may be computed using:

$$\frac{\Delta V_o}{V_o} = \frac{D}{RCf}$$

Equation 3.18

f denotes the switching frequency Capacitance can also be described as a function of the output voltage ripple.

$$C = \frac{D}{R\left(\frac{\Delta V_o}{V_o}\right)f}$$

Equation 3.19

3.5. Control Methods for boost converter

PV's current-voltage (I-V) characteristic is affected by irradiance and temperature. The photovoltaic output voltage is affected by temperature, whereas the photovoltaic output current is affected by sun irradiation. Because it has a maximum value Power Point, the array operates at maximum efficiency; it is based on the impedance matching idea. When the source impedance equals the load impedance, the circuit's output power is maximized. The MPPT algorithm achieves impedance

56

matching by altering the DC-DC converter's duty cycle D (Manna et al., 2023). The expression is linked to input output impedance.

$$R_{in} = (1 - D^2)\, R_{Load}$$ Equation 3.20

Where D stands for duty cycle, R_{in} stands for PV impedance, and R_{Load} stands for load impedance. The proposed MPPT method has two operating regions: MPP ($P_{PV} > \beta \cdot P_{MPP}$) and non-MPP ($P_{PV} < \beta \cdot P_{MPP}$) as shown in Figure 3.7, where β is an MPP region coefficient. Starting with VPV = VOC, the operating point swiftly shifts toward the MPP (VMPP, PMPP). ΔP_{PV} and ΔV_{PV} are used to determine the operating point's direction, where β is the difference between the current and past values. In order to calculate the MPP, the current PPV is compared to the PMPP (Fathah, 2013).
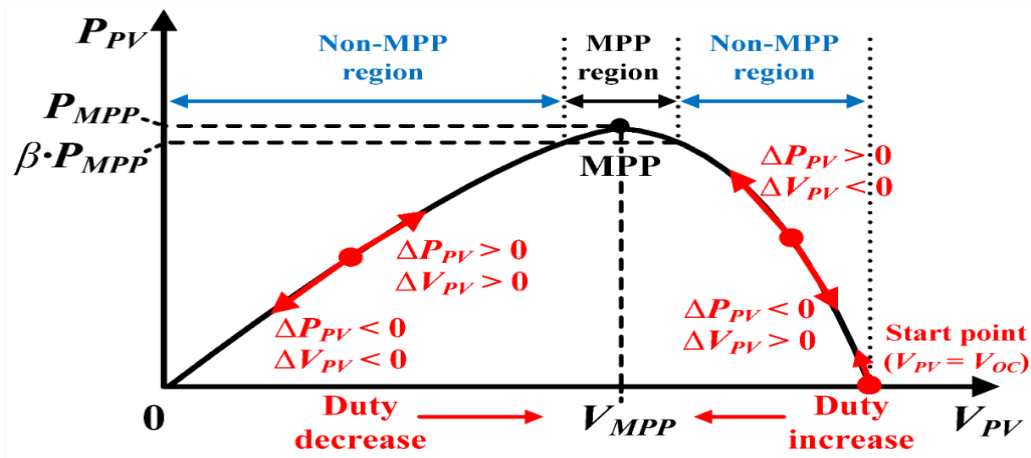
Figure 3.7: The suggested MPPT algorithm's operating principle

The P&O algorithm is used for MPPT in this text. The reference voltage is disrupted in this manner, and the direction of the next disturbance is established by analyzing the system reaction. The reference voltage is altered in the direction that the power should grow.

The control circuitry consists of two PI controllers with integral gains of 100 and time constants of 0.1. The reference voltage is sent into the first PI controller, which manages voltage and shifts the PV system voltage in the direction of the MPPT voltage. Following that, a second PI controller acts as a current controller, directing the system current in the direction of the MPPT current (Esram & Chapman, 2007). The comparator receives the output of the control loops and generates PWM to drive the boost converter to guarantee that the system operates at the stated maximum power point. The MPPT follow-up flowchart utilizing the P&O approach is shown in the Figure 3.8.

57
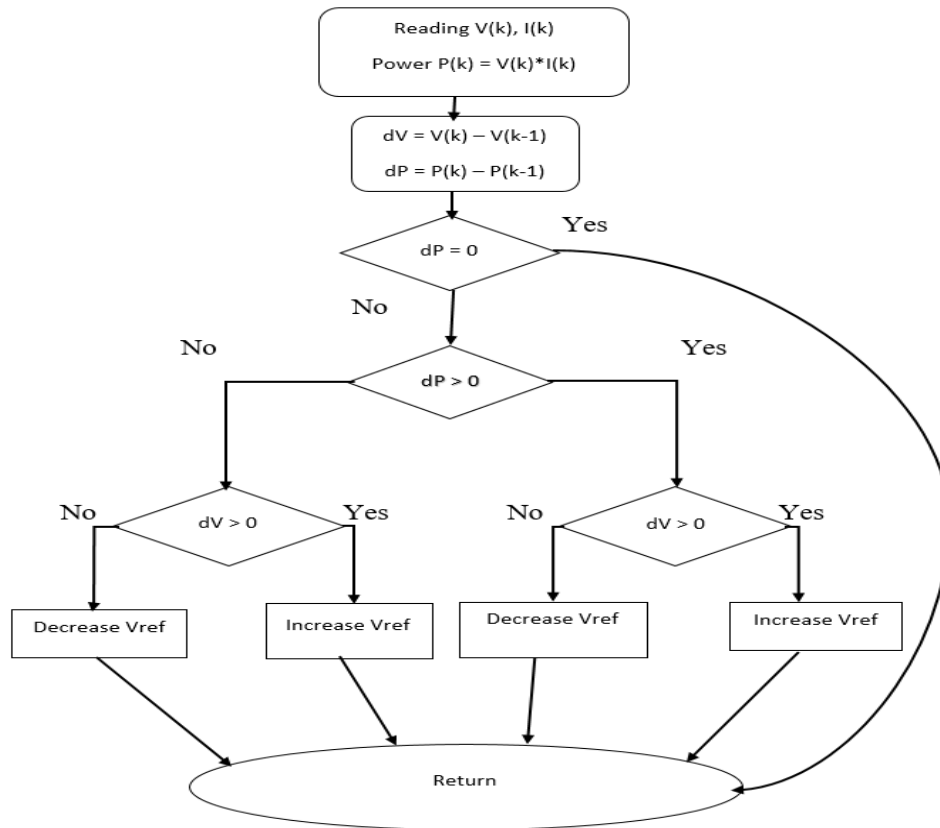
Figure 3.8: MPPT Algorithm flowchart

3.6. Modelling of DC-AC Converters

An inverter is a direct-alternating converter (DC-AC) which, from a source DC, enables an AC load to be supplied (Chapman, 2012). They can be single phase or three-phase according to the desired application.

3.7. Grid-tied Inverter

3.7.1. Three phase half bridge Inverters

This type of inverter is generally recommended for high-power applications. The structure of such a converter is made by the association, in parallel, of three single-phase half-bridge (or bridge) inverters giving three phase-shifted output voltages of 120 degrees, one relative to the other (Chapman, 2012). The three-phase inverter said two levels is illustrated by its power circuit of Figure 3.9. The inverter used in this project is a three-phase half-bridge inverter composed of 3 half-bridges, one per phase, and each half-bridge is composed of two IGBTs, and the DC bus is made up of two capacitors which are connected in series so that the midpoint of these capacitors gives

access to the midpoint of the DC bus in fact the output voltage of the inverter (AC side) will always be respectful to the Intermediate point of the DC bus.
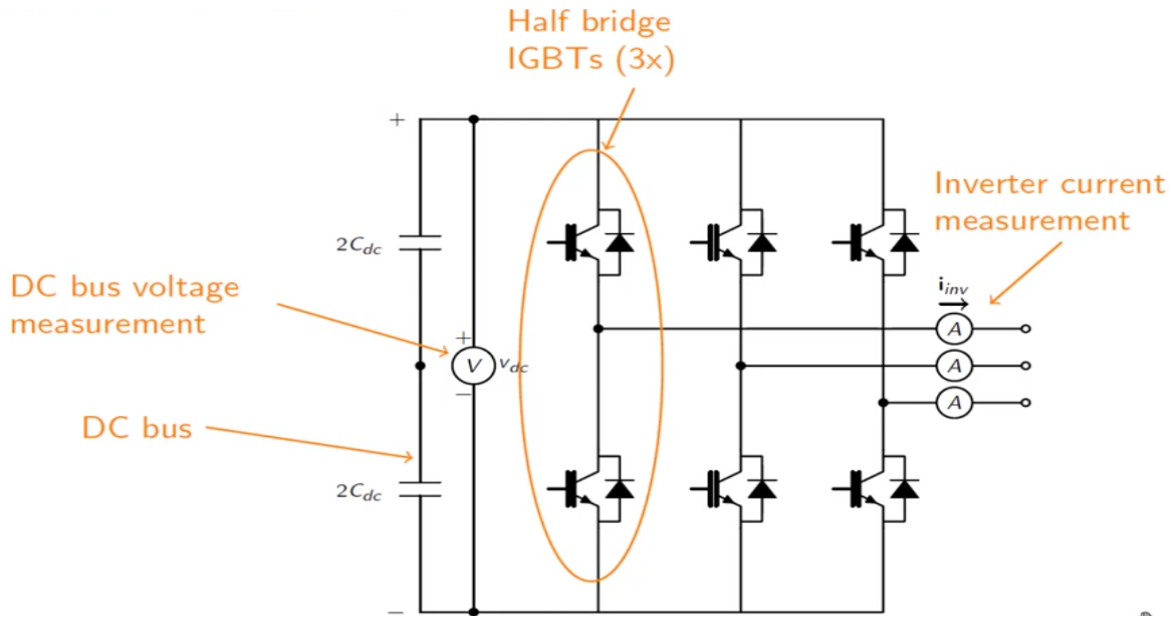
Figure 3.9: Three-phase grid convert control.

The inverter current can be measured by the output of each half-bridge midpoint IGBTs and the output voltage of the inverter is controlled by the switching period of the half-bridge IGBTs.

3.7.2. Three Phase Voltage Inverter Model

One must distinguish on the one hand the branch voltages V_{AN}, V_{BN}, and V_{CN} measured by with respect to the negative terminal of the DC voltage, on the other hand, there are the voltages of phases V_{An}, V_{Bn}, V_{Cn} measured with respect to a floating neutral point representing a star-connected balanced load. From simple tensions, one can easily deduce phase-to-phase voltages V_{AB}, V_{BC}, and V_{CA} (Chapman, 2012).

In the power circuit of the three-phase inverter illustrated in Figure 3.9, the states of the switches on the same arm are complementary. We can calculate the inverter output string voltages measured against the negative terminal of the DC side voltage using these switch states (Haider et al., 2012):

$$\begin{cases} V_{AN} = S_1 * V_{pu} \\ V_{BN} = S_2 * V_{pu} \\ V_{CN} = S_3 * V_{pu} \end{cases}$$

Equation 3.21

S1, S2, and S3 designate respectively the states of the switches of phases A, B and C.

$$\begin{cases} V_{AB} = V_{AN} + V_{BN} = (S_1 - S_2) * V_{pu} \\ V_{AB} = V_{BN} + V_{CN} = (S_2 - S_3) * V_{pu} \\ V_{AB} = V_{CN} + V_{AN} = (S_3 - S_1) * V_{pu} \end{cases}$$

Equation 3.22

The voltages between phases are expressed in the following system:

$$\begin{bmatrix} V_{AB} \\ V_{BC} \\ V_{CA} \end{bmatrix} = \begin{bmatrix} 1 & -1 & 0 \\ 0 & 1 & -1 \\ -1 & 0 & 1 \end{bmatrix} \begin{bmatrix} S_1 \\ S_2 \\ S_3 \end{bmatrix} V_{dc}$$

Equation 3.23

From this system of equations, we deduce the following equation in matrix form

$$\begin{cases} V_{AN} = \left(\frac{2}{3}\right) V_{AN} \left(\frac{1}{3}\right) (V_{BN} + V_{CN}) \\ V_{BN} = \left(\frac{2}{3}\right) V_{BN} \left(\frac{1}{3}\right) (V_{AN} + V_{CN}) \\ V_{CN} = \left(\frac{2}{3}\right) V_{CN} \left(\frac{1}{3}\right) (V_{AN} + V_{BN}) \end{cases}$$

Equation 3.24

$$\begin{bmatrix} V_{An} \\ V_{Bn} \\ V_{Cn} \end{bmatrix} = \frac{V_{dc}}{3} \begin{bmatrix} 2 & -1 & -1 \\ -1 & 2 & -1 \\ -1 & -1 & 2 \end{bmatrix} \begin{bmatrix} S_1 \\ S_2 \\ S_3 \end{bmatrix}$$

Equation 3.25

3.7.3. Presentation of the Grid-Inverter system

The grid-side converter shown in Figure 3.10 is connected to the grid via a LCL filter. The DC bus is connected to a capacitor of capacitance C under a voltage Vcc. The purpose of this converter is to keep the voltage constant at the terminals of the bus continue as well as adjust the power factor at the point of connection with the network (Izah & Prastiyanto, 2018)
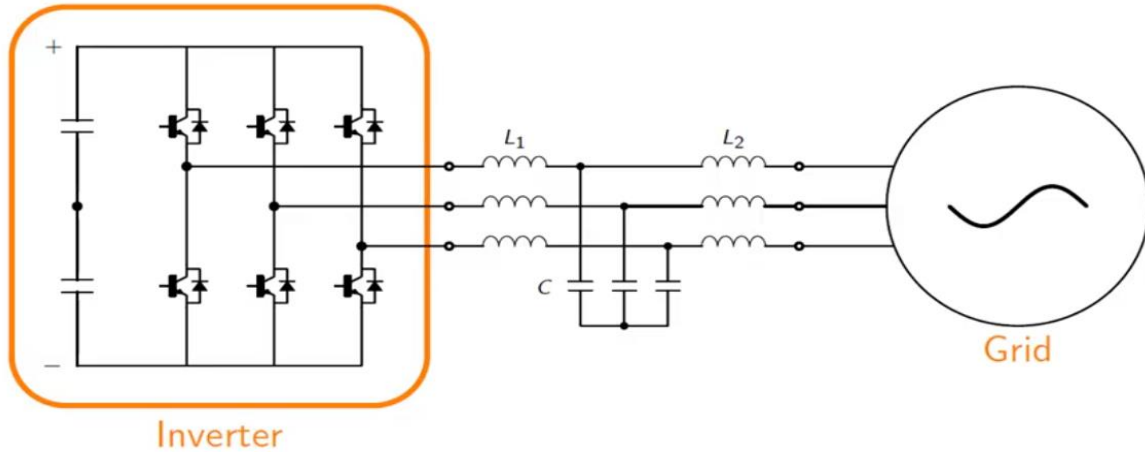
Figure 3.10: DC to AC Convector Connected to Grid

Where the following components are used to design the DC to AC convector connecting to the grid systems:

C: capacity value

V_{dc}: DC bus voltage

I_c: current flowing through the capacitor

I_{rip}: current rippled by the DC-AC converter on the network side

I_o: chopper output current

I_{In}: inverter input current

R_f: resistance

L_f: inductance of the filter

V_{in}: I= A, B and C phase-to-neutral network voltages

I_f: I= A, B and C currents through the filter

3.8. Presentation of the PV-chopper-inverter-grid system

The global photovoltaic system is composed of the following element that we present in this part:

a) A photovoltaic panel;
b) A Boost converter with its control;
c) An inverter also equipped with its control;
d) The three-phase network.

The Figure 3.11 depicts the overall layout of a solar plant that is linked to the network.
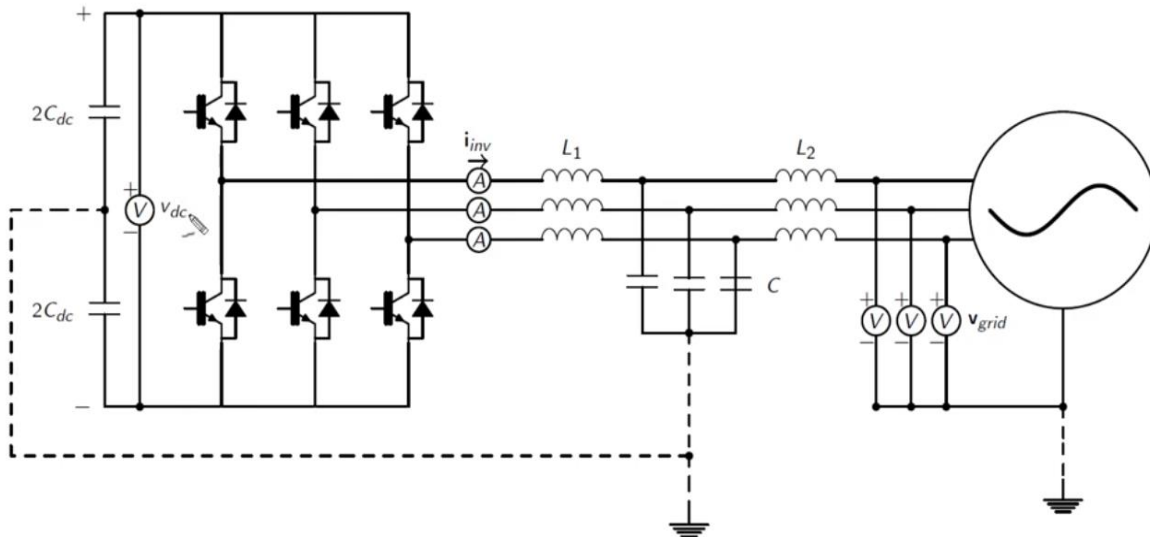
Figure 3.11: Grid-Adapted PV System

3.9. Modeling of LCL Filter

An LCL filter is a critical component in a grid-connected PV system as it helps to ensure the stability and reliability of the electrical grid by reducing the amount of harmonic distortion and ripple current in the output waveform of the inverter. Figure 3.12 shown the electrical circuit of LCL filter for grid connected photovoltaic systems. (Yasmeena & Das, 2015).
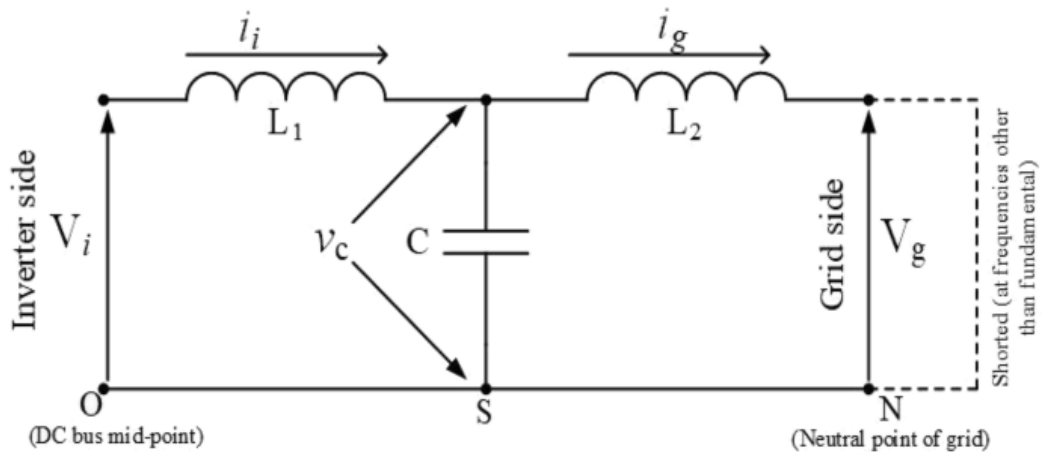
Figure 3.12: Electrical circuit of LCL filter

By using the Figure 3.2 we can determine the required filter parameters following with the Equations bellow:

$$\frac{V_i - V_C}{sL_1} = I_g + \frac{V_C}{\frac{1}{sC}}$$

<div align="right">Equation 3.26</div>

$$V_C = I_g * s * L_2$$

<div align="right">Equation 3.27</div>

Take Equation 3.27 into Equation 3.26:

$$\frac{I_g}{V_i} = \frac{1}{s^3 L_1 L_2 C + (L_1 + L_2)} \text{ Let } L_1 + L_2 = L \text{ then } L_P = \frac{L_1 L_2}{L_1 + L_2}$$

$$\frac{I_g}{V_i} = \frac{1}{sL(1 + s^2 C L_P)}$$

<div align="right">Equation 3.28</div>

Where:

V_i : Voltage inverter side

I_i: Current Inverter side

V_C : Voltage across the capacitor

I_g: Current grid side

V_i : Voltage grid side

L_1 and L_2 Inductor inverter side and grid side

3.10. Control system of grid connected

There are various issues with directly connecting solar systems to the grid; we will need a one-of-a-kind control circuit that, when used in grid interfacing, fits the Grid properties like as voltage, current, and frequency with those of the Inverter. Only by maintaining constant the voltage, current, frequency, and phase of the two sources can synchronism be maintained.

There are several strategies for controlling the grid with various energy sources; which approach is best depending on the criteria of the sources. In this project we have two different sources PV and grid that as to be synchronise and a suitable method used in this project is PLL Phase locked loop.

3.10.1. P.L.L. techniques are used in inverter control

Disturbances due to the electrical network. Among these disturbances, we have the phase jump, voltage sag, harmonic and frequency jump. To remedy these network faults which influence the frequency and therefore the phase position, the purpose of the PLL is to synchronize the frequency

of the phase voltages between the network and the inverter. There PLL regulation loop comprises three essentials: the phase detector (DP); THE corrector and integrator as shown in Figure 3.13 the traction for Synchronize rotating reference frame (SRF) (Jiang et al., 2018). The more developed diagram is illustrated below:
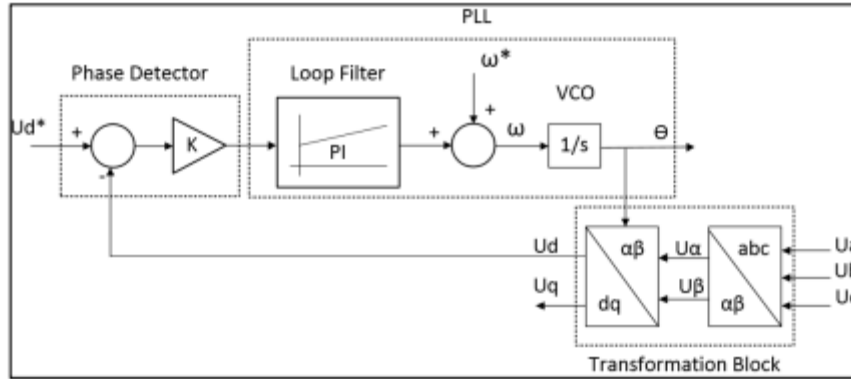
Figure 3.13: Basis traction for SRF PLL

3.10.2. Synchronize rotating reference frame

The SRF PLL is simply a PI-managed feedback device that tracks the phase angle. Voltage indications V_A ; V_B and V_C are converted from a three-phase stationary system to a two-phase stationary system V_α and V_β. V_A ; V_B and V_C are the grid voltages.

3.10.3. Transfer three phases voltage to stationary two phases

We must convert the three-phase signals in order to track the phase angle, V_a, V_b and, V_c, from three phases to a two-phase stationery, V_α and V_β, the grid voltage is provided as:

$$V_a = Vm(sin\,\theta) \hspace{4cm} \text{Equation 3.29}$$

$$V_b = Vm(sin(\theta - \frac{2\pi}{3})) \hspace{3cm} \text{Equation 3.30}$$

$$V_c = Vm(sin(\theta + \frac{2\pi}{3})) \hspace{3cm} \text{Equation 3.31}$$

Where θ is the phase angle $2\pi f$.

The $\alpha\beta$ transformation matrix is given bellow

$$T\,\alpha\beta = \frac{2}{3}\begin{vmatrix} 1 & -\frac{1}{2} & -\frac{1}{2} \\ 0 & -\frac{\sqrt{3}}{2} & \frac{\sqrt{3}}{2} \end{vmatrix} \hspace{2.5cm} \text{Equation 3.32}$$

The matrix multiplication $V_{\alpha\beta} = \text{T } \alpha\beta V_{abc}$ yields

$$\begin{vmatrix} V_\beta \\ V_\alpha \end{vmatrix} = \begin{vmatrix} V_m \ (sin\ \theta) \\ V_m \ (cos\ \theta) \end{vmatrix}$$

Equation 3.33

The matrix in Equation 3.36 depicts two signals that only care about the phase angle of one of the phases Va**.**

3.10.4. Synchronous rotating or Transform

synchronous rotating or Transform V_α , V_β to V_q , V_d In the SRF, the phase angle of V alpha is monitored by synchronizing the voltage space vector along the Q or D axis (Natesan & Venkatesan, 2016; Ögren & Ögren, 2011). Figure 3.14 indicates that the voltage space vector is not in sync with the Q- or D-axes.
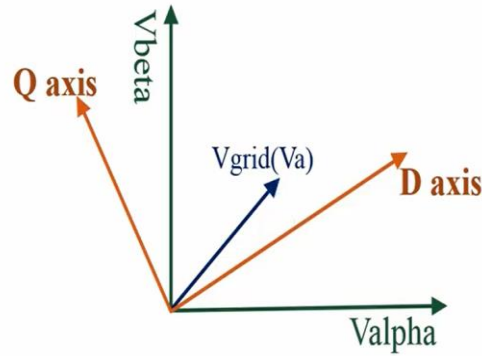
Figure 3.14: Not synchronous phase diagrams of abc-frame to dq-frame

The transformation matrix is to be synced with the voltage space vector**:**

$$\textbf{T } qd = \begin{vmatrix} cos\ \theta^* & sin\ \theta^* \\ sin\ \theta^* & cos\ \theta^* \end{vmatrix}$$

Equation 3.34

Where:

θ^*Is the PLL system's anticipated phase angle output.

Using the trigonometric addition rules and the transformation.

$$\begin{vmatrix} V_d \\ V_q \end{vmatrix} = \begin{vmatrix} -V_m \ sin(\theta - \theta^*) \\ V_m \ (cos\ \theta - \theta^*) \end{vmatrix}$$

Equation 3.35

The PI regulator's gain is designed so that V_q follows the reference value $V_d{}^*= 0$. if $V_d = 0$, the anticipated frequency is locked to the system frequency once the space voltage vector is synced along the D axis. The voltage space vector is synchronized with the D-axis in Figure 3.15, with the active component aligned with alpha and the reactive component aligned with beta.
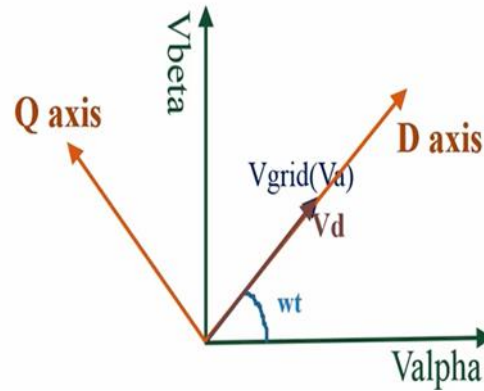
Figure 3.15: Phase diagram of Vgrid synchronous with D axis or Q axis

To obtain excellent performance and minor steady-state errors in size and phase, the compensator design (Ögren & Ögren, 2011) technique shown in Figure 3.15 is not a simple process.

3.10.5. Transfer function

Because this program will be running in a sampled system, the delay impact must be considered (Gao & Barnes, 2016). The transfer function (TF) of the plant is just a lag and an integrating element.

$$G_p = \left(\frac{1}{1+TS}\right) * \left(\frac{1}{S}\right) \qquad \text{Equation 3.36}$$

Ts is the sample simulation period for the system's open-loop TF, as shown below:

$$G_{ol} = \left(kp\frac{1+s\tau}{s\tau}\right) * \left(\frac{1}{1+ST}\right)^* * \left(\frac{Vm}{S}\right) \qquad \text{Equation 3.37}$$

To transition from an open-loop to a closed-loop system, the relationship between the transfer functions is as follows:

$$G_{cl} = \frac{G_{ol}}{1+G_{ol}} \qquad \text{Equation 3.38}$$

3.10.6. Integration and going from s-domain to z-domain

The Euler forward technique is the most fundamental approach for solving integration. In fact, the voltage input signal for the PLL system is sampled from a grid-connected PV system. The system was built to handle the signals. The plant's integration elements are as follows:

$$G_{(s)} = \frac{F(s)}{E(s)} = \frac{1}{s} * \Longleftrightarrow \frac{df}{dt} = e(t)$$
Equation 3.39

Using the Mathematical Expression Z-transform and applying Euler forward (Nurujjaman, 2020; Ögren & Ögren, 2011) yields:

$$S = \frac{Z-1}{Ts}$$
Equation 3.40

The PI-regulator in the z-domain is determined using equation 3.39 as follows:

$$G_{pi} = kp\frac{1+s\tau}{s\tau} = kp\frac{z-1+\frac{Ts}{\tau}}{z-1}$$
Equation 3.41

The PLL system's transfer function (Tf) in equation (4.19) may be rewritten as follows

$$G_{ol} = (kp\frac{1+s\tau}{s\tau}) * (\frac{1}{1+ST}) * (\frac{Vm}{S}) = kp\frac{z-1+\frac{Ts}{\tau}}{s^2(s+\frac{Ts}{\tau})} = kp\frac{Vm}{aTs} * \frac{(\frac{a}{\tau}+as)}{s^2(s+\frac{1}{T})}$$
Equation 3.42

Where:

      Ts: sampling period in second,

      Kp: Regulator gain.

      $\frac{1}{1+ST}$: lag term of the system,

      $\frac{1}{s}$: The integrating element illustrates a voltage-driven oscillator.

      V_a: Amplitude voltage level

      G_{ol}: open loop transfers function

      G_p: Transfer of the of the full system,

In the rest of this work, we used the P.L.L in a balanced system. However, in an unbalanced system the efficiency of the P.L.L deteriorates, hence the use of a multi-variable filter becomes a necessity to filter these disturbances.

3.11. Summary

In this Chapter, we cover several topics related to modelling and control of PV systems. The chapter starts with the modelling of PV modules using the single-diode model, which is a widely used and accurate model for PV modules. The model takes into account the effects of temperature and irradiance on the performance of the PV module. The chapter explains the mathematics of the boost converter, including the derivation of the transfer function and the design of the control loop.

The chapter then moves on to the modelling of a DC-AC converter, which converts the DC voltage from the boost converter into AC voltage suitable for feeding into the grid. The chapter explains the modelling of the DC-AC converter and the design of the control system, including the use of a PLL to synchronize the AC output voltage with the grid voltage. The final topic covered in the chapter is the control system of a grid-connected PV system, including the design of a controller to track the maximum power point of the PV module and the use of an LCL filter to reduce the harmonic content of the output current.

The chapter concludes by noting that the next chapter will cover the modelling and design methodologies for a complete grid-connected PV system, including the integration of energy storage systems and the impact of PV systems on the stability of the grid.

CHAPTER 4: MODELING USING MATLAB SIMULINK AND TYPHOON HIL

4.1 Introduction.

This chapter places a significant focus on the crucial task of sizing the PV system, a pivotal element in optimizing its performance within the grid-connected framework. We delve deeply into the intricacies of designing and calculating both the boost converter and LCL filter. Furthermore, within this section, our exploration extends to the modeling and design of key parameters, including MPPT control, DC Voltage Controller, Open-loop Power Controller, Current Controller, and the intricate nuances of PLL design.

It's worth highlighting that these evaluations are conducted within two distinct software environments, bolstering the robustness and reliability of our findings. In addition to our analytical endeavors, we provide comprehensive visual representations of all circuit parameters integrated within the simulated model. This visual elucidation proves invaluable for identifying potential issues and refining our operational insights.

To ensure the utmost precision and comprehensiveness in our analysis, we leverage the unique capabilities of both MATLAB Simulink and Typhoon HIL simulation package with HIL402 configuration in the virtual environment. This approach enables us to deliver a holistic assessment of the grid-connected photovoltaic system under rigorous scrutiny, thereby ensuring the reliability and completeness of our findings.

4.2. Sizing of PV system

In the process of evaluating the number of PV modules necessary to fulfill the power requirements of a 100 kW load system, we employed equations 4.1, 4.2, 4.3, and 4.5. we present the results detailing the sizing of the PV system to meet this specific demand.

   a) Using Equation 4.1, calculate the amount of energy necessary to cover the area covered by a PV array.

$$P_{required} = \frac{P_{load}}{\eta_{inverter}}$$ Equation 4.1

   Where:

   $P_{required}$: The amount of energy required to cover a PV array.

P_{load} : Load in watt-hour

$\eta_{inverter}$: Inverters efficiency.

b) Using Equation 4.2, calculate the energy output of modules each day.

$$P_{module} = P_{max} \times t_{peak}$$
Equation 4.2

Where:

P_{module}: Modules energy output per day.

t_{peak}: Average daily peak sunshine hours

c) Using Equation 4.3, determine the number of modules required to satisfy power demands for mixed with the grid.

$$\eta_{pv} = \frac{P_{array}}{P_{module}}$$
Equation 4.3

Where:

η_{pv}: Total number of PV modules

P_{array}: Output of PV array in watt-hour

P_{module}: Output of one PV module in watt-hour

d) Using equation 4.4, determine the number of modules linked in series.

$$n_{series} = \frac{Vbus}{Vm}$$
Equation 4.4

Where:

n_{series}: PV modules connected in series

$Vbus$: DC bus voltage of the system

Vm: PV rated voltage

e) Using Equation 4.5, calculate the number of threads linked in parallel.

$$n_{parallel} = \frac{n_{pv}}{n_{series}}$$
Equation 4.5

Where:

$n_{parallel}$: PV strings connected in parallel

n_{pv}: Total number of PV modules

Using Equation 4.3, determine the number of modules required to cover the power demands to feed into the grid.

$$\eta_{pv} = \frac{100KW}{360} = 277.77 \approx 278$$

Using Equation 4.4, get the number of modules linked in series (number of strings).

$$n_{series} = \frac{300v}{39.6v} = 7.6 \approx 8 \, modules$$

Determining the number of strings connected in parallel by using Equation 4.5

$$n_{parallel} = \frac{278}{8} = 35.75 \approx 35 strings$$

4.3 Boost converter designed.

The Boost converter circuit is utilized as the DC to DC converter in a two-stage PV production system (Fathah, 2013). Because the PV cell's output voltage is low, a boost converter circuit can be used to transform an unstable DC voltage of 250-300Vdc to a stable DC voltage of 600Vdc.

Determining the value of inductor and capacitor needed for the boost converter using Equation 4-8 and 4-9 first we need to calculate input current and ripple values, the following steps show bellow:

$D = 1 - \frac{V_s}{V_o}$ Equation 4.6

$R_{l=} \frac{V_o{}^2}{P}$ Equation 4.7

$C = \frac{I*(V_o - V_{S\,(min)})}{f_S * \Delta_v * V_o}$ Equation 4.8

$L = \frac{V_s*(V_o - V_{S(max)})}{f_{sw} * \Delta_i * V_o}$ Equation 4.9

Where:

   D: Duty circle

   V_s: Voltage source

71

V_o: Voltage output

Rl: Resistant Load

P: Power

ΔV: ripple voltage

Δ_i: current Ripple

f_{sw}: switching frequency

Calculate input current by using power formula: P=I*V

$$I = \frac{100k}{250} = 400A,$$

Current ripple is 5% of input current

$$\Delta_i = \frac{400}{100} *5 = 20A$$

Voltage ripple is 1% of voltage out:

$$\Delta_v = \frac{600}{100} *1 = 6V$$

$$output\ current = \frac{100k}{600} = 166A$$

Calculate Duty circle by using Equation 4-6

$$D = 1 - \frac{300}{600} = 0.5$$

Determining the value of Resister needed for the boost converter using Equation 4.7

$$R_l = \frac{600^2}{100k} = 3.6\ ohms$$

Determining the value of capacitor needed for the boost converter using Equation 4.8

$$C = \frac{166*(600-300)}{5k* 6* 600} = 2.8mF$$

3. Determining the value of inductor needed for the boost converter using Equation 4.9

$$L = \frac{300*(600-300)}{5k*20*600} = 1.5mH$$

4.4 LCL Filter Design and calculations

The switching frequency using for the designer of LCL filter is:

Fsw = 10Khz and the resonant frequency is calculated by using formula bellow:

$$f_{res} = \frac{Fsw}{10} = \frac{10k}{10} = 1000Hz$$

Fist is to find the resonance frequency: $f_{res} = \frac{f_{sw}}{10}$

The power factor of the inverter must 1unit then S=100kva, Voltage phase 230v and f=50hz

Determining the value of capacitor needed for LCL Filter using Equation 3.24 and Equation 3.25

$$C_f = 0.05 * C_b$$

$$C_b = \frac{S}{V^2 * 2\pi * f}$$

$$C_b = \frac{100k/3}{230^2 * 2\pi * 50} = 2005.73uF$$

$C_f = 0.05 * C_b = 0.05 * 2005.73 = 100.29uF$

The values of inductor need for LCL filter:

Phase current by grid side

$Ig = \frac{100k/3}{230} = 144.9A$

The current grid switch is 0.3% of the current grid is: 0.003*144.92= 0.434A

The Voltage inverter switch = 0.9*Vg = 0.9*230 = 207V

Determining the value of inductors needed for LCL Filter using Equation 3.28

$$L_i = \frac{V_{DC}}{16 * f_{sw} * \Delta I_{L-max}}$$

$$L_i = \frac{1}{(2\pi*10k)*\left(\frac{0.434}{207}\right)*(1-\frac{(2\pi*10k)^2}{(2\pi*1k)^2}} = 76.68uH$$

Let Li = Lg = $\frac{L}{2} = \frac{76.68u}{2}$ = 38.34uH

And for maximum inductor L(max) we calculate the voltage is 20% of voltage grid therefore we have:

73

$$L_{max} = \frac{0.2 * Vgrid\ in\ phase}{2\pi * f_{grid} * I_{grid}} = \frac{0.2 * 230}{2\pi * 50 * 144.92} = 1mH$$

$$Li = Lg = \frac{Lmax}{2} = 500mH$$

4.5 Modeling using MATLAB Simulink

This paragraph exemplifies the parameter blocks modeling process using MATLAB Simulink. The system has been meticulously designed and modeled in accordance with precise calculations and established parameters. The fundamental building blocks designed within the MATLAB environment include MPPT, Filter & AC Measurement, PLL, and voltage and current protection control.

These integral components are crafted with precision, and voltage and current control systems are engineered using MATLAB Simulink. This comprehensive approach allows for a detailed examination of system behavior, dynamics, and the intricate interactions of these vital subsystems, essential for optimizing overall performance and ensuring robust protective measures. In summary, this paragraph underscores the significant role of MATLAB Simulink in the design and modeling of these critical system components.

The MPPT system was meticulously designed using MATLAB Simulink to accurately track both Ipv and Vpv. As demonstrated in Figure 4.1, the comprehensive block diagram of the MPPT showcases the integration of Ipv and Vpv inputs into the MPPT algorithm. Additionally, the Start MPPT voltage is supplied through a changeover switch, enabling voltage measurement and subsequent adjustment. This dynamic process allows for voltage fine-tuning, both incrementally and decrement, as necessary. The Vmpp output is then precisely optimized to meet the project's voltage requirements.
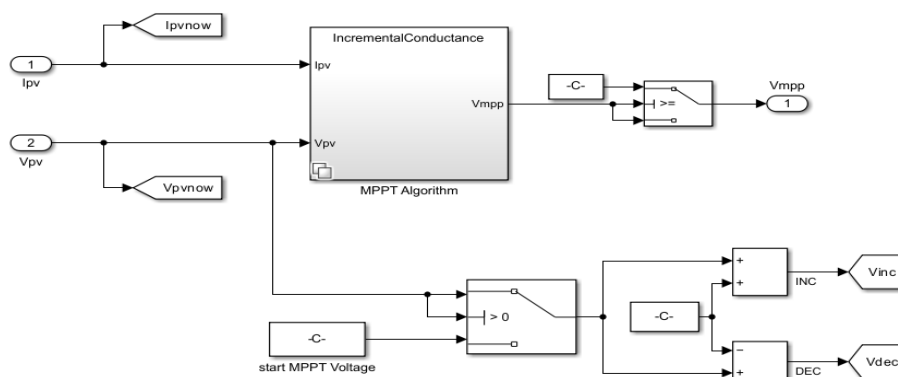
Figure 4.1: MPPT Block Diagram

Figure 4.2 illustrates the design of the Filter & AC Measurements in MATLAB Simulink blocks. The three-phase line from the power inverter is connected to a filter, and the output is subsequently linked to current sensor 1. Current sensor 1 relays information to a second current sensor, which provides stable and dynamic readings of the system's instantaneous current. The second pin of current sensor 1 is connected to a voltage sensor, and the output of this voltage sensor captures the dynamic voltage, rendering it both stable and dynamic. The output of this block yields dynamic three-phase AC current and voltage data in the form of Iabc and Vabc.
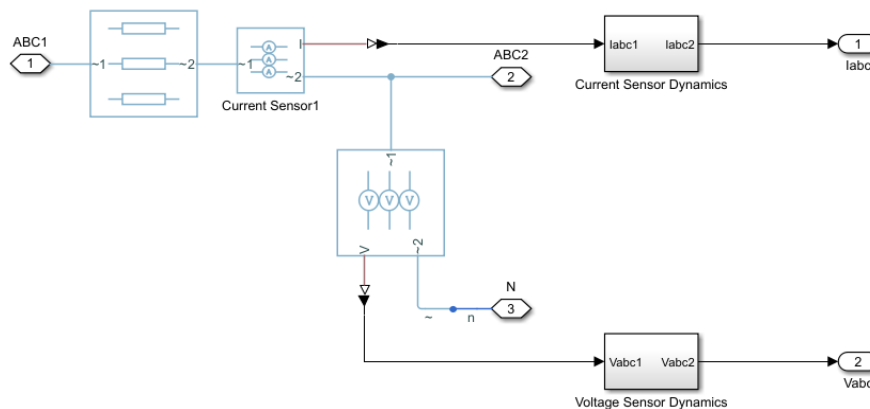
Figure 4.2: Filter & AC Measurements. Block

Figure 4.3 illustrates the block diagram design of the PLL connected to the protection block in MATLAB Simulink. In this block diagram, you can observe that the three grid voltages are directly connected to the PLL input pins for tracking and sinusoidal measurement.

The output from this connection is subsequently transformed into three separate pins, one for frequency, another for phase angle, and the last for magnitude. The frequency and voltage information are then linked to the protection system. This configuration allows us to generate a trip signal when the PLL fails to accurately track the grid voltage, ensuring a safeguard mechanism in the event of tracking failure.
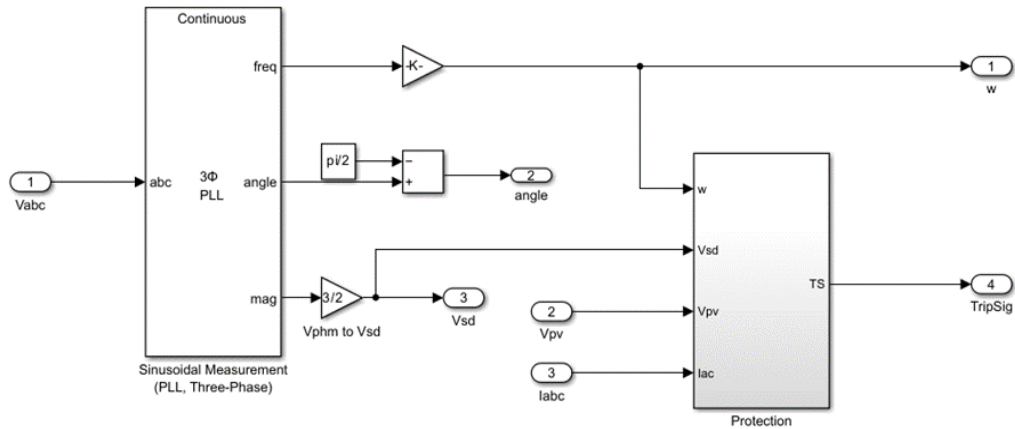
Figure 4.3: PLL and Protection block

Figure 4.4 displays the control block designed in MATLAB Simulink. As observed below, the input variables Vmpp and Vpv are supplied to the initial block, which transforms them into controller voltage. The output of this transformation is then connected to the Id control, which subsequently feeds into the D-axis current control and q-axis current control blocks.

The output of this control process yields two controllable parameters, Vd and Vq. These parameters are then used to supply current to the dq control, involving both Id and Iq, driven by angle and Iabc grid current inputs.
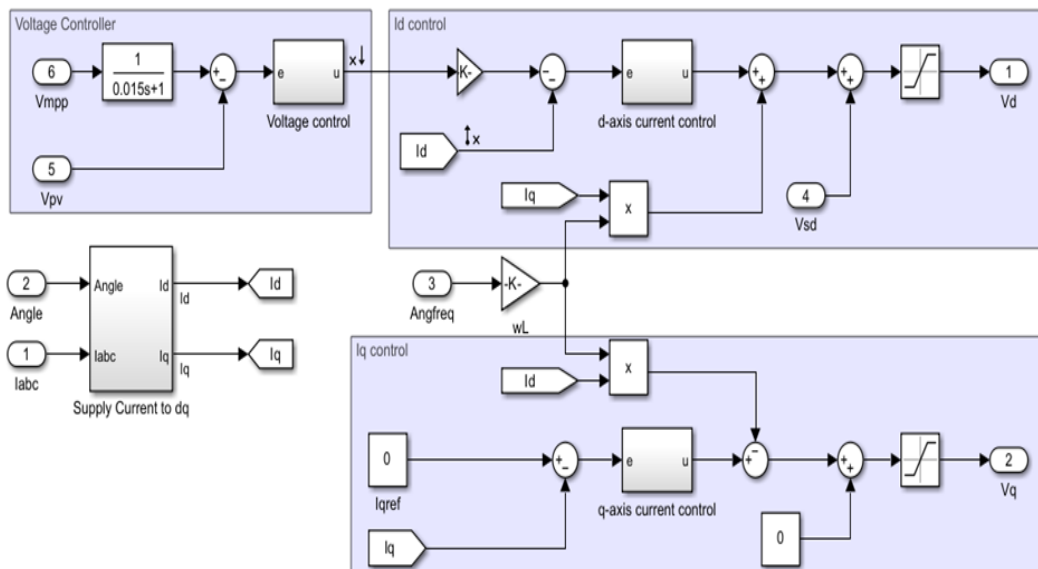
Figure 4.4: Control systems

4.6 Modelling using Typhoon HIL402 System/Platform

The Typhoon HIL simulation is based on a virtual machine that brings all functionalities of the physical HIL device with a real-time environment considering all the limitations. For the current simulation study. Similar model of grid connected to PV system is developed in the HIL schematic editor consists of signal processing blocks and grid tied inverter model. The signal processing blocks are coded using C language. The piecewise linear approach of HIL simulation divides the whole system into subsystems considering the processing power available.

Standard processing core helps in the subsystem simulation with the required processing power. The subsystem is created for each calculation in the HIL schematic editor. The parameters common to all the subsystems are initialized in the python script like execution rate etc. The instrumentation subsystem consists of the differently labeled probes for data acquisition. The data labeled probes are accessed directly from the HIL SCADA interactive panel for data representation. The linear time-invariant signals are obtained from the linearized circuit.

The model is build based on a state-space approach with weights assigned for each element. Grid inverter model is developed in HIL schematic editor and validation is carried out with the successful generation of the C code of the model. The C code is loaded into a virtual environment of the HIL simulator having VHIL configuration. The user system configuration for the virtual HIL simulation is as shown in Table 4.1.

TABLE 4.1. SYSTEM CONFIGURATION

System Parameters	Specified Values
Manufacturer	Intel
CPU Model	i7-5600U
Base Clock Speed (GHz)	2.60GHz
Maximum Clock Speed (GHz)	8GHz
RAM Capacity (GB)	16
Junction Temperature ($\circ$C)	100

The interactive HIL SCADA panel is built using the widgets available. The scope, data logger, and analog display are primarily used for the development of the HIL SCADA panel which is displayed in Fig. 4.5.
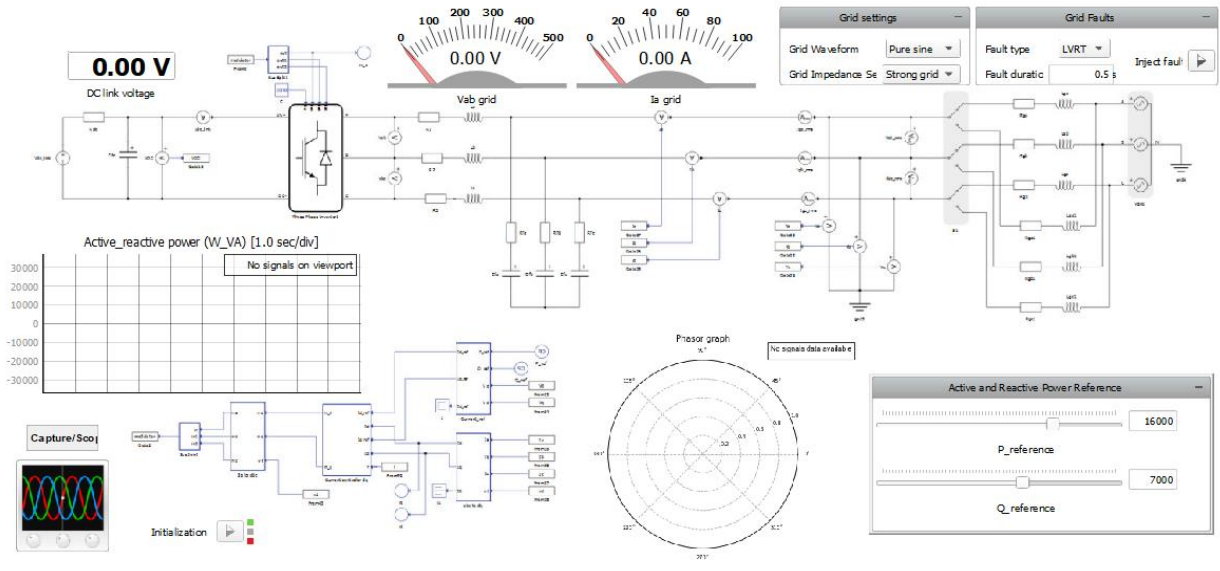
Figure 4.5:Typhoon HIL SCADA panel

The design and modeling of the system were accomplished using Typhoon HIL, incorporating various blocks. In Figures 4.6, we can observe the PLL Blocks. These PLL block take in a three-phase voltage input from the grid. Subsequently, they transform this input into two voltages, Vd and Vq. Furthermore, the PLL block provides the capability to track the grid's angular position (wt) and frequency with precision.
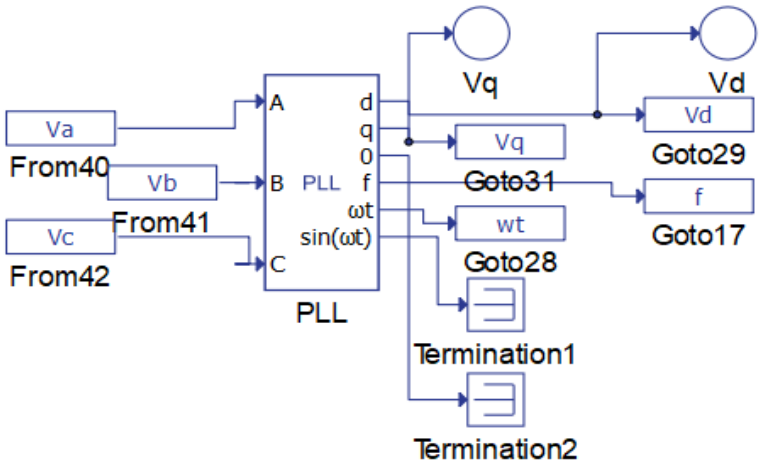
Figure 4.6:PLL Blocks

Figure 4.7 displays the designed block of the voltage controller in Typhoon HIL-402. This block, as indicated in the diagram, involves the modulation of incoming DC voltage and the feedback voltage. These two signals are combined with varying polarities and processed using the PI (Proportional-

78

Integral) control method. This approach allows precise control of the DC voltage originating from the solar panels as it enters the boost convector.
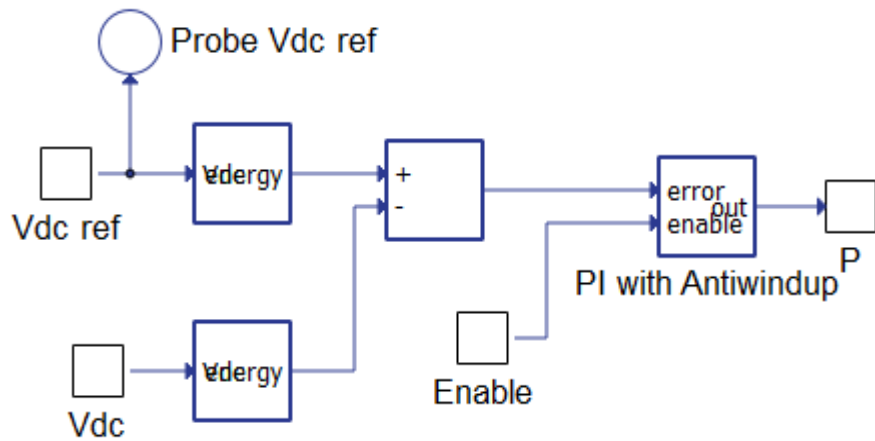
Figure 4.7: DC Voltage Controller

4.7 Summary

The process of determining the required number of PV modules to meet a 100 kW load system's power demands involves employing a set of equations (4.1, 4.2, 4.3, and 4.5). The subsequent results provide a precise configuration for the PV system tailored to fulfill this specific requirement. A critical component in this setup is the Boost converter circuit, serving as the DC to DC converter in a two-stage PV production system. This choice is mainly driven by the low output voltage of the PV cells, with the boost converter effectively elevating an unstable DC voltage of 250-300Vdc to a stable 600Vdc.

The selection of the switching frequency plays a pivotal role in designing the LCL filter. This paragraph illustrates the parameter block modeling process using MATLAB Simulink. The system's design and modeling meticulously adhere to precise calculations and established parameters. The primary building blocks within the MATLAB environment encompass MPPT, Filter & AC Measurement, PLL, and voltage and current protection control. Each of these components is engineered with precision, and the voltage and current control systems are implemented through MATLAB Simulink.

CHAPTER 5: SIMULATION RESULTS AND DISCUSIONS

5.1 Introduction

Since renewable energy sources are becoming an essential part of the world's energy mix, they must be thoroughly tested and validated before being successfully incorporated into the power systems that already operate. The use of HIL modelling to model the operation of a grid-connected solar energy system is covered in detail in Chapter 5 of this dissertation. The findings obtained from MATLAB/Simulink and the Typhoon HIL 402 simulation platform, which is an essential tool for examining the electrical responses of the system in a variety of environmental scenarios, are presented in this chapter. Verifying the system's operational integrity and improving the control schemes that manage its communication with the grid are the two main goals. This chapter attempts to evaluate the system's behaviour using a variety of scenario simulations, supporting the usefulness of HIL simulations in predicting the system's performance in real life. The findings summarised here give significant insights into the dynamics of the solar energy system and a thorough knowledge that is anticipated to drive future developments in solar technology integration.

5.2. Simulation result using MATLAB/Simulink
5.2.1. Grid-Connected PV System in MATLAB/Simulink

In this project, we employed two simulation software tools to enable the comparison and validation of results. Figure 5.1, presented below, showcases the circuit block design of the grid-connected photovoltaic system using MATLAB/Simulink. The simulations were executed within a 45-millisecond timeframe, and a detailed explanation of all results is included. The circuit incorporates various blocks, including solar panels, power circuit filters, PLL, protection blocks, controllers, MPPT, and measurement blocks.
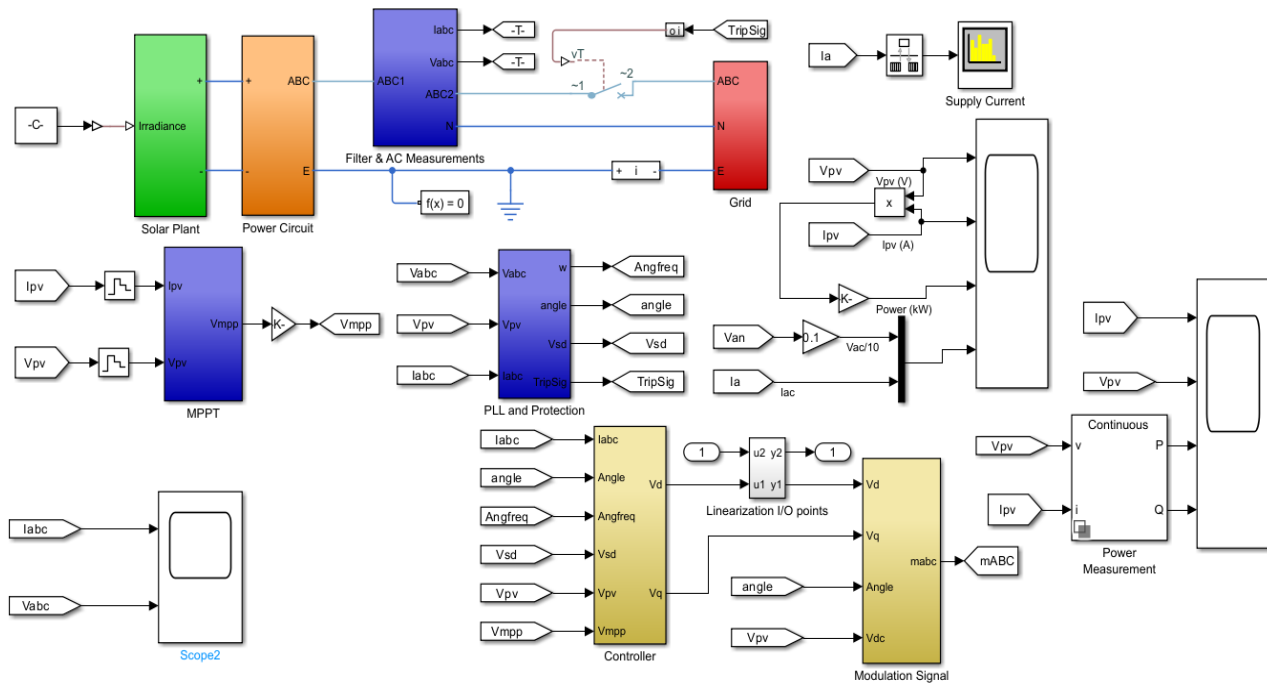
Figure 5.1: Block Diagram of grid-connected PV system in MATLAB/SIMILINK

The PLL control mechanism, a mainstay in grid synchronisation, is simulated to assess its accuracy in preserving coherence between inverter output and grid frequency. The capacity of the PLL to lock onto the grid frequency with low phase error is crucial for the reliable functioning of the grid-connected PV system, which is rigorously modelled in the simulation.

Furthermore, the simulation framework's protection blocks are meant to imitate the safety procedures that protect the system against abnormalities. This includes overcurrent protection, voltage control, and islanding avoidance, all of which are critical to the grid-connected PV system's operational integrity.

Critically, the MATLAB/Simulink environment can simulate these components and their interactions in 45 milliseconds, resulting in a near-real-time simulation of the system's behaviour. This quick modelling capacity is critical for validating system performance under transient situations, such as unexpected changes in solar irradiation or load demand.

When the discourse is synthesised, it becomes clear that the MATLAB/Simulink platform serves not only as a testing ground for theoretical constructions, but also as a bridge to practical application. The simulation findings are critical for the iterative process of system optimisation, enabling researchers to fine-tune control algorithms and system designs prior to physical instantiation.

81

5.2.2. Grid Voltage and Current Phase under Irradiation of 250 and 500 W/m² and a Temperature of 25°C in MATLAB/SIMILINK

Figure 5.2 depicts the simulation results showcasing grid voltage and current variations under different irradiation levels, specifically 250W/m² and 500W/m², in MATLAB/Simulink, with the temperature maintained at a constant 25°C. It is noteworthy that throughout these scenarios, the grid voltage remains stable, while the current exhibits an increase corresponding to changes in irradiation levels. However, a minor synchronization delay of approximately 4 microseconds is observed as the current adjusts to the modified irradiation levels. Subsequently, the current realigns itself with the grid voltage.

Figure 5.2: Grid voltage and current phase under irradiation of 250 and 500W/m² and a temperature of 25°C in MATLAB/SIMILINK

The stability and effectiveness of renewable energy integration into the electrical grid greatly depend on the fidelity of grid-connected photovoltaic (PV) systems, especially in the presence of fluctuating irradiation circumstances. Critical insight into the performance dynamics of such systems at defined irradiation intensities of 250 and 500 W/m² at a steady temperature of 25°C is provided by the simulation results produced using MATLAB/Simulink software. Understanding how the inverter current behaves in respect to the grid voltage phase—a relationship that is critical to

preserving the consistency and quality of power supplied to the grid—requires the use of these simulations

In order to guarantee the smooth integration of the PV system into the grid infrastructure, a certain level of grid voltage stability is anticipated. This stability is confirmed by the MATLAB/Simulink simulations, even when the irradiation levels and, therefore, the PV cells' potential power production, change. This demonstrates how resilient the grid's voltage control systems are, since they are intended to keep the voltage constant even in the face of fluctuating input from renewable sources.

However, there is a noticeable phase shift in the simulation results that indicates the inverter current's phase is sensitive to variations in irradiation levels. Any phase displacement may result in inefficient power transmission and possible grid disruptions, hence it is essential that the inverter current and grid voltage be aligned phase-to-phase. This sensitivity is shown by the simulations run at 250 and 500W/m² irradiation levels, which show a short asynchrony of around 4 microseconds when switching between irradiation levels. But this asynchrony is quickly corrected by the system's control algorithms, which most likely include both PLL and PI controllers. This realigns the current phase with the grid voltage.

Contend that the accumulation of these small differences can have a compounding effect on the stability of the grid. This is especially true as PV systems become more and more integrated into the grid.

5.2.3. Grid Voltage and Current Phase under Irradiation of 750 and 1000W/m² and a Temperature of 25°C in MATLAB/SIMILINK

Figure 5.3 further illustrates the simulation outcomes for grid voltage and current under varying irradiation conditions (750W/m² and 1000W/m²) using MATLAB/Simulink, with a constant temperature of 25°C. Throughout each scenario, the grid voltage remains stable, while the current levels dynamically adjust to the changing irradiation. A brief asynchrony of approximately 4 microseconds is observed as the current aligns itself with the modified irradiation levels. However, the current eventually returns to synchronization with the grid voltage. These results offer valuable insights into the behavior of the grid-tied PV system under dynamic irradiation conditions.
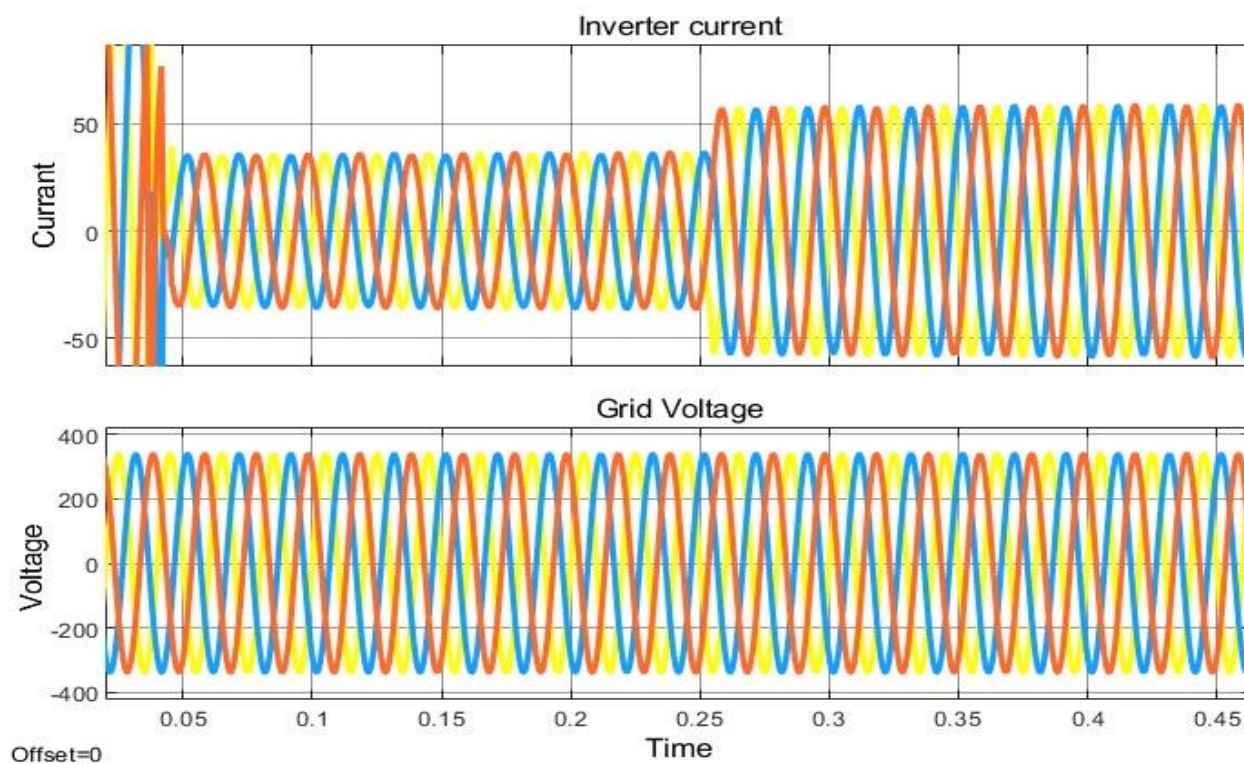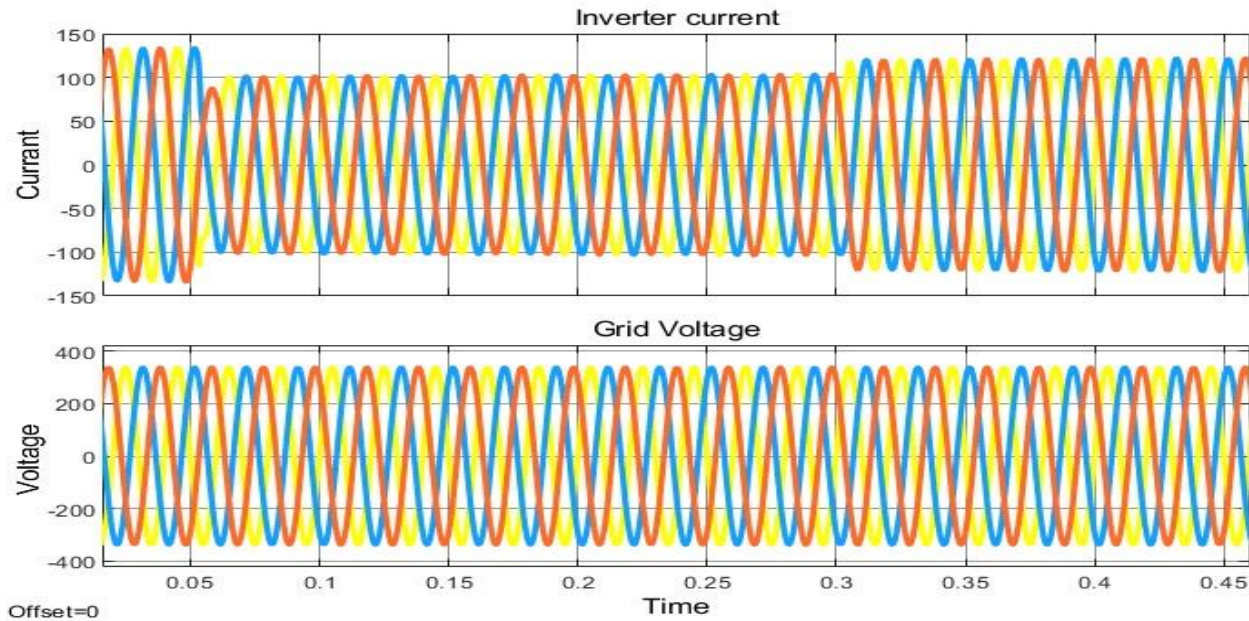
Figure 5.3: Grid voltage and current phase under irradiation of 750 and 1000W/m² and a temperature of 25°C in MATLAB/SIMILINK

Knowledge the performance of grid-connected PV systems requires a knowledge of the grid voltage and current phase behaviour under higher irradiation situations. Higher irradiance levels of 750 and 1000W/m² MATLAB/Simulink simulations give deeper insights into the PV system's dynamics, providing an accurate evaluation of its reaction to solar irradiance variations at a constant temperature of 25°C. The capacity to effectively estimate and forecast these reactions is critical for PV system design and optimisation, improving reliability and efficiency in real operating conditions.

The MATLAB/Simulink model exhibits an increase in photovoltaic current (Ipv) at these increased irradiation circumstances, which is predicted given the direct connection between irradiance and the current produced by PV cells. Simultaneously, the model shows an increase in active power output, confirming the system's capacity to convert more solar energy into electrical power, as report. An intriguing discovery from the simulation is the drop in photovoltaic voltage (Vpv) despite increasing irradiance, which is indicative of the intrinsic properties of PV cells and their temperature coefficients, as stated by.

The constant value of the reactive power output (PV_out_Q) throughout the simulations is an indicator of effective inverter control in maintaining a unity power factor, which is critical for integrating PV systems into the grid without introducing reactive power disturbances. Because reactive power is neither used nor created under variable irradiance levels, this part of the

84

simulation highlights the efficacy of the inverter's management algorithms in regulating power quality.

The grid voltage and inverter current phase behaviour under these circumstances demonstrates the complexity of contemporary grid-tied inverters. These inverters are intended to manage the fluctuation of renewable energy generation while keeping a steady phase connection with the grid voltage. This stability is critical for preventing harmonic distortions and ensuring a smooth flow of energy into the power system.

The MATLAB/Simulink simulation results not only serve as a proof of concept, but also as a baseline for real-time HIL testing. The data given by the simulation environment is useful in optimising control techniques prior to testing them in an HIL context, ensuring that the system performs as predicted when linked to real grid infrastructure.

The capabilities of the MATLAB/Simulink platform to model these situations with great precision helps researchers to anticipate and handle any concerns that may come from high irradiation levels. For example, stated that the fall in Vpv with higher irradiation, although paradoxical, may be attributable to the non-linear properties of PV modules and their sensitivity to temperature variations.

5.2.4. Simulation Results for Ipv, Vpv, PV_out. P, and PV_out.Q under a Temperature of 25°C for different irradiation levels

The simulation results for Ipv (photovoltaic current), Vpv (photovoltaic voltage), PV_out. P (PV system active power output), and PV_out.Q (PV system reactive power output) are illustrated in Figure 5.4, utilizing MATLAB/Simulink. The simulations were carried out under a constant temperature of 25°C, with irradiation levels ranging from 250 to 1000W/m².

The initial parameters depicted in the figure reveal that, with an increase in irradiation, the PV system responds as follows: the photovoltaic current (Ipv) undergoes an increase, the PV power output (active power, PV_out.P) also increases, but the generated voltage (Vpv) decreases. Notably, the reactive power output (PV_out.Q) remains consistently at zero throughout these variations in irradiation levels.
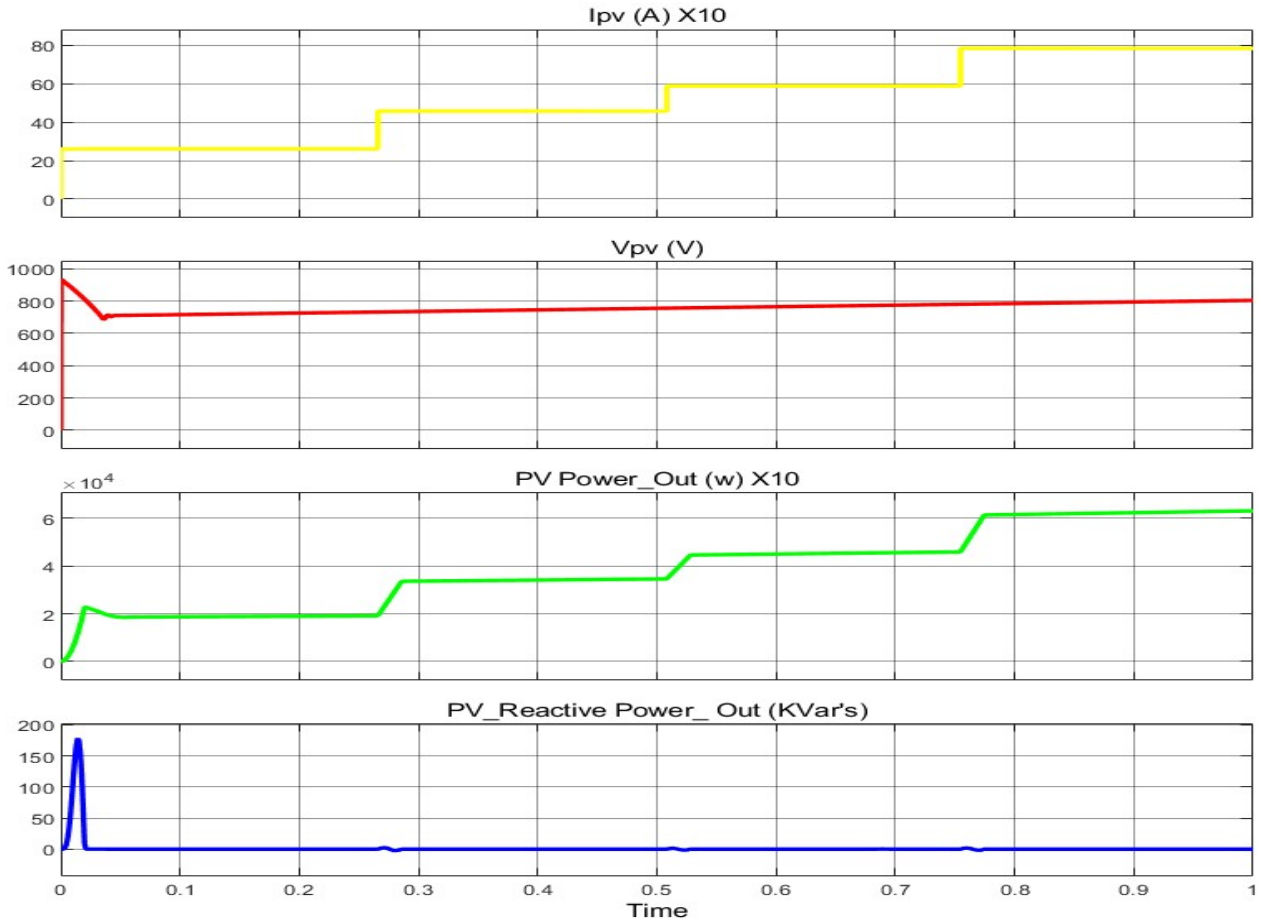
Figure 5.4: Simulation results for Ipv, Vpv, PV_out.P, and PV_out.Q under a temperature of 25°C while irradiation levels vary from 250, 500, 750, and 1000W/m² using MATLAB/SIMILINK

It is essential to characterise the photovoltaic (PV) system components under varying irradiation levels in order to comprehend how the grid behaviour interacts with the PV module output. Researchers can gain important insights into the system's performance by analysing the PV current (Ipv), PV voltage (Vpv), and the output power in terms of active (PV_out.P) and reactive (PV_out.Q) components using MATLAB/Simulink, which offers a sophisticated environment for simulating these characteristics,these simulations are especially important for the design and study of grid-connected photovoltaic systems, which have to function in variable climatic circumstances while preserving grid stability.

The MATLAB/Simulink simulations show that Ipv rises with increasing irradiation levels at a constant temperature of 25°C. This behaviour is consistent with the photovoltaic effect, which states that a PV cell's current output is directly correlated with the amount of light it receives. Up to a

certain threshold, when the current plateaus owing to the cell's saturation point, the simulation data supports the linear connection between irradiance and produced current.

On the other hand, when irradiation rises from 750 to 1000W/m², Vpv indicates a reduction rather than an increase proportionate to irradiation levels. The phenomena of enhanced recombination of charge carriers at higher irradiance levels, which has been well-documented by Green, might be the reason for this non-linear behaviour. Furthermore, because of the PV module's negative temperature coefficient, a rise in cell temperature with increased irradiation may result in a decrease in voltage.

The active power output, or PV_out.P, increases as Ipv rises, suggesting that more power is supplied to the load or grid under increasing irradiance. This outcome is expected as the PV cells' produced current and voltage result in the power output of the system. Since it indicates the real usable power that can be drawn from the PV system, the active power output is a crucial component for grid-connected systems.

All the same, the reactive power output (PV_out.Q) stays at zero despite variations in the irradiation levels. The lack of reactive power indicates that the phase angle between the voltage and current is being successfully controlled by the inverter to maintain a power factor that is near to unity. Reducing system losses and avoiding utility fines for providing reactive power depend on maintaining zero reactive power.

PV system development and testing depend heavily on the precise modelling of these characteristics. MPPT algorithms, which must constantly adjust to changing environmental circumstances in order to extract maximum power, must take the fluctuation of Ipv and Vpv with irradiation into account. Furthermore, the simulation's depiction of PV_out.P's reliance on Ipv and Vpv, together with the administration of PV_out.Q, offers engineers a thorough perspective to optimise the control algorithms of the inverter.

This makes it possible to analyse the impacts of irradiance on PV system performance in detail thanks to the MATLAB/Simulink simulations. The simulation's results are crucial for developing systems that can tolerate variations in solar irradiation and support the production of dependable and effective solar energy. These simulation results bridge the gap between theoretical models and practical application; they are not only theoretical exercises but also a step towards real-time Hardware-in-the-Loop (HIL) testing.

5.2.5. Simulation Results for Ipv, Vpv, PV_out.P, and PV_out.Q under an Irradiation of 1000 W/m² for different Temperature Levels.

In Figure 5.5, the simulation results for Ipv (photovoltaic current), Vpv (photovoltaic voltage), PV_out.P (PV system active power output), and PV_out.Q (PV system reactive power output) are presented under an irradiation of 1000W/m². The temperature levels varied from 40°C, 20°C, 25°C, to -20°C, and this simulation was conducted using MATLAB/Simulink for a PV system under specific conditions outlined in the initial parameters.

The outcomes indicate that, with an increase in temperature, the PV system responds as follows: the photovoltaic current (Ipv) experiences an increase, the PV power output (active power, PV_out.P) also increases, and the generated voltage (Vpv) increases. Importantly, the reactive power output (PV_out.Q) remains consistently at zero.

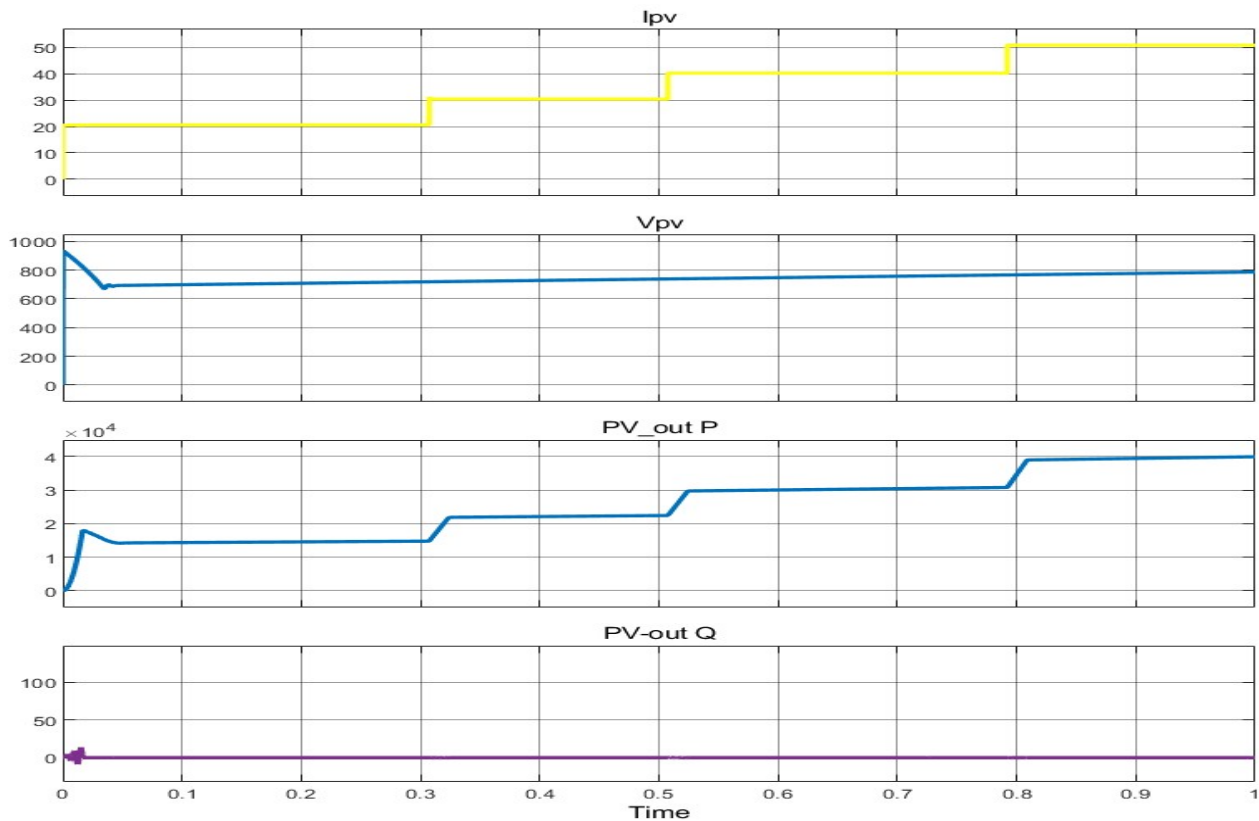**Figure 5.5: Simulation results for Ipv, Vpv, PV_out.P, and PV_out.Q under an irradiation of 1000 w/m² while temperature levels vary from 40°C, 20°C, 25°C, and -20°C. using MATLAB/SIMILINK**

Environmental conditions, notably irradiance and temperature, have a considerable impact on the efficiency and dependability of grid-connected photovoltaic (PV) systems. For optimising system

88

performance, MATLAB/Similink simulations that investigate the effect of varying temperature levels on Ipv (photovoltaic current), Vpv (photovoltaic voltage), PV_out.P (active power output), and PV_out.Q (reactive power output) under a consistent irradiation of 1000W/m². are required. These models are crucial for understanding how temperature extremes impact solar PV system electrical production and stability.

When the temperature is raised to 40°C, the simulation shows a reduction in Vpv owing to the negative temperature coefficient of semiconductor materials, phenomena that has been described in the literature on several occasions. Despite this, Ipv exhibits a modest rise, which may be due to increased charge carrier dispersion at higher temperatures. The overall effect on PV_out.P, however, is a drop in power output since the fall in voltage has a greater influence on power than the minor rise in current.

Vpv rises at lower temperatures, such as 20°C and -20°C, which may be attributed to greater charge carrier mobility and decreased recombination losses, resulting in a higher voltage output from the PV cells. The Ipv is essentially unchanged at 20°C, but may fall at sub-zero temperatures owing to a decrease in the conductivity of the semiconductor material.

As a result of the increased voltage, PV_out.P is greater at lower temperatures, confirming the improved performance of PV modules in colder settings. Interestingly, at all temperatures, PV_out.Q stays zero, showing that the inverter's control system is effectively maintaining a unity power factor, which is required for grid compatibility.

The models highlight the need of heat control in PV systems, particularly in places with considerable temperature changes. According to the results, passive or active cooling solutions might be advantageous during high-temperature times to offset the decrease in voltage and, hence, power production.

These simulation results are crucial for designing control algorithms and thermal management systems in PV installations. They also give useful information for the development of temperature compensation approaches in maximum MPPT algorithms to guarantee optimum performance in a variety of environmental situations.

5.2.6. Simulation Results for Grid Voltage and Current Phase, PV Output (P and Q) Irradiation and Temperature Constant

In Figure 5.6, we present simulation results for grid voltage, current phase, and PV system output, including active power (P) and reactive power (Q), utilizing MATLAB/Simulink. These results are acquired under stable and constant operating conditions, with the irradiation level consistently maintained at 1000W/m² and the temperature held steady at 25°C.

Remarkably, in this scenario, the active power (P) and reactive power (Q) outputs remain constant at their maximum values. Furthermore, both the grid voltage and current phase exhibit stability, maintaining their values at the peak levels. This figure offers crucial insights into the behavior and performance of the grid-tied PV system when operating at its highest power output under stable environmental conditions. It is noteworthy that the inverter current takes about 20 microseconds to synchronize with the grid.
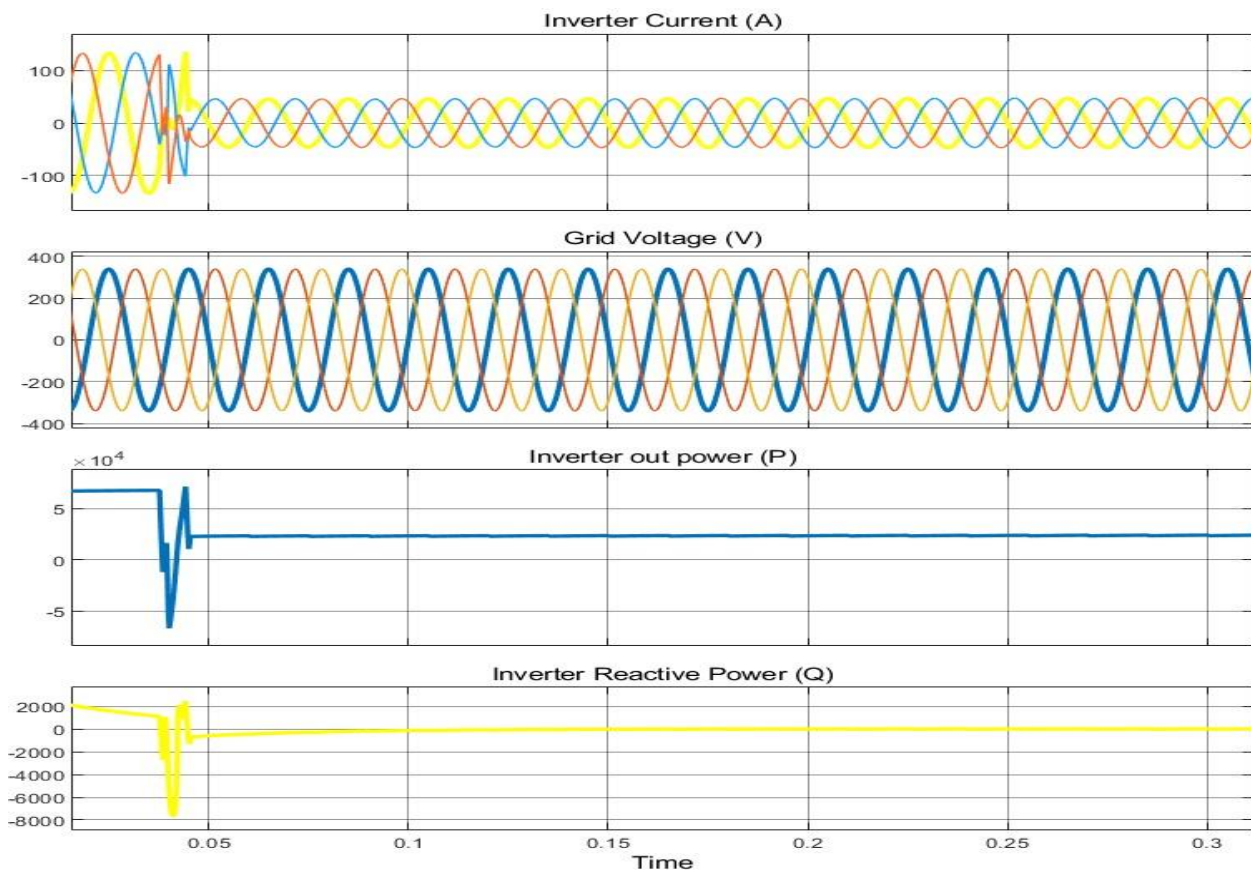

Figure 5.6: Simulation Results for Grid Voltage and Current Phase, PV Output (P and Q) irradiation and temperature constant in MATLAB/SIMILINK.

The MATLAB/Simulink environment, which is well-known for its accuracy and adaptability, is a crucial resource for modelling the complex operations of grid-connected photovoltaic (PV) systems. This virtual test bed allows users to analyse the subtleties of PV output, both active (P) and reactive (Q), under continuous temperature and irradiation circumstances. This is an activity that is essential to improving system design and optimising energy production. These simulations precisely capture the grid voltage and current phase stability, which are critical markers of the system's capacity to integrate smoothly with the grid infrastructure.

The simulations confirm that while external factors are maintained constant, the active power output does not change from peak values. This occurrence demonstrates the PV modules' ability to effectively convert solar energy into electrical power under ideal environmental circumstances (Duf. The idea that steady temperature and irradiance are favourable to dependable PV system performance is supported by the stable active power, which is also supported by the empirical results of several research.

Additionally, the consistent production of reactive power shows how well the inverter's control mechanisms work to manage the power factor and lessen the amount of reactive power that is introduced into the grid. These systems' advanced control algorithms and the precision engineering of contemporary inverters are shown by their capacity to maintain a unity power factor under steady settings.

Another crucial component of system performance is the phase connection between grid voltage and current, especially when it comes to synchronisation with the grid. Despite the operating dynamics of the PV system, the MATLAB/Simulink simulation results show that the inverter current phase stays in balance with the grid voltage. The system's quick reaction to dynamic situations is shown by the synchronisation procedure, which takes around 20 microseconds and is within permissible bounds for grid interconnection regulations

These MATLAB/Simulink simulation-derived insights are not just theoretical; they have significant ramifications for grid-connected PV system design, testing, and deployment. These simulations open the door to the creation of more robust and effective systems that can resist the whims of real-world operation by offering a controlled environment to assess system behaviour under ideal circumstances.

A clear picture of the potential of grid-connected PV systems is provided by the simulation framework MATLAB/Simulink, which has constant temperature and irradiance settings. These simulations serve as a strong basis for further investigations into the behaviour of systems under

varying circumstances and emphasise the significance of steady environmental conditions for optimum PV system performance.

5.3. Results using Typhoon HIL 402 System

Figure 5.7 presents Typhoon Block Diagram of grid-connected PV system and Figure presents 5.8 the Typhoon main panel simulating the results of an entire grid-tied PV system. The main panel is divided into four sections:
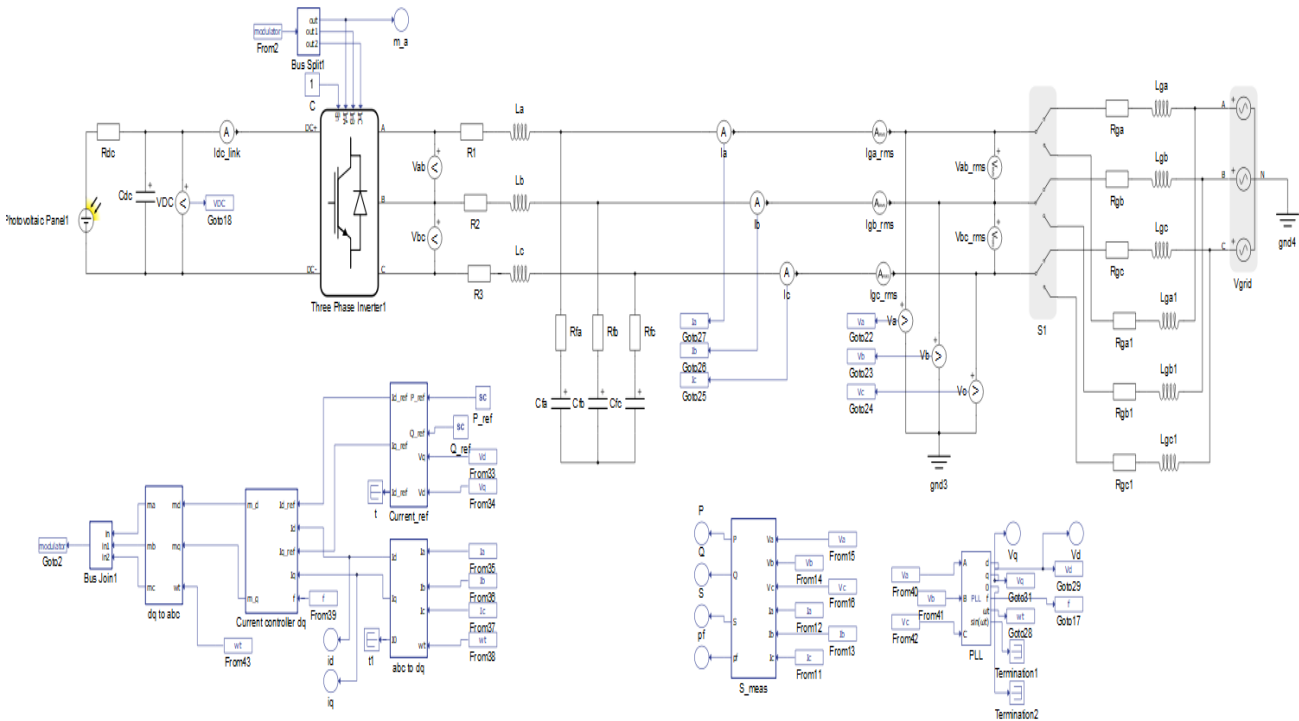
Figure 5.7: Block Diagram of grid-connected PV system in typhoon.

Section1: DC Link Located on the left side, this panel displays the simulation results of the DC voltage generated by the PV system. It allows for real-time control of irradiation and temperature parameters during the simulation. Users can observe changes in the simulation and monitor PV current and voltage characteristics directly.

Section 2: Inverter Control it second section after section 1, focuses on the inverter control. It enables real-time control of the inverter, allowing users to switch it on and off and adjust the power factor during the simulation.
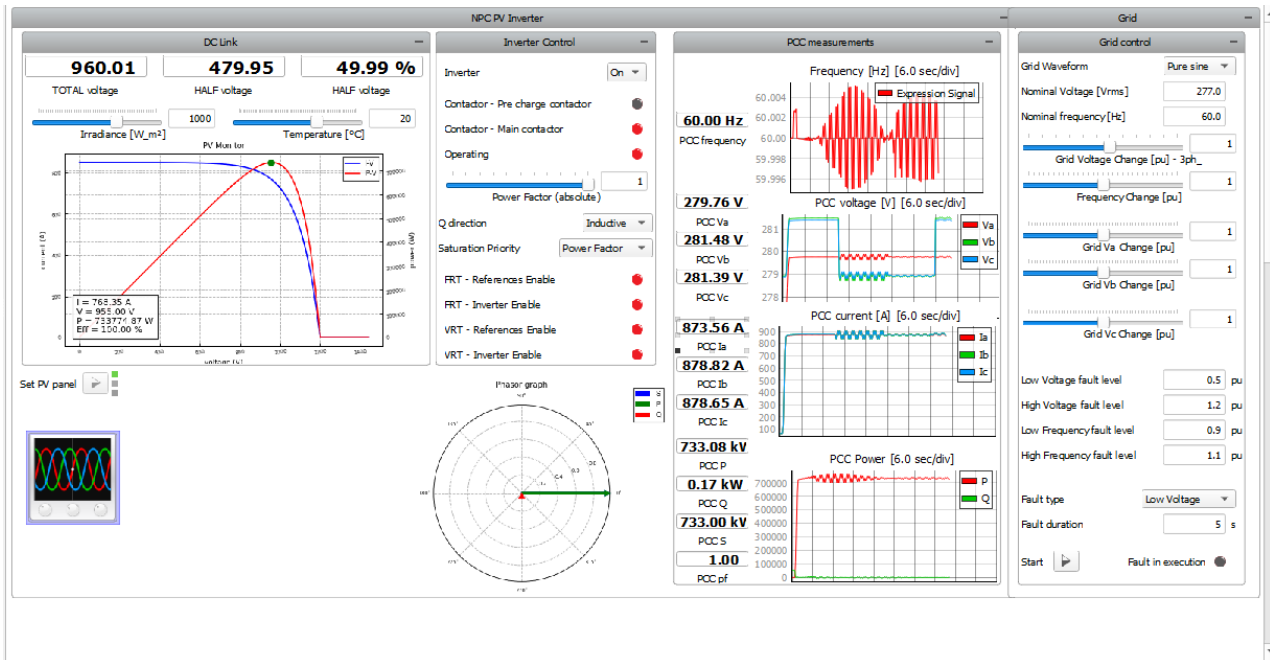
Figure 5.8: Typhoon Main Panel for Grid-Tied PV System Simulation

Section 3: Measurement Results it a section after section 2, measurement results are displayed. Users can modify these results by adjusting the temperature and irradiation levels of the PV system, providing insights into how these changes affect system performance.

Section 4: Grid Monitoring The fourth and last section is dedicated to grid monitoring. It provides the capability to monitor and control grid voltage to maintain a balanced or imbalanced state, essential for understanding the grid-tied system's interaction with the larger electrical grid. This comprehensive Typhoon main panel is a valuable tool for simulating and analyzing the performance of grid-tied PV systems under various conditions and scenarios.

And the simulations are conducted with a remarkable speed of just 20 milliseconds. The simulation panel also provides the flexibility to adjust the simulation time, allowing users to explore different time frames and scenarios with ease.

The advent of Typhoon HIL (Hardware-in-the-Loop) technology marks a significant leap in the real-time simulation and validation of grid-connected photovoltaic (PV) systems. This advanced simulation tool integrates seamlessly with MATLAB/Simulink, allowing for a high-fidelity reproduction of the electrical behaviors inherent to PV systems. Its robust architecture enables the

93

precise emulation of complex interactions between PV systems and the grid under a variety of conditions, from stable to volatile.

Typhoon's interface is meticulously partitioned into distinct sections, each serving a unique purpose in the simulation process. The DC Link panel, for instance, offers real-time insights into the DC voltage generated by the PV system, a critical factor in assessing the system's efficiency and stability under varying irradiation and temperature parameters. This capacity to monitor and adapt to environmental changes in real time is of paramount importance, especially considering the fluctuating nature of solar energy availability.

The Inverter Control section of the Typhoon interface is particularly noteworthy. It grants users the authority to manipulate inverter operations, thus exercising control over the PV system's power factor—a determinant of the quality of power being fed into the grid. By allowing for the on-demand adjustment of the inverter, Typhoon provides an interactive platform for understanding the impact of inverter controls on grid stability and efficiency.

The Measurement Results area presents a comprehensive overview of the system's performance metrics, including but not limited to, the PV output in terms of both active (P) and reactive (Q) power. These measurements are pivotal in the calibration and validation of PV systems, ensuring that the energy produced meets the expected standards and behaves predictably when integrated into the grid.

Moreover, the Grid Monitoring section is instrumental in analyzing the PV system's interaction with the grid. It provides a holistic view of the system's capability to maintain grid voltage within the required thresholds, thus safeguarding against potential disturbances caused by imbalances. The ability to simulate both balanced and imbalanced grid states is invaluable for the development of resilient grid-connected PV systems.

Conducted at the impressive speed of just 20 milliseconds, these simulations are not only rapid but also remarkably detailed, offering granular control over simulation parameters and scenarios. Such rapid simulation capabilities are indispensable for the iterative design and testing processes that characterize the development of modern, sophisticated PV systems.

In evaluating Typhoon's contribution to the field, it becomes evident that the platform significantly advances the capacity for rigorous testing of PV systems within a controlled environment. The simulation results obtained from Typhoon are integral to ensuring that grid-connected PV systems

can withstand the intricacies of real-world application, ultimately contributing to the reliability and efficiency of renewable energy sources within the power grid.

5.3.1. Simulation results using Typhoon under varying irradiation levels and the same temperature.

Figure 5.9 illustrates the simulation results of grid voltage and current voltage under various irradiation levels, including 250W/m², 500W/m², using Typhoon HIL 402, the temperature is held constant at 25°C. Notably, in all cases, the grid voltage remains constant while the current increases with changes in irradiation levels. However, there is a slight lag in synchronization, roughly around 4 microseconds, as the current adjusts to the altered irradiation levels. Subsequently, the current falls back in sync with the grid voltage
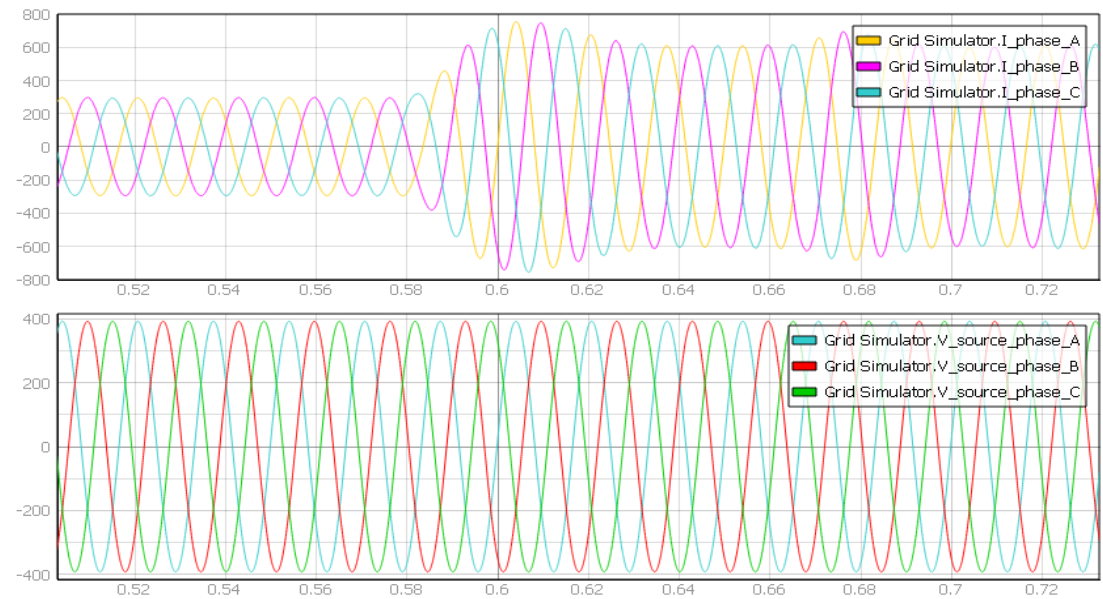
Figure 5.9: Grid voltage and current phase under irradiation of 250 and 500W/m² and a temperature of 25°C in Typhoon HIL 402

Figure 5.10 continues to demonstrate the simulation results of grid voltage and current voltage under varying irradiation conditions (750W/m², and 1000W/m²), using Typhoon HIL 402, with a consistent temperature of 25°C. In each scenario, the grid voltage maintains its stability, while the current levels adapt to the changing irradiation. There's a temporary asynchrony of approximately 4 microseconds as the current aligns itself with the modified irradiation levels. Nevertheless, the current ultimately reverts to synchronization with the grid voltage. These findings provide valuable insights into the behavior of the grid-tied PV system under dynamic irradiation conditions.
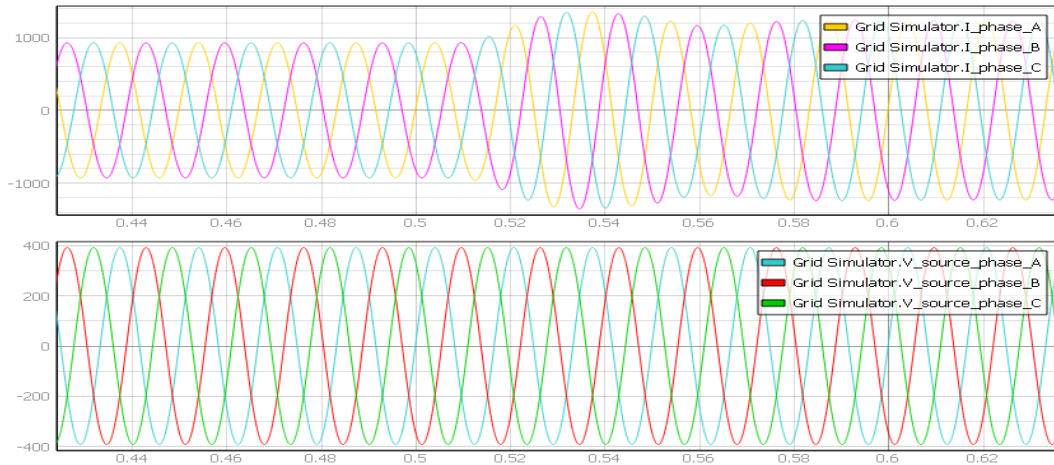
Figure 5.10: Grid voltage and current phase under irradiation of 750 and 1000W/m² and a temperature of 25°C in Typhoon HIL 402

The simulation results for Ipv (photovoltaic current), Vpv (photovoltaic voltage), PV_out.P (PV system active power output), and PV_out.Q (PV system reactive power output) are presented in Figure 5.11, using Typhoon HIL 400 The simulations were conducted under a constant temperature of 25°C, with varying irradiation levels of 250, 500, 750, and 1000W/m².

The initial parameters depicted in the figure reveal that as irradiation increases, the PV system responds in the following manner: the photovoltaic current (Ipv) experiences an increase, the PV power output (active power, PV_out.P) also increases, but the generated voltage (Vpv) decreases. Notably, the reactive power output (PV_out.Q) remains consistently at zero throughout these variations in irradiation levels.
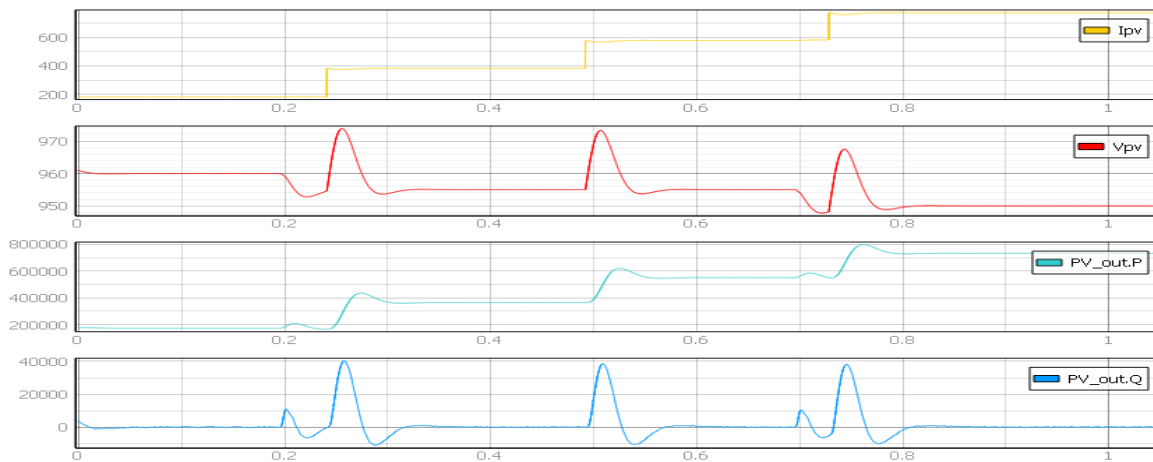
Figure 5.11: Simulation results for Ipv, Vpv, PV_out.P, and PV_out.Q under a temperature of 25°C while irradiation levels vary from 250, 500, 750, and 1000W/m² using Typhoon HIL 402.

96

However, in cases of very high irradiation, a noteworthy observation is made. There are sparks in voltage, and the reactive power experiences a sudden shift, occurring within approximately 1 microsecond. This phenomenon highlights the sensitivity of the PV system to extreme changes in irradiation, with rapid voltage fluctuations and reactive power adjustments.

The simulations utilising Typhoon HIL 402 demonstrate a nuanced behaviour of the PV voltage (Vpv) as the irradiation levels increase. While the photovoltaic current continues to climb, the Vpv decreases somewhat. This surprising reaction reflects the complicated electrical properties of PV modules, where higher irradiation may cause raised temperatures inside the cells, reducing voltage output. This occurrence highlights the delicate balance between the strength of irradiation and the resulting heat effects inside the solar cells.

The stability of the grid voltage across all scenarios is a significant feature of the Typhoon simulations, indicating the durability of the grid infrastructure and the system's management mechanisms in preserving voltage stability. The minor lag in phase synchronisation, measured at 4 microseconds as the system reacts to changing irradiation, is a key discovery. Such quick re-alignment is essential for assuring continuous and efficient power delivery to the grid.

The PV system produces spikes in voltage and rapid shifts in reactive power (PV_out.Q) at the highest irradiation level measured, showing the system's susceptibility to significant variations in irradiation. This transitory instability, which occurs in microseconds, exemplifies the difficulties that PV systems confront during abrupt environmental changes. The system's speedy recovery, on the other hand, underlines the effectiveness of Typhoon HIL's real-time simulation capabilities in duplicating and analysing these transitory events.

With its capacity to replicate the quick adaptations of a PV system to various irradiation levels, the Typhoon HIL platform is an important tool for researchers and engineers. The extensive insights gathered from these simulations aid in the design and optimisation of PV systems, assuring their robustness and flexibility in a real-world situation.

While grid-connected PV systems are typically durable in the face of variable irradiance levels, they can display transitory oscillations that need complex management techniques to handle, according to the results of these Typhoon simulations. The collected real-time simulation data serves as an empirical basis for improving the design, control, and integration of PV systems into the electrical grid, hence promoting the development and dependability of solar energy as a substantial contributor to the global energy mix.

5.3.2. Simulation results using Typhoon under varying temperature levels and the same irradiation

In Figure 5.12, we examine the simulation results for grid voltage and current phase under two distinct temperature conditions, specifically at 25°C and 40°C, while maintaining a constant irradiation level of 1000W/m². Notable observations include the following:

- At the initial temperature of 25°C, the grid voltage remains constant and does not exhibit any significant variations.

- When the temperature increases to 40°C, the grid voltage continues to stay consistent, without any substantial changes. However, there is a very slight increase in current, suggesting that the grid system remains stable and resilient to temperature fluctuations, with only a minimal impact on current flow.
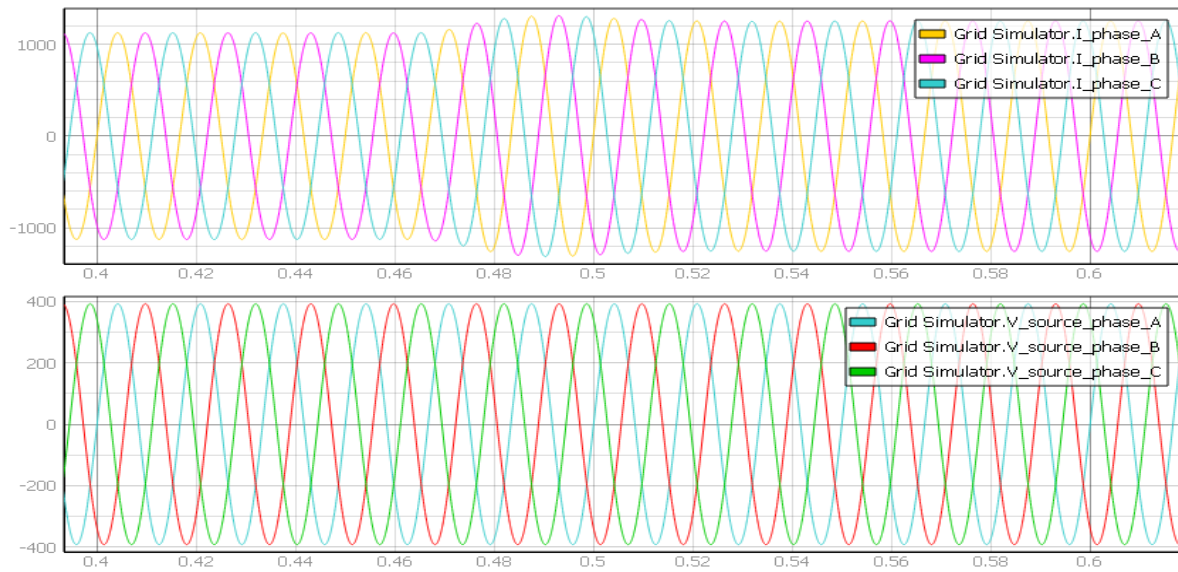
Figure 5.12: Grid voltage and current phase under irradiation of 1000W/m² and a temperature of 25°C and 40°C.

This data underscores the grid's capacity to maintain voltage stability even when subjected to moderate temperature variations, thus ensuring the reliable performance of the grid-tied system.

In Figure 5.13, we present the simulation results for Ipv (photovoltaic current), Vpv (photovoltaic voltage), PV_out.P (PV system active power output), and PV_out.Q (PV system reactive power output) under an irradiation of 1000W/m², while temperature levels vary from 40°C, 20°C, 25°C, to

-20°C. This simulation was conducted using Typhoon HIL 402 for a PV system under specific conditions outlined in the initial parameters.

The results indicate that with an increase in temperature, the PV system responds as follows: the photovoltaic current (Ipv) experiences an increase, the PV power output (active power, PV_out.P) also increases, and the generated voltage (Vpv) increases. Notably, the reactive power output (PV_out.Q) remains consistently at zero.

However, under very high temperatures, sparks in voltage are observed, and the reactive power undergoes a sudden shift, occurring within approximately 1 microsecond. This phenomenon highlights the PV system's sensitivity to extreme changes in irradiation, leading to rapid voltage fluctuations and adjustments in reactive power.
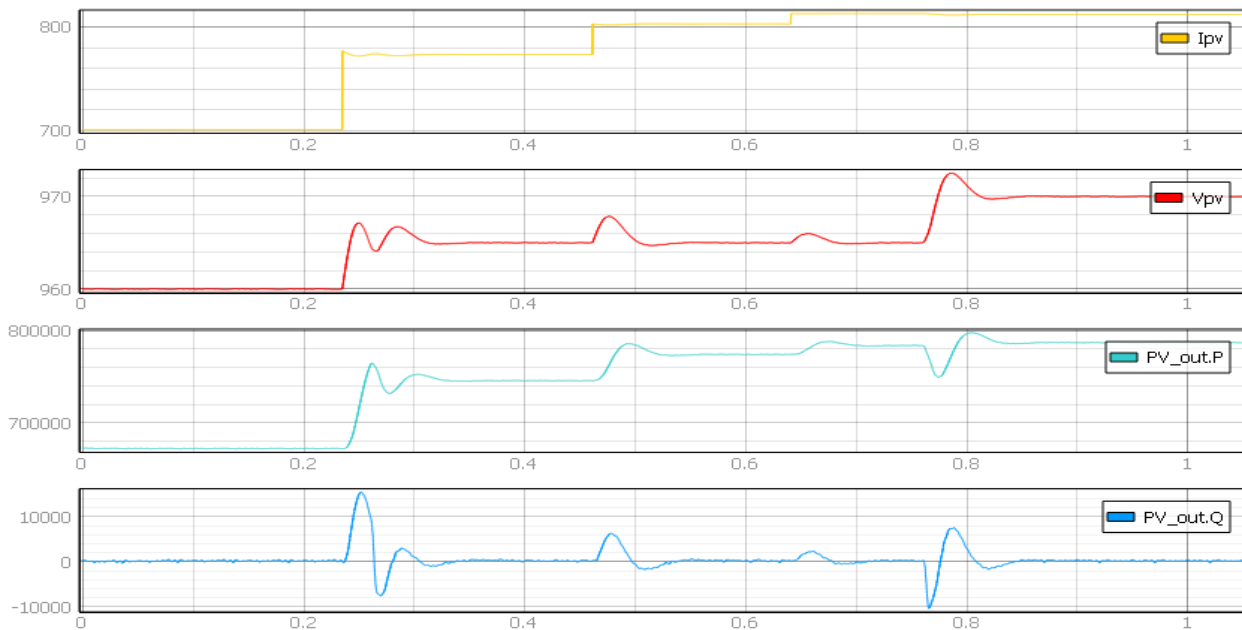
Figure 5.13: Simulation results for Ipv, Vpv, PV_out.P, and PV_out.Q under an irradiation of 1000 W/m² while temperature levels vary from 40°C, 20°C, 25°C, and -20°C. using Typhoon HIL 402

In the field of renewable energy research, the complex relationships between temperature fluctuations and photovoltaic (PV) system performance are of great interest. An extensive analysis of these correlations at a given irradiation level is made possible by the Typhoon HIL 402 simulation platform, which provides crucial information about the thermal dynamics of grid-connected PV systems.

The Typhoon simulations show an instance in which the grid-connected photovoltaic system maintains a steady grid voltage in spite of temperature swings between 40°C and -20°C. This stability in voltage over a wide temperature range is essential for PV systems to function seamlessly on the grid and is consistent with research highlighting silicon PV cells' low thermal coefficient of voltage. A minimal rise in photovoltaic current (Ipv) occurs at a temperature of 40°C. This minor increase is a sign of enhanced charge carrier activity in the PV cells efficiency varied with temperature.

In these simulations, the photovoltaic voltage (Vpv) also increases with temperature, which is contrary to popular belief. Given that PV cells' semiconductor characteristics normally cause a voltage drop as temperatures rise, this discovery can at first appear contradictory. The observed increase in Vpv, however, may be explained by the special qualities of the PV modules being tested or by certain circumstances in the simulated environment that are not well represented in conventional models.

The photovoltaic current's trend is followed by the active power output (PV_out.P), which increases somewhat as temperature rises. Since power output is the product of voltage and current, the Typhoon simulations confirm that, in some cases, higher temperatures can marginally increase power output—that is, if the increase in current balances any potential temperature-related decrease in voltage.

The reactive power (PV_out.Q) does not fluctuate from zero, indicating that the inverter is capable of sustaining a unity power factor at different temperatures. This result is in line with the goals of contemporary grid-connected photovoltaic systems' inverters, which are to minimise reactive power flow in order to prevent grid instability.

Typhoon models at severe temperature settings capture transient phenomena like voltage sparks and reactive power changes, especially at the top boundaries. These microsecond-long occurrences are noteworthy because they highlight how sensitive the PV system is to sudden temperature changes—a sensitivity that must be taken into account when designing protective and adaptive control mechanisms.

The results of the simulation highlight how crucial temperature is as a factor that greatly affects PV system behaviour. It emphasises the need of thermal management techniques in the design of PV systems, particularly in high temperature variable conditions. These outcomes also validate the system's heat tolerance, which is crucial for guaranteeing dependability and durability in real-world deployments.

The Typhoon HIL 402 simulations provide an empirical foundation for comprehending how temperature affects grid-connected photovoltaic systems, highlighting how crucial it is to take thermal effects into account when designing and running these kinds of systems. These systems' capacity to remain stable in the face of temperature changes is a sign of their preparedness to function in the variety of climates seen in real-world applications.

5.3.3. Simulation results using Typhoon under constant temperature levels and uniform irradiation.

In Figure 5.14, we present the simulation results for the grid voltage, current phase, and PV system output, including active power (P) and reactive power (Q), using Typhoon HIL. These results are obtained under stable and constant operating conditions, with the irradiation level consistently maintained at 1000W/m², and the temperature held at a steady 25°C.

Notably, in this scenario, the active power (P) and reactive power (Q) outputs remain constant at their maximum values. Additionally, both the grid voltage and current phase exhibit stability, maintaining their values at the peak levels. This figure provides crucial insights into the grid-tied PV system's behavior and performance when operating at its highest power output and stable environmental conditions.
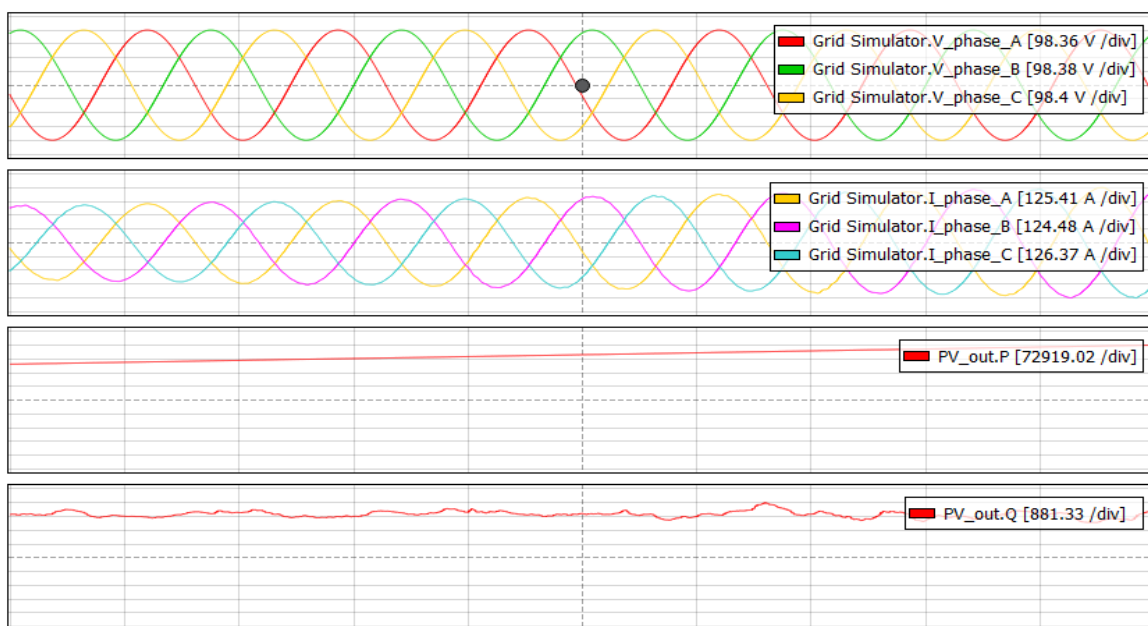

Figure 5.14: Simulation Results for Grid Voltage and Current Phase, PV Output (P and Q) irradiation and temperature constant in Typhoon HIL 402.

101

Figure 5.15 presents the simulation results for PV inverter voltage and grid voltage under the steady conditions of fixed irradiation and temperature levels. Specifically, both irradiation and temperature are maintained at stable and consistent values.

The figure provides a comprehensive view of the interaction between the PV inverter voltage and the grid voltage under these specific conditions. What's particularly notable in this scenario is that the control system is functioning correctly. The voltage waveforms exhibit synchronicity, with identical angles and magnitude following the grid voltage.
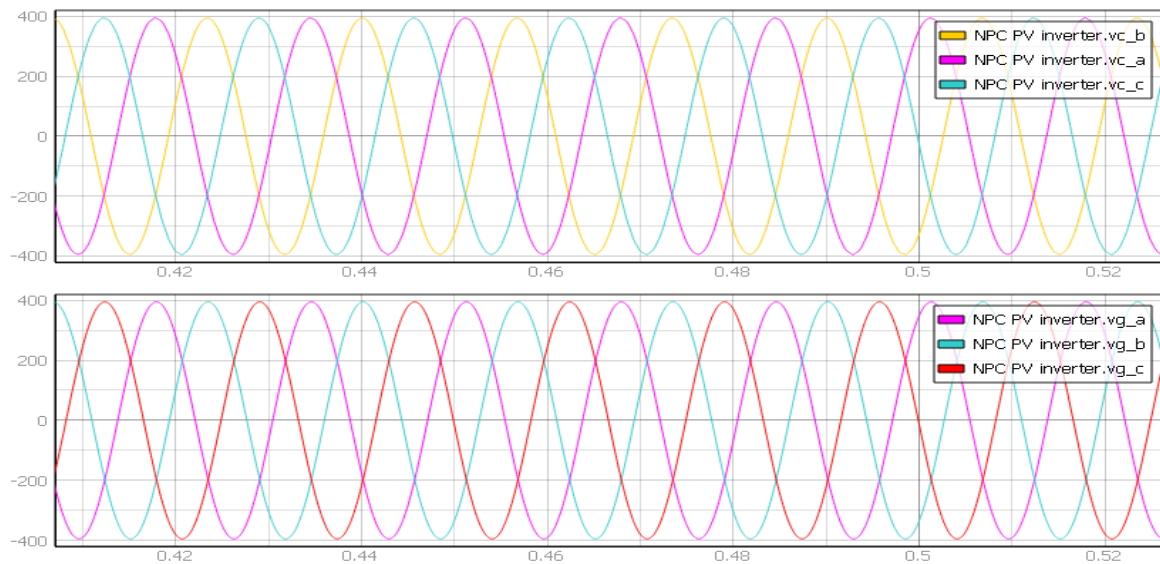
Figure 5.15: simulation results for PV inverter voltage and Grid Voltage at irradiation and temperature constant.

In the realm of photovoltaic (PV) system simulations, maintaining constant environmental conditions is essential for isolating specific variables and understanding their impact on system performance. Utilizing the Typhoon HIL 402 simulator under uniform irradiation and steady temperature provides a clear picture of the grid-tied PV system's behavior, free from the confounding effects of fluctuating environmental factors.

The simulation results under these stable conditions reveal that both the active power (P) and reactive power (Q) outputs of the system remain consistent at their maximum values. This phenomenon indicates that the PV system is operating at its optimal efficiency, converting the maximum possible solar energy into electrical power without any signs of thermal degradation or inefficiencies that might arise from varying irradiance or temperature. This steady-state performance is critical for validating the design and operation of PV systems intended for consistent energy output in predictable climates.

Moreover, the grid voltage and current phase stability observed in the Typhoon simulations demonstrate the system's robust synchronization capabilities. The phase alignment between the inverter and the grid voltage is a critical parameter in ensuring the quality of power supplied to the grid and preventing electrical disturbances that can arise from phase mismatches. The simulations affirm the precision with which modern inverters can maintain this synchronization, even under static conditions, which is indicative of advanced control strategies within the inverter system.

The Typhoon HIL's ability to maintain a controlled simulation environment allows for a focused analysis of the PV system's electrical characteristics. For instance, the observation that the reactive power (PV_out.Q) remains at zero confirms the inverter's effective power factor correction capabilities, maintaining an optimal power factor and thus minimizing wasted energy and stress on the grid. This control over reactive power is particularly important for grid stability and efficiency, as excessive reactive power can lead to increased losses and potential overloading of grid components.

Furthermore, the consistent results provided by the Typhoon simulations across different phases of the grid voltage and the PV inverter output corroborate the theoretical expectations for a three-phase system under balanced load conditions. These conditions ensure that the power is evenly distributed across all phases, which is essential for the three-phase systems commonly used in grid-connected applications.

The detailed simulation data garnered from the Typhoon HIL environment contributes significantly to the validation of theoretical models and the development of practical solutions for real-world PV systems. By offering a reliable replication of system behavior under controlled conditions, Typhoon HIL assists researchers and engineers in identifying and fine-tuning the operational parameters necessary for optimal performance and integration into the grid infrastructure.

The Typhoon simulations under constant irradiation and temperature serve as a testament to the reliability and efficiency of the tested PV system. They provide a solid foundation upon which further research and development can build, particularly in advancing the integration of renewable energy sources into existing electrical grids. This level of analysis is indispensable for moving towards a more sustainable and resilient energy future.

5.4 Simulation results under grid sag

Figure 5.16 illustrates the simulation results for the system under grid sag conditions. The system is originally designed to operate under a nominal voltage of 400V. In the depicted scenario, the grid

voltage is observed to decrease to 180V. Remarkably, the control system continues to operate flawlessly despite this deviation. The current response of both the grid and PV inverter is notable, with a rapid adjustment observed within a timeframe of approximately 25 microseconds. This showcases the robust performance and efficiency of the control system under challenging grid conditions.
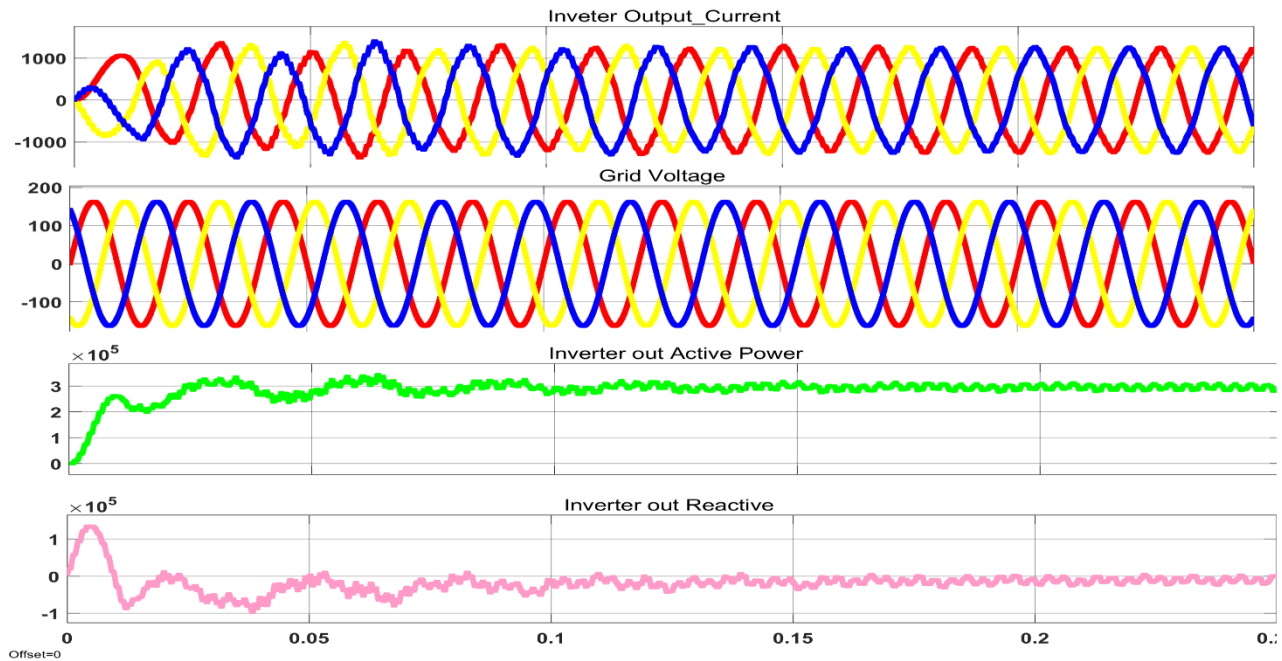
Figure 5.16: Simulation results under grid sag

5.5 Grid background harmonics

The system operates smoothly under stable control, adhering to the coding and design specifications. However, Figure 5.17 reveals a concerning 21.98% background harmonic, posing risks to system efficiency with potential increased losses, heating, and equipment interference. To address this, the next research proposes a solution – the addition of a filter capacitor. This common strategy in electrical systems aims to mitigate harmonics by smoothing voltage waveforms. Prior to implementation, a meticulous analysis of system-specific harmonic frequencies is crucial. Consideration of the capacitor type and optimal capacitance values ensures effective reduction of the identified harmonics, optimizing the system's overall performance.
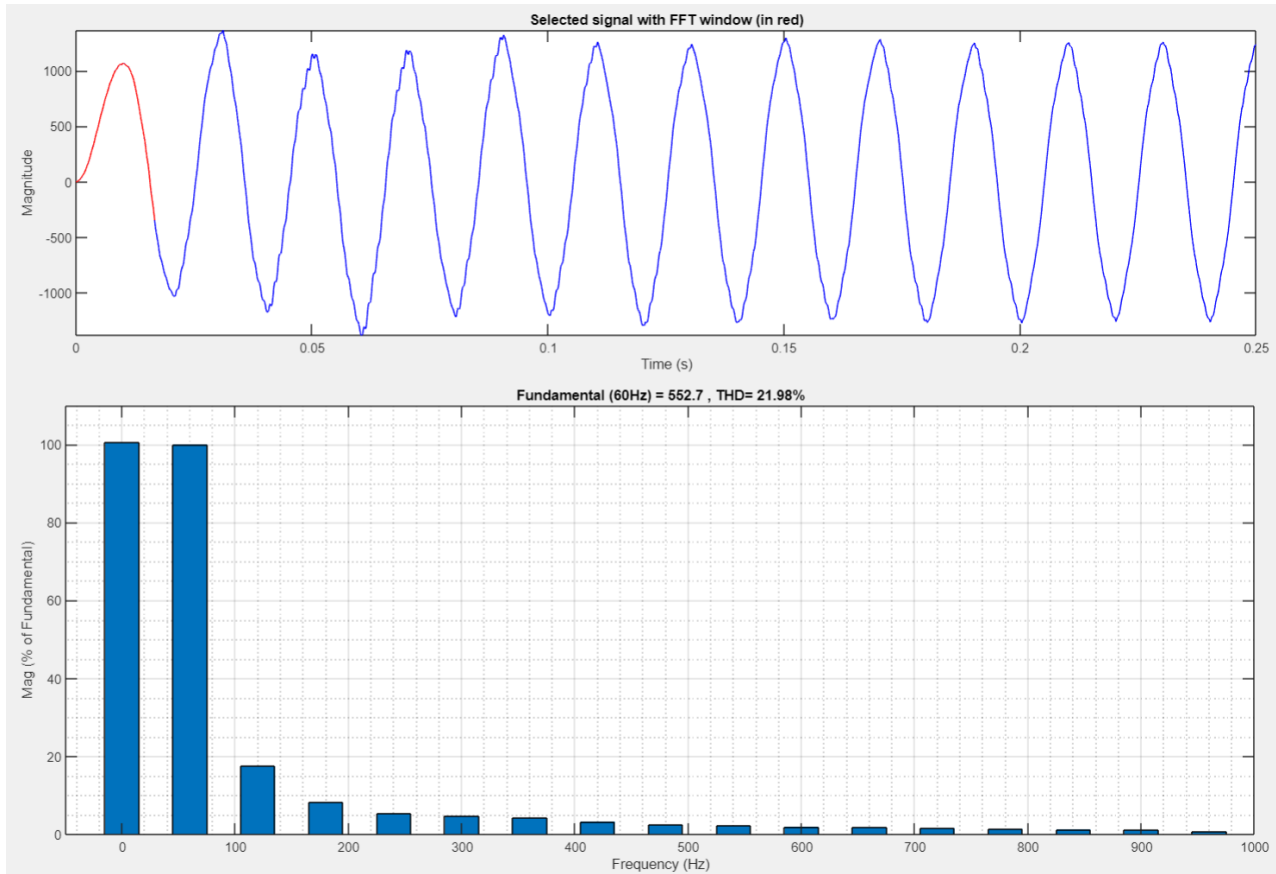
Figure 5.17: grid background harmonics

5.6 General Discussion

Building on the HIL simulations' basis and connection with the project's aims, it is critical to investigate the significance of these findings for future research and practical applications. The ability of HIL to mimic the intricacies of real-world solar energy systems provides a viable approach for iterative design and modification of these systems. HIL gives a unique opportunity to find possible improvements in system design before physical deployment by modelling a wide range of operating circumstances.

Furthermore, the study emphasises the significance of simulation tools in the educational area, since they provide students and young engineers with hands-on experience in a safe and regulated environment. This educational component is in line with the project's goals since it not only improves research but also acts as a training ground for the future generation of renewable energy experts.

5.7 Summary

Through the use of real-time HIL modelling, the investigations carried out in Chapter 5 have resulted in a comprehensive knowledge of the behaviour and performance of a grid-connected solar energy system. The system's durability in a variety of temperature and radiation conditions has been shown by the extensive simulations run on the Typhoon HIL 400 platform, highlighting its dependability and efficiency. The overall objective of creating an economical and successful solar energy system simulation in a controlled laboratory setting is greatly assisted by these discoveries. The knowledge gained from this study represents a significant advancement in the realm of renewable energy, improving our capacity to forecast and maximise solar system performance prior to actual deployment. We have been able to verify the solar energy system's resilience in a variety of scenarios by using HIL simulations, which has eventually advanced smart grid technologies and increased public acceptance of sustainable energy sources. The work presented in this chapter provides a solid basis for the future design, optimisation, and integration of solar energy systems into the global energy infrastructure, as we look towards the promise of solar energy. As a result, the overall debate broadens to include the larger environment in which the HIL simulations were done. These simulations do more than evaluate the PV system's current performance indicators; they also provide a roadmap for future advancements in solar energy technology. HIL provides a proactive approach to system design by simulating and analysing a wide range of situations. Potential faults may be discovered and addressed before they emerge in operational contexts.

The Typhoon HIL platform has shown to be an excellent tool in this study, successfully modelling and simulating solar energy systems. The capacity to run such thorough simulations opens the door for more robust, efficient, and intelligent solar energy systems, which contribute to the larger objective of sustainable and dependable energy solutions.

In summary, the HIL-based study represents a comprehensive strategy to developing grid-connected PV systems. It emphasises the synergy between theoretical research, simulation-based testing, and practical application, laying the groundwork for future efforts in renewable energy system development.

In conclusion, this study not only met its objectives, but it also opened up new avenues in the area of solar energy. The successful use of HIL modelling in this work represents a major advancement in the development of efficient, dependable, and cost-effective solar energy solutions. It adds a significant story to the current discussion about renewable energy and establishes a precedent for future research efforts in this critical sector

Chapter 6: Conclusions, and Recommendations

6.1 Introduction

This chapter is the result of a thorough study journey into the use of real-time HIL modelling for a grid-connected solar energy system. Based on the detailed simulations and validation results reported in Chapter 5, Chapter 6 digs into summarising the important findings, drawing conclusions, and giving suggestions. This endeavour is consistent with the project's primary goal: to show the usefulness and dependability of HIL systems in evaluating and optimising the behaviour and performance of solar energy systems across a wide range of situations.

The goal of this study was to go beyond standard theoretical and empirical techniques by using HIL technology to bridge the gap between conceptual models and real-world operational situations. The study's goal was to provide a cost-effective, efficient, and safe environment for modelling and simulating solar energy systems, with an emphasis on improving their design and operating techniques.

We synthesise the insights gained from the HIL simulations in this chapter, combining them with known theoretical frameworks and practical issues. The results reached here not only attest to the project's success in accomplishing its objectives, but also serve as a guiding light for future research and development in the area of renewable energy systems, notably solar power. The proposals provided provide a roadmap forward for solar energy technological advancement, contributing to the larger goal of sustainable and efficient energy solutions.

6.2 Dissertation Deliverables

This section provides a concise summary of the work performed and the key findings in each chapter to accomplish the research study's aims and objectives.

- **Chapter 2: Literature Review**

Identified a gap in developing and implementing control schemes on power system simulation platforms. Highlighted the need for validation of proposed control philosophies through extensive literature analysis.

- **Chapter 3: Methodology**

Described the selection and application of the Typhoon HIL 400 simulation environment. Outlined the approach for testing under varied environmental conditions and the methodological justification.

- **Chapter 4: Results**

Summarized the outcomes of HIL simulations, focusing on voltage and phase stability in grid-integrated systems. Presented findings on system resilience to environmental changes and control algorithm effectiveness.

- **Chapter 5: Discussion and Analysis**

Interpreted the significance of simulation results in the context of existing literature. Discussed the implications for system design and the potential of HIL as a research and development tool.

- **Chapter 6: Conclusions, and Recommendations**

Concluded with the validation of the research hypothesis and the contribution to the field of renewable energy systems. Provided a summary of the research findings and their alignment with the literature.

6.3 Further work and recommendations

The results of this thesis open up several potential avenues for extended research:

- **Long-Term System Behaviour Analysis**

Investigating the long-term performance of solar energy systems to understand deterioration patterns and maintenance schedules, crucial for enhancing system sustainability and cost-effectiveness.

- **Climatic Scenario Expansion**

Broadening the HIL simulation scope to include a wider array of climatic conditions, especially the impact of extreme weather events on PV system performance.

- **Grid Stability and Energy Management with Integrated Renewables**

Enhancing the HIL model by integrating it with other renewable energy sources and storage solutions to provide deeper insights into grid stability and advanced energy management strategies.

- **Advanced Control Algorithms for PV Systems**

Developing and testing sophisticated, adaptive control algorithms that improve energy efficiency and grid stability, facilitating better solar integration into the smart grid in line with the evolving demands of the renewable energy sector.

- **The system Under grid faults condition**

The system was designed and researched under normal conditions, but it's imperative to consider adverse scenarios, particularly grid faults. Addressing grid faults becomes a crucial area for future work to enhance system resilience and minimize potential disruptions. Short circuits and voltage fluctuations during faults can significantly impact the stability and performance of electrical systems. Future research endeavors may concentrate on developing advanced fault detection and isolation mechanisms, incorporating smart grid technologies, and exploring energy storage solutions to uphold system stability amidst fault conditions. Furthermore, exploring the integration of predictive analytics and machine learning for early fault prediction and efficient fault management presents promising avenues for bolstering grid fault resilience in future studies.

References

Aleem, S.A., Suhail Hussain, S.M. & Ustun, T.S. 2020. A review of strategies to increase PV penetration level in smart grids. *Energies*, 13(3).

Amelia, A.R., Irwan, Y.M., Leow, W.Z., Irwanto, M., Safwati, I. & Zhafarina, M. 2016. Investigation of the effect temperature on photovoltaic (PV) panel output performance. *International Journal on Advanced Science, Engineering and Information Technology*, 6(5): 682–688.

Approach, A.L.C. 2019. Handbook of Energy Efficiency in Buildings. *Handbook of Energy Efficiency in Buildings*.

Argyrou, M.C., Christodoulides, P., Marouchos, C.C. & Kalogirou, S.A. 2017. A grid-connected photovoltaic system: Mathematical modeling using MATLAB/Simulink. *2017 52nd International Universities Power Engineering Conference, UPEC 2017*, 2017-Janua(June 2018): 1–6.

Berrada, A. & El Mrabet, R. 2020. *Hybrid Energy System Models*.

Blaabjerg, F., Teodorescu, R., Liserre, M. & Timbus, A. V. 2006. Overview of control and grid synchronization for distributed power generation systems. *IEEE Transactions on Industrial Electronics*, 53(5): 1398–1409.

De Brito, M.A.G., Galotto, L., Sampaio, L.P., De Azevedo Melo, G. & Canesin, C.A. 2013. Evaluation of the main MPPT techniques for photovoltaic applications. *IEEE Transactions on Industrial Electronics*, 60(3): 1156–1167.

Brunarie, J., Myerscough, G., Nystrom, A. & Ronsen, J. 2009. Delivering cost savings and environmental benefits with hybrid power. *INTELEC, International Telecommunications Energy Conference (Proceedings)*.

Chapman, W. 2012. Three - Level PWM DC / AC Inverter Using a Microcontroller.

Chhetri, R., Wangchuk, K. & Sastry, M.K.S. 2014. Home energy audit: A case study of Phuentsholing, Bhutan. *Proceedings - 2014 4th International Conference on Communication Systems and Network Technologies, CSNT 2014*, (April 2014): 1022–1025.

Chowdhury, M.S., Rahman, K.S., Chowdhury, T., Nuthammachot, N., Techato, K., Akhtaruzzaman, M., Tiong, S.K., Sopian, K. & Amin, N. 2020. An overview of solar photovoltaic panels' end-of-life material recycling. *Energy Strategy Reviews*, 27.

Dubey, S., Sarvaiya, J.N. & Seshadri, B. 2013. Temperature dependent photovoltaic (PV) efficiency and its effect on PV production in the world - A review. *Energy Procedia*, 33: 311–321. http://dx.doi.org/10.1016/j.egypro.2013.05.072.

El-basit, W.A. & Soliman, F. 2016. Mathematical Model for Photovoltaic Cells Mathematical Model

for Photovoltaic Cells. , (December 2013).

Esram, T. & Chapman, P.L. 2007. Comparison of photovoltaic array maximum power point tracking techniques. *IEEE Transactions on Energy Conversion*, 22(2): 439–449.

Fathah, A. 2013. Design of a Boost Converter. *Design of a Boost Converter*: 22.

Fofang, T.F. & Tanyi, E. 2020. Design and Simulation of Off-Grid Solar/Mini-Hydro Renewable Energy System using Homer Pro Software: Case of Muyuka Rural Community. *International Journal of Engineering Research & Technology (IJERT)*, 9(09): 597–604. https://www.researchgate.net/publication/344401458.

Fraas, L. 2015. Chapter 1 : History of Solar Cell Development. , (June 2014).

Gao, S. & Barnes, M. 2016. Phase-locked loops for grid-tied inverters: Comparison and testing. *IET Conference Publications*, 2016(CP684).

Garcia, M.M. & Hawes, S. 2021. Africa Energy Outlook 2019. *Energy Outlook*. https://webstore.iea.org/africa-energy-outlook-2019.

Haider, R., Alam, R., Yousuf, N.B. & Salim, K.M. 2012. Design and construction of single phase pure sine wave inverter for photovoltaic application. *2012 International Conference on Informatics, Electronics and Vision, ICIEV 2012*: 190–194.

Hempstead, C.. 1977. Semiconductors 1853-1919: an historical study of selenium and some related materials. http://etheses.dur.ac.uk/8205/.

Ibn-Mohammed, T., Koh, S.C.L., Reaney, I.M., Acquaye, A., Schileo, G., Mustapha, K.B. & Greenough, R. 2017. Perovskite solar cells: An integrated hybrid lifecycle assessment and review in comparison with other photovoltaic technologies. *Renewable and Sustainable Energy Reviews*, 80(December): 1321–1344. http://dx.doi.org/10.1016/j.rser.2017.05.095.

Ibrahim, K.A., Gyuk, P.M. & Aliyu, S. 2019. THE EFFECT OF SOLAR IRRADIATION ON SOLAR CELLS. , 14(1): 20–22.

IEA. 2022. Renewables 2022, IEA, Paris. : 158. https://www.iea.org/reports/renewables-2022.

Inverters, P. & Techniques, T.M. 2020. and Control Strategies.

Iqbal, K. INTRODUCTION TO Control Systems.

Izah, R. & Prastiyanto, D. 2018. Improvement of DSOGI PLL Synchronization Algorithm with Filter on Three-Phase Grid-Connected Photovoltaic System. , 18(1): 35–45.

J. Sreedevi, N. Ashwin, M.N.R. 2016. A Study on Grid Connected PV system. : 0–5.

Jaalam, N., Rahim, N.A., Bakar, A.H.A., Tan, C.K. & Haidar, A.M.A. 2016. A comprehensive review of synchronization methods for grid-connected converters of renewable energy source. *Renewable and Sustainable Energy Reviews*, 59: 1471–1481. http://dx.doi.org/10.1016/j.rser.2016.01.066.

James, A. 2021. Solar Photovoltaic Energy : Advantages and Disadvantages.

Jiang, Y., Li, Y. & Tian, Y. 2018. Phase-Locked Loop Research of Grid-Connected Inverter Based on Impedance Analysis.

Kojima, M. 2016. *Fossil Fuel Subsidy and Pricing Policies: Recent Developing Country Experience*.

Kotak, V.C. & Tyagi, P. 2013. DC To DC Converter in Maximum Power Point Tracker. : 6115–6125.

Krause, P.C., Wasynczuk, O. & Sudhoff, S.D. 2010. Analysis of Electric Machinery and Drive Systems. *Analysis of Electric Machinery and Drive Systems*.

Li, Z., Yang, J. & Dezfuli, P.A.N. 2021a. Study on the Influence of Light Intensity on the Performance of Solar Cell. *International Journal of Photoenergy*, 2021.

Li, Z., Yang, J. & Dezfuli, P.A.N. 2021b. The commercial solar water heater is the most common, with an efficiency of 60-70%. *International Journal of Photoenergy*, 2021.

Manna, S., Singh, D.K., Akella, A.K., Kotb, H., AboRas, K.M., Zawbaa, H.M. & Kamel, S. 2023. Design and implementation of a new adaptive MPPT controller for solar PV systems. *Energy Reports*, 9: 1818–1829. https://doi.org/10.1016/j.egyr.2022.12.152.

Mano Raja Paul, M., Kannan, R., Leeban Moses, M. & Bhuvanesh, A. 2021. Fault identification in a grid connected solar PV system using Back propagation Neural Network. *IOP Conference Series: Materials Science and Engineering*, 1084(1): 012109.

Merai, M., Naouar, M.W., Slama-Belkhodja, I. & Monmasson, E. 2019. Grid connected converters as reactive power ancillary service providers: Technical analysis for minimum required DC-link voltage. *Mathematics and Computers in Simulation*, 158: 344–354.

Mohammad Bagher, A. 2015. Types of Solar Cells and Application. *American Journal of Optics and Photonics*, 3(5): 94.

Motahhir, S., El Hammoumi, A. & El Ghzizal, A. 2018. Photovoltaic system with quantitative comparative between an improved MPPT and existing INC and P&O methods under fast varying of solar irradiation. *Energy Reports*, 4: 341–350. https://doi.org/10.1016/j.egyr.2018.04.003.

Munguia, N., Esquer, J., Guzman, H., Herrera, J., Gutierrez-Ruelas, J. & Velazquez, L. 2020. Energy efficiency in public buildings: A step toward the UN 2030 agenda for sustainable development. *Sustainability (Switzerland)*, 12(3).

Natesan, S. & Venkatesan, J. 2016. A SRF-PLL Control Scheme for DVR to Achieve Grid Synchronization and PQ Issues Mitigation in PV Fed Grid Connected System. , (August): 2996–3015.

Ngoc, T.N., Sanseverino, E.R., Quang, N.N., Romano, P., Viola, F., Van, B.D., Huy, H.N., Trong, T.T. & Phung, Q.N. 2019. A hierarchical architecture for increasing efficiency of large

photovoltaic plants under non-homogeneous solar irradiation. *Solar Energy*, 188(July): 1306–1319. https://doi.org/10.1016/j.solener.2019.07.033.

Nurujjaman, M. 2020. Enhanced Euler's Method to Solve First Order Ordinary Differential Equations with Better Accuracy. *Journal of Engineering Mathematics & Statistics* , 4(1): 1–13. https://www.researchgate.net/publication/341150578_Enhanced_Euler's_Method_to_Solve_ First_Order_Ordinary_Differential_Equations_with_Better_Accuracy.

Ögren, J. & Ögren, J. 2011. PLL design for inverter grid connection Simulations for ideal and non-ideal grid conditions.

Padmanaban, K., Shunmugalatha, A. & Kamalesh, M.S. 2022. Design and Implementation of a New Fast and Efficient MPPT Controller under Different Solar Irradiance Conditions. *International Journal of Photoenergy*, 2022.

Pal, S. & Sahay, K.B. 2018. Modeling of Solar Energy Grid Integration System Using Typhoon HIL. *2018 International Electrical Engineering Congress (iEECON)*, 1: 1–5.

Rakesh, N., Banerjee, S., Subramaniam, S. & Babu, N. 2020. A simplified method for fault detection and identification of mismatch modules and strings in a grid-tied solar photovoltaic system. *International Journal of Emerging Electric Power Systems*, 21(4).

RASHID, M.H. 2001. *POWER ELECTRONICS Academic Press Series in Engineering.*

Romero-cadaval, E., Engineers, E., Spagnuolo, G. & Franquelo, L.G. 2013. Grid Connected Photovoltaic Generation Plants . , (September).

Saïd-Romdhane, M. Ben, Naouar, M.W., Belkhodja, I.S. & Monmasson, E. 2016. Simple and systematic LCL filter design for three-phase grid-connected power converters. *Mathematics and Computers in Simulation*, 130(October): 181–193. http://dx.doi.org/10.1016/j.matcom.2015.09.011.

Salah, J.A. 2019. Agenda Introduction Photovoltaic effect Electron-hole formation A solar panel (or) solar array Types of Solar cell Principle , construction and working of Solar cell Advantage , disadvantage and. , (October).

Santhoshi, B.K., Sundaram, K.M., Padmanaban, S., Holm-Nielsen, J.B. & Prabhakaran, K.K. 2019. Critical review of PV grid-tied inverters. *Energies*, 12(10).

Sapountzoglou, N., Raison, B., Sapountzoglou, N., Raison, B., Connected, A.G., System, P. V, Diagnosis, F., Sapountzoglou, N. & Raison, B. 2019. To cite this version : HAL Id : hal-02072272 A Grid Connected PV System Fault Diagnosis Method.

SEA. 2017. Sustainable energy solutions for South African local government: a practical guide. *Sustainable Energy Africa*: 24. https://www.sustainable.org.za/userfiles/process(2).pdf.

Shariar, K. & Control, P. 2016. Fabrication & Characterization of Natural Dye Sensitized Solar Cell

(NDSC) Fabrication & Characterization of Natural Dye Sensitized Solar Cell Part - 1 & Part - 2 Prepared By : Kazy Fayeen Shariar (072457) Md . Tauhidul Islam (072457) Supervised By . , (October 2011).

Sharma, D.K. & Purohit, G. 2014. Analysis on the efficiency of solar PV system for improved design of MPPT. *The 6th World Conference on Photovoltaic Energy Conversion*, (November): 1281– 1282. https://www.researchgate.net/profile/Dinesh-Sharma-19/publication/269390463_Analysis_of_the_Effect_of_Fill_Factor_on_the_Efficiency_of_Sol ar_PV_System_for_Improved_Design_of_MPPT/links/55405ee70cf2736761c2766d/Analysis -of-the-Effect-of-Fill-Factor-on-the-.

Shrestha, Ram M, Acharya, Jiwan. 2018. *Sustainable Energy Access Planning: A Case Study*. https://www.adb.org/sites/default/files/publication/448631/sustainable-energy-access-planning-case-study.pdf.

Singh, B.P., Goyal, S.K. & Siddiqui, S.A. 2019. Grid Connected-Photovoltaic System (GC-PVS): Issues and Challenges Grid Connected-Photovoltaic System (GC-PVS): Issues and Challenges.

Sultana, G. & U, H.H. 2016. Electrical Energy Audit a Case Study. *IOSR Journal of Electrical and Electronics Engineering Ver. III*, 10(3): 2278–1676. www.iosrjournals.org.

Szabo, L. 2018. The History of Using Solar Energy. , (June 2017).

EL Tayyan, A.A. 2013. A simple method to extract the parameters of the single-diode model of a PV system. *Turkish Journal of Physics*, 37(1): 121–131.

Tripathi, S.M. & Singh, S. 2020. Hardware-in-the-Loop Simulation of Grid-tied Converter for Unity Power Factor Operation. , (4): 250–253.

Tunahan Işık Isik. 2015. Solar Cells review Faculty of Arts and Science Department of Physics Project - I Solar Cells Review by Tunahan Işık Supervised by : Prof . İsmail Karakurt January-2015. *Solar Cells Review*, (January).

USAID. 2014. Greenhouse Gas Emissions in South Africa. *Greenhouse Gas Emissions Factsheet*, (July): 1–3. [12/12/2017 14:15] Frederic Hans: %0Ahttps://www.environment.gov.za/sites/default/files/docs/greenhousegas_invetorysouthaf rica.pdf %0A %0A.

Villegas Aguilar, P. 2018. Benefits of Solar Energy for Belize. *The Belize Times*, 4(April): 18.

W. Hart Danial. 2011. *Power Electronics*. Indiana: McGraw-Hill.

Wang, L. 2020. Chapter 1 Basics of PID Control. , (March).

Yang, Y., Member, I., Hadjidemetriou, L., Member, Ieee Student, Blaabjerg, F., Fellow, I., Kyriakides, E. & Member, Ieee Senior. 2015. Benchmarking of Phase Locked Loop based

Synchronization Techniques for Grid-Connected Inverter Systems. : 2167–2174.

Yasmeena, S. & Das, G.T. 2015. A Review of Technical Issues for Grid Connected Renewable Energy Sources. *International Journal of Energy and Power Engineering International Journal of Energy and Power Engineering. Special Issue: Energy Systems and Developments*, 4(5): 22–32. http://www.sciencepublishinggroup.com/j/ijepe.

Yi, G.C. 2012. *Semiconductor Nanostructures for Optoelectronic Devices: Processing, Characterization and Applications*.

Zabihian, F. 2021. Solar Energy and Photovoltaic Solar Units. *Power Plant Engineering*, (June): 759–904.

Zina, B., Mouna, B.H. & Lassaad, S. 2017. Photovoltaic Cell Mathematical Modelling. , 6(06): 884–887. www.ijert.org.